6-1974

Electron Attachment to Molecules in Very High Pressure Gases

Ronald Earl Goans
University of Tennessee, Knoxville

To the Graduate Council:

I am submitting herewith a dissertation written by Ronald Earl Goans entitled "Electron Attachment to Molecules in Very High Pressure Gases." I have examined the final electronic copy of this dissertation for form and content and recommend that it be accepted in partial fulfillment of the requirements for the degree of Doctor of Philosophy, with a major in Physics.

L. G. Christophorou, Major Professor

We have read this dissertation and recommend its acceptance:

R. J. Lovell, R. O'brilly, F. Williams

Accepted for the Council:

Carolyn R. Hodges

Vice Provost and Dean of the Graduate School

(Original signatures are on file with official student records.)

February 28, 1974

To the Graduate Council:

I am submitting herewith a dissertation written by Ronald Earl Goans entitled "Electron Attachment to Molecules in Very High Pressure Gases." I recommend that it be accepted in partial fulfillment of the requirements for the degree of Doctor of Philosophy, with a major in Physics.

L. G. Christophorou

Major Professor

We have read this dissertation and recommend its acceptance:

R. J. Lovell

R. O. Bentley

Truman Williams

Accepted for the Council:

Hilton A. Smith

Vice Chancellor for
Graduate Studies and Research

NV

ELECTRON ATTACHMENT TO MOLECULES IN VERY HIGH PRESSURE GASES

A Dissertation

Presented to

the Graduate Council of

The University of Tennessee

In Partial Fulfillment

of the Requirements for the Degree

Doctor of Philosophy

---

by

Ronald Earl Goans

June 1974

ACKNOWLEDGEMENTS

The author wishes to thank Dr. L. G. Christophorou for suggesting this research and for his guidance throughout the project. He is also grateful to Ada Carter, J. A. Harter, D. Pittman, and J. G. Carter for experimental assistance and to V. E. Anderson for computational assistance.

The author was priviledged to use the research facilities in the Health Physics Division of the Oak Ridge National Laboratory where the research was sponsored by the U. S. Atomic Energy Commission under contract with Union Carbide Corporation. He is appreciative of the hospitality shown him by many people during his stay there.

Special thanks are extended to K. Gant for her many helpful and stimulating discussions. The author is also especially grateful to his wife, Judy, for her patience and understanding during the years of graduate study.

Appreciation is also extended to Oak Ridge Associated Universities for financial assistance through a Special Fellowship in Health Physics and an ORAU Laboratory Participantship. Without this assistance, the present work could not have been completed.

ABSTRACT

In this thesis, electron capture mechanisms and reaction schemes have been developed for electron attachment to O_2, C_6H_6, and C_2H_5Br embedded in high densities of N_2 ($P_{N_2} \leq 36$ atm), Ar ($P_{Ar} \leq 56$ atm), C_2H_4 ($P_{C_2H_4} \leq 22$ atm), and C_2H_6 ($P_{C_2H_6} \leq 23$ atm). As the density of each medium increases, each is found to affect the attachment rate in a different manner, indicating the profound effect and importance of the environment on the electron attachment process. The results of a study on the capture of slow (< 1 eV) electrons by O_2 in high pressures of N_2, C_2H_4, and C_2H_6 media are presented and discussed and a model is presented to account for the experimental observations in each case. Benzene has also been found to capture slow electrons in high pressures of N_2 and Ar media and a model is presented to account for the observed results. The finding that C_6H_6 captures electrons in the gas phase forces the conclusion that $(EA)_B > 0$ eV in contrast to the accepted view that $(EA)_B < 0$ eV. Bromoethane has been found to capture slow (< 3 eV) electrons in high pressures of N_2 and Ar and a reaction mechanism is presented which accounts for the relative magnitudes of the rate constants for autoionization, dissociation, and collisional stabilization. The high pressure data for electron attachment to O_2, C_6H_6, and C_2H_5Br to form the respective negative ions have been extrapolated to liquid densities to yield values of the attachment rate in the liquid state. These values generally are in reasonable agreement with those obtained by other investigators using liquid solutions.

TABLE OF CONTENTS

LIST OF TABLES

LIST OF FIGURES

CHAPTER I

INTRODUCTION

I. IMPORTANCE OF ELECTRON ATTACHMENT STUDIES

The study of low energy electron attachment to molecules is of fundamental importance in both the physical and biological sciences. These processes are important in the physical sciences because many molecular parameters can be directly or indirectly determined from electron attachment studies. Such parameters include electron affinities of molecules, electron attachment rate constants and cross sections, autoionization lifetimes of transient negative ion species, bond dissociation energies, and shapes of molecular and negative ion potential energy curves. Electron attachment studies are important in biology because of the large number of low energy electrons that are produced when ionizing radiation interacts with matter. The elucidation of reaction mechanisms for these electrons is a crucial step in the development of a coherent picture of radiation biology. The importance of electron attachment studies in the physical and biological sciences is obvious, and related details have been discussed in several books [see, e.g., McDaniel (1964), Szent-Gyorgyi (1960, 1968) and Christophorou (1971a)].

II. REACTION CHANNELS OF INTEREST IN ELECTRON ATTACHMENT STUDIES

It is instructive to consider the various reaction channels available when a free electron is captured by a molecule. These are as follows:

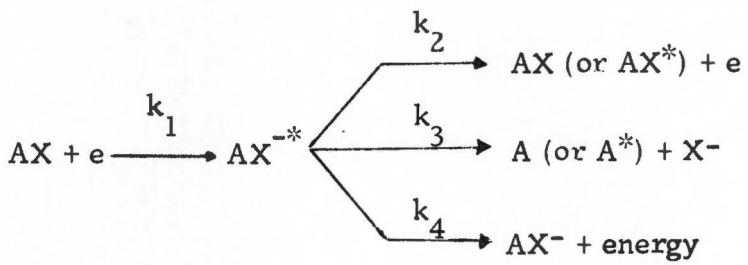

(I-1)

(I-2)

(I-3)

where k_i ($i = 1, \ldots 4$) are the rate constants for the various channels. k_1 is the absolute rate for formation of the compound negative ion AX^{-*}. This compound system may autoionize either elastically or inelastically with a lifetime $\tau_a = k_2^{-1}$ as short as $10^{-14} - 10^{-15}$ seconds. Dissociation [Equation (I-2)] can be in competition with autoionization and is energetically possible when the incident electron energy exceeds D(AX) - EA(X) where D(AX) is the dissociation energy of AX and EA(X) is the electron affinity of X. The electron affinity of a molecule is defined as the difference in energy between the neutral molecule and the negative ion when both are in their ground electronic, vibrational, and rotational states. By convention, EA is positive if the $v = 0$ level of AX^- lies below the $v = 0$ level of AX, where v is the vibrational quantum number.

Channel (I-3) is the nondissociative electron attachment process resulting in the formation of the parent negative ion AX^-. This reaction is possible when EA(AX) > 0 eV and there is a mechanism for removing the excess excitation energy. Generally, radiative stabilization of AX^{-*} is improbable and stabilization occurs through interaction with a third body, i.e.,

$$e + AX \longrightarrow AX^{-*} \xrightarrow{+S} AX^- + S^* + \text{energy} \qquad \text{(I-4)}$$

where S may be AX or another molecule or atom. Complete stabilization of transient ions with $10^{-13} \leq \tau_a \leq 10^{-6}$ sec can be achieved in high pressure swarm experiments ($10^3 \leq P \leq 10^5$ Torr) if the density of the stabilizing body is such that the autoionization lifetime is much longer than the time between collisions of AX^{-*} and S.

III. METHODS USED TO STUDY MOLECULAR NEGATIVE IONS

Three groups of negative ions have been distinguished [Christophorou (1971a)] on the basis of the magnitude of the negative ion lifetime τ_a.

1. Extremely short lived ions ($10^{-15} \leq \tau_a \leq 10^{-13}$ sec). These ions are observed as resonances in electron scattering experiments.

2. Moderately short lived ions ($10^{-13} \leq \tau_a \leq 10^{-6}$ sec). Collisional stabilization can occur in this time interval at high pressures and the negative ions can be observed in high pressure swarm experiments.

3. Long lived negative ions ($\tau_a \geq 10^{-6}$ sec). The lifetimes of many of these ions can be determined under single collision conditions in a time of flight mass spectrometer (TOFMS).

The two methods used most often for observing molecular negative ions are the electron beam and the electron swarm. In the electron beam method, a nearly monoenergetic beam of electrons collides under single collision conditions with the molecule of interest. Beam experiments using a TOFMS are utilized to measure the negative ion yield $I(\epsilon)$ and to mass analyze and find the energy dependence of the reaction products. Under appropriate experimental conditions the yield $I(\epsilon)$ is proportional to the attachment cross section thereby giving a relative cross section spectrum. The mean autoionization lifetime of long-lived negative ions ($\tau_a \geq 10^{-6}$ sec) can also be determined in a TOFMS by measuring the ratio of the total current (neutral + ion) to the neutral current for various values of the accelerating potential. The TOFMS method has been improved with the development of the retarding potential difference technique (RPD) [Fox et al. (1955)]. This technique has a resolution of ~ 0.2 eV and thereby provides a lower limit to the width of a negative ion resonance that can be measured experimentally.

The electron swarm method combined with the swarm unfolding technique (see Chapter II) is ideally suited for low energy electron attachment studies in the high pressure gas phase ($0.2 \text{ atm} \leq P \leq 100 \text{ atm}$). Such a range of pressures can be utilized to stabilize negative ions in the lifetime range

$10^{-13} \leq \tau_a \leq 10^{-6}$ sec. This type of experiment is important because such negative ions are undetectable in a conventional TOFMS. The high pressure swarm experiment is crucial in relating the abundant knowledge on isolated molecules (low pressure gases) to that in the condensed phase. Such studies are useful in developing an understanding of the environmental influences on reaction mechanisms accompanying the interaction of radiation with matter. Furthermore, an understanding of the role of the physicochemical properties of molecules in biological reactions requires knowledge as to how these isolated molecule properties change when the molecule is embedded in gradually denser and denser gaseous and, finally, into condensed phase environments. Through the high pressure swarm experiment one is capable of determining the pressure dependence of certain molecular parameters and, in some cases, is capable of extrapolating these values to the liquid phase.

IV. SCOPE OF THE PRESENT WORK

In this thesis, results on electron attachment to molecules embedded in high pressure gaseous media will be given. In Chapter II, we review both the analytical and experimental methods and the experimental modifications which were necessary in order to extend measurements to 55 atm. In Chapter III, we present results of a study on the capture of slow (< 1 eV) electrons to O_2 in very high pressures of nitrogen, ethylene, and ethane. In addition, we present various models for attachment in these three environments and utilize the proposed models to calculate a value for

the lifetime of O_2^{-*}. The high pressure data on O_2 are also extrapolated to liquid state behavior. In Chapter IV, gaseous electron attachment to benzene in dense media is presented. These data along with certain models are used to calculate the autodetachment lifetime of $C_6H_6^{-*}$. In Chapter V, ultrahigh pressure studies on the dissociative attachment processes in C_2H_5Br are presented. In Chapter VI, the present work is summarized.

CHAPTER II

EXPERIMENTAL AND ANALYTICAL METHODS

In this chapter we review work performed with the electron swarm method and comment on the experimental modifications introduced in the present work in order to study electron attachment in ultrahigh pressure gas mixtures. Furthermore, the accuracy of the experimental data has been significantly improved by addition of a new electronics system and by modifications on the chamber. These details will be discussed first and then, the methods of determining electron attachment cross sections will be presented.

I. EXPERIMENTAL PROCEDURE

1. Description of the Electron Swarm Method

In the electron swarm method, electrons drift through a gas at high pressures under the influence of a uniform electric field E. Because of the high pressures employed, these electrons rapidly come into equilibrium with the gas and attain an energy distribution $f(\epsilon, E/P)$ which is characteristic of the gas, the temperature, and the pressure-reduced electric field E/P (volt-cm^{-1} $Torr^{-1}$). The electron swarm distribution is broad and is defined by $f(\epsilon, E/P)\, d\epsilon$ = fraction of electrons in the energy interval between ϵ and $\epsilon + d\epsilon$. One therefore determines quantities, such as the attachment

rate, $(\alpha w)_o$, in a high pressure swarm experiment which are averages over the electron energy distribution $f(\epsilon, E/P)$.

In the electron swarm method employed in the present study, the attaching gas is mixed in very small proportions with another gas called the carrier gas which does not capture electrons in the energy region of interest and whose role is to establish the electron distribution function at each E/P. In this study, ethylene (C_2H_4), ethane (C_2H_6), nitrogen (N_2) and argon (Ar) were used as carrier gases. The electron energy distribution functions for these gases will be discussed in a subsequent section.

The swarm method of Bortner and Hurst (1958), modified for ultrahigh pressures (0.5 atm $\leq$ P $\leq$ 100 atm), was used for measurement of electron attachment rates. The swarm apparatus as modified by Christophorou et al. (1965) is shown in Figure II-1. Briefly, in this method, electrons are produced in a plane by α-particle ionization at a known distance between two parallel plate collectors. Because of the high pressures involved, these electrons ($\sim 1.5 \times 10^5$ per α particle) come into equilibrium with the gas quickly and attain the energy distribution $f(\epsilon, E/P)$. A uniform electric field E causes the electron swarm to drift toward the positive collector. Let N be the number of electrons at a distance from the source and let dN be the number of electrons removed from the swarm by the attaching species while the swarm drifts through the distance dx. We then have

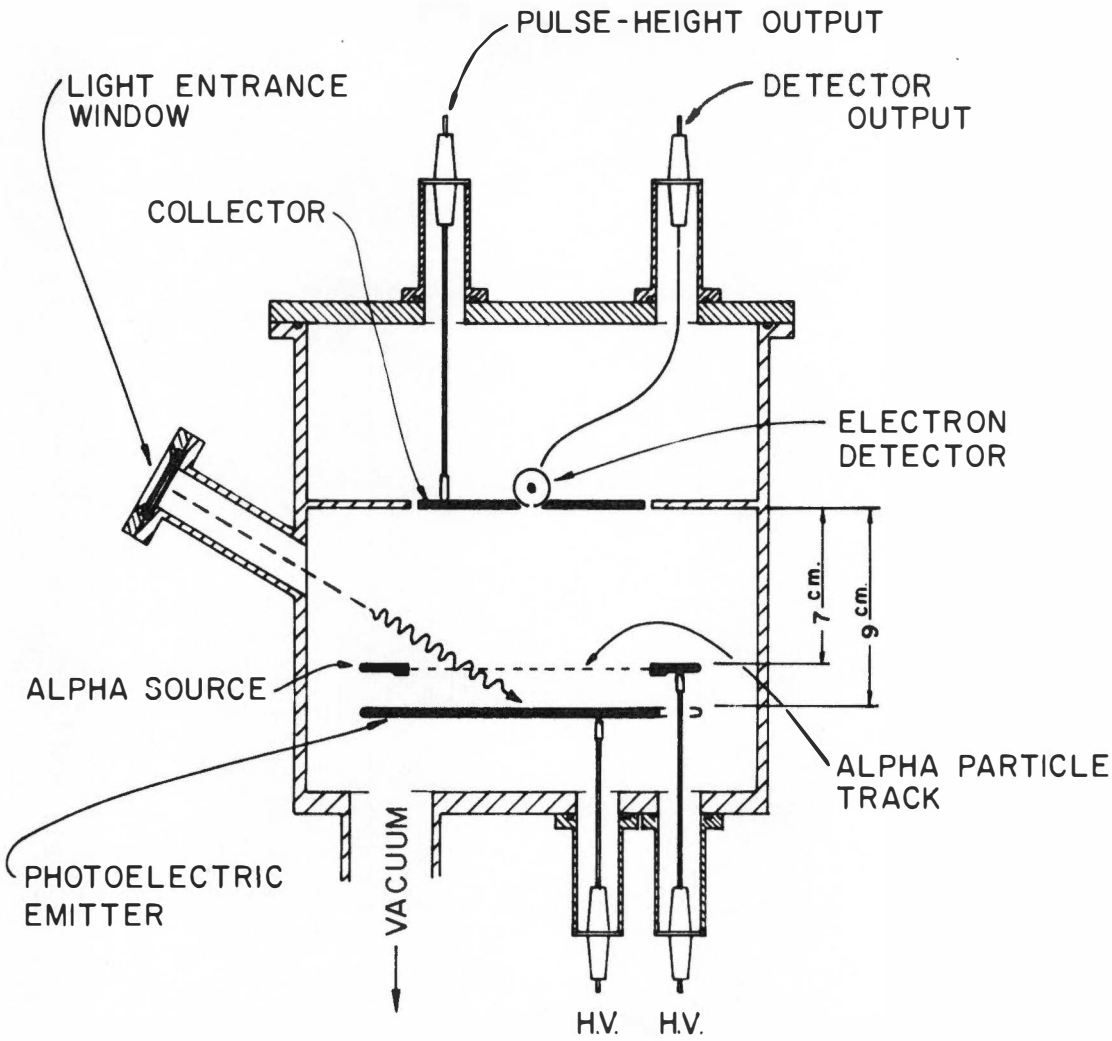

SWARM APPARATUS FOR MEASUREMENT OF ELECTRON ATTACHMENT COEFFICIENT AND DRIFT VELOCITY

Figure II-1. Swarm Apparatus of Bortner and Hurst as Modified by Christophorou et al.

$$dN = -\alpha N(x) P_A \, dx \qquad \text{(II-1)}$$

where α is the attachment coefficient and P_A is the pressure of the attaching species. Integrating Equation (II-1) gives

$$N(x) = N(0) \, e^{-\alpha P_A x} \, . \qquad \text{(II-2)}$$

As the electron swarm drifts a distance dx, the potential variation dV at the positive electrode is given by

$$dV = \frac{N(x) V_o \, dx}{d} \qquad \text{(II-3)}$$

where d is the distance between the α source and the collector and V_o is the change in the collector potential due to a single electron traversing the distance d. The time variation of the collector potential V(t) is given by

$$V(t) = \frac{A}{f}(1 - e^{-ft/\tau_o}) \qquad \text{(II-4)}$$

where $A = N(0) V_o$, $\tau_o = d/w$ is the collection time of a swarm of drift velocity w and $f = \alpha P_A d$.

2. Description of the Electronics System

The height of the pulse given by Equation (II-4) is measured (i) for the pure carrier gas and (ii) in a binary mixture in which the attaching gas is mixed in minor proportions with the carrier gas under identical experimental conditions and total pressure. The pulse V(t) is fed into a Tennelec

TC161D charge sensitive preamplifier and through a TC200 Tennelec linear pulse amplifier. The TC200 pulse amplifier contains a main amplifier section of gain A' and wave shaping networks consisting of two differentiators and a single integrator, each with separately adjustable time constants τ. The transfer function of the pulse amplifier is [see Kowalski (1973)]

$$\frac{E_o(s)}{E_i(s)} = \left(\frac{s\tau_{d1}}{1+s\tau_{d1}}\right)\left(\frac{s\tau_{d2}}{1+s\tau_{d2}}\right)\frac{A'}{1+s\tau_{int}} \qquad \text{(II-5)}$$

where s is the Laplace transform variable, $E_o(s) = \mathcal{L}[e_o(t)]$ is the transform of the output signal $e_o(t)$, $E_i(s) = \mathcal{L}[e_i(t)]$ is the transform of the input signal, and τ_{d1}, τ_{d2}, and τ_{int} are the first differentiator, second differentiator, and integrator time constants, respectively. The input to this amplifier is the collector signal V(t) so that

$$e_o(t) = \mathcal{L}^{-1}\left\{\frac{s^2\tau_{d1}\tau_{d2}A'V(s)}{(1+s\tau_{d1})(1+s\tau_{d2})(1+s\tau_{int})}\right\} \qquad \text{(II-6)}$$

where $\mathcal{L}^{-1}$ is the inverse Laplace transform operator, $e_o(t)$ is the output signal in the time domain, and $V(s) = \mathcal{L}[V(t)]$. Equation II-6 can be inverted to yield

$$e_o(t) = \frac{AA'}{\tau_o\tau_{int}}\sum_{i=1}^{4}\frac{P(\alpha_i)}{Q'(\alpha_i)}e^{\alpha_i t} \qquad \text{(II-7)}$$

where $P = s$, $Q = \prod_{i=1}^{4} (s + \alpha_i)$ and α_i $(i = 1, \ldots 4) = 1/\tau_{d1}$, $1/\tau_{d2}$, $1/\tau_{d3}$ and f/τ_o, respectively. $e_o(t)$ may either be a bipolar or unipolar pulse depending on the relative magnitudes of the time constants. The noise can be shown [Fairstein (1961)] to be minimized when the differentiator and integrator time constants are equal. $e_o(t)$ is then inputed into a 512 channel Nuclear Data analyzer and the output of the multichannel analyzer is printed out using a teletype. At a given E/P, the pulse $e_o(t)$ will be stored in channel c_1 for the pure carrier gas (i) and will be stored in channel $c_2 < c_1$ for the binary mixture (ii). From the ratio $R = c_2/c_1$ of the heights of the collector pulses for the binary gas mixture and the carrier gas itself, the attachment coefficient α can be determined [Eldridge (1962)]. The tables of Eldridge considered the response of an amplifier with single integrator and differentiator shaping networks to the input pulse V(t). These tables may be used, however, with the more complicated situation II-6 because the ratio R is independent of the shaping networks.

The product of α and the electron swarm drift velocity, w (in cm sec^{-1}), at each E/P gives the absolute rate of electron attachment, αw (in sec^{-1} $Torr^{-1}$), at that E/P. Drift velocities used in this work were taken from Christophorou (1971a) and represent averages of the best experimental data available. Attachment rates can be obtained as a function of mean energy $\langle \epsilon \rangle$ if $\langle \epsilon \rangle$ is known as a function of E/P. $\langle \epsilon \rangle$ is generally known as a function of E/P for the common carrier gases N_2, Ar, and C_2H_4 [Christophorou (1971a)] and can often be found from D_L/μ data for other gases.

The electronics system used in the high pressure swarm apparatus has very little drift (< 1 channel per day) and consequently can be used to measure low attachment rates ($\sim 10^3$ sec^{-1} $Torr^{-1}$). Such low rates are difficult to measure because the pulses for the carrier gas and the binary mixture are nearly the same size. However, the stability of the system has allowed reasonably precise measurement of αw where the pulses for the binary system are more than 5 channels below the pulses for the pure carrier gas.

3. Source Modifications

Due to the wide range of high pressures employed it was necessary to build α-particle sources of different dimensions. A number of these were constructed by electroplating either ^{252}Cf (α-particle energies: 6.12, 6.08 MeV; half life: 2.65 yr.) or ^{239}Pu (α-particle energies: 5.16, 5.15, 5.11 MeV; half life: 24390 yr.) on a thin ribbon of plutonium and locating it in a circular groove as shown in Figure II-2 at a distance R from the inside edge of the annulus. The dimensions R and D (see Figure II-2) were decreased as the pressure was increased because an increase in pressure causes a corresponding decrease in α-particle track length. Sources with $1.5 \leq D \leq 8.6$ cm and $0.038 \leq R \leq 0.014$ cm were found to be effective. Care was also taken to have a thin source so that the fraction of the α-particle energy lost in the source was small. Collimation of the α-particles is extremely important in order to have narrow pulse-height distributions; this objective was achieved

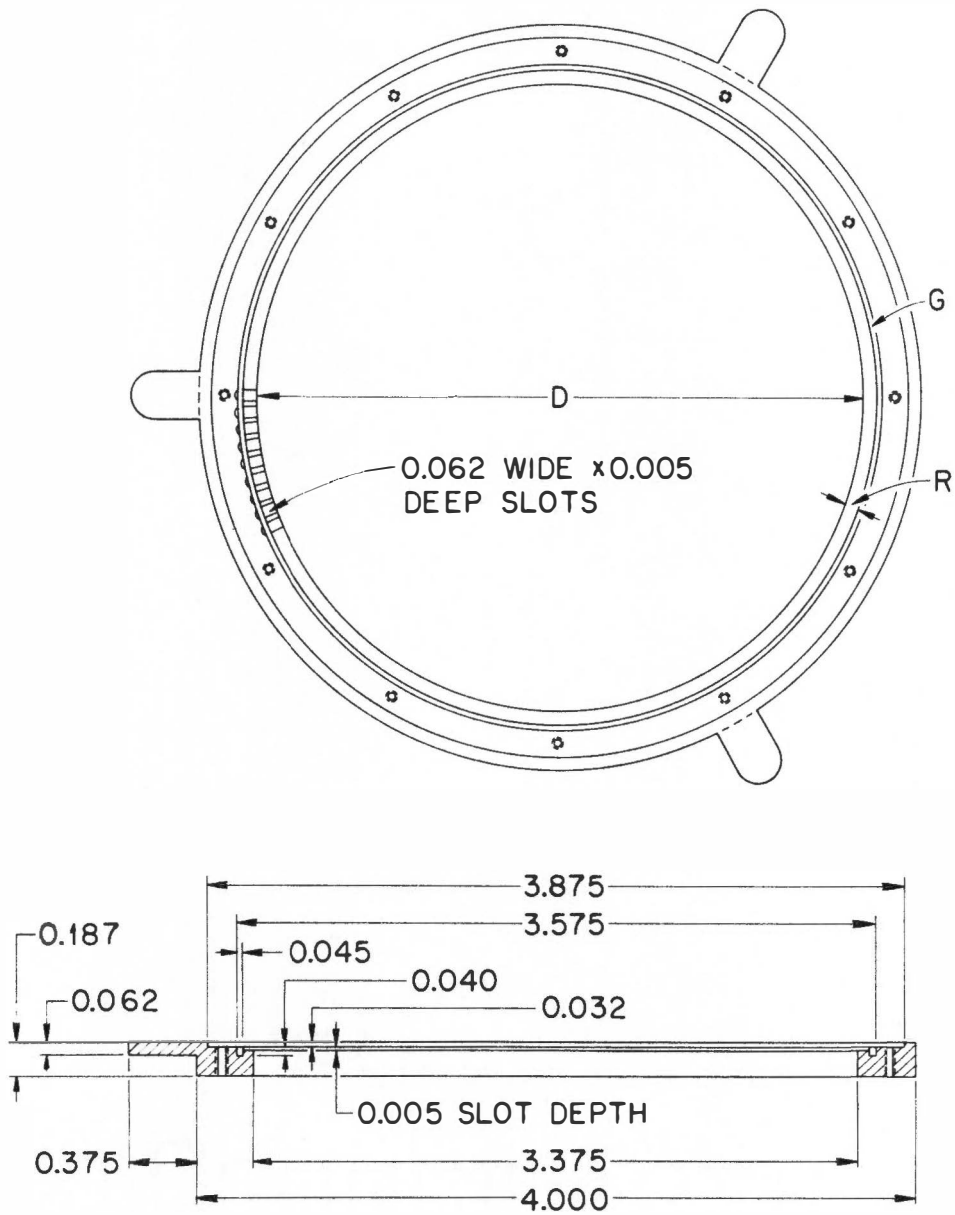

Figure II-2. Dimensions of α Source in Inches.

by accepting only those α-particles coming from a series of equally spaced collimating holes. The holes are arranged in a 360° pattern and the number of holes varied from 120 for D = 8.6 cm to 24 for D = 1.5 cm. To maintain a convenient counting rate, the source activity was increased from 0.5 μC for the source with the largest D to $\sim$ 5 μC for the source with the smallest D. In general, use of sources with high activity tended to give better results.

4. Chamber Modifications

The use of high pressures required the construction of a new ionization chamber of the same general design as that in Figure II-1, page 9. The chamber was milled from a single piece of nonmagnetic stainless steel to reduce outgassing and noise pickup and was structurally designed using ASME (American Society of Mechanical Engineers) boiler standards to support internal pressures of up to $\sim$ 80,000 Torr. All seals were inside welded and copper gaskets were used to facilitate bakeout. Varian flanges and Nupro high pressure valves were used at critical points in the chamber. Pump-out pressures were $\leq 1 \times 10^{-8}$ Torr and the outgas rate was normally ≤ 0.2 μ/hr.

5. Experimental Results

The carrier gases N_2 and Ar were obtained from Matheson Company and were of a quoted purity of 99.997%. Due to the large quantities of carrier gases needed in high pressure experiments it is uneconomical to use gases of extreme purity. However, since traces of impurities could be

troublesome, a tank of extra pure N_2 (99.9995%) was purchased and it was found that the extra purity had no effect on the attachment rates. The carrier gases C_2H_4 and C_2H_6 were of a quoted purity of 99.95% and were purified extensively by use of liquid nitrogen traps. In all experiments the carrier gas was introduced first into the chamber for pulse height measurements. When this set of measurements on the pure gas was completed the gas was collected in liquid nitrogen traps and was reused in subsequent measurements on the mixture. This procedure allowed use of a carrier gas that was of exactly the same relative purity for both sets of measurements. Furthermore, it helped avoid the difficulty of distilling larger quantities of carrier gas and of containing this amount in the liquid nitrogen traps. The cost of the experiment is also significantly reduced in view of the large quantities of carrier gas needed.

The attaching gas pressures were measured with an MKS capacitance manometer; the carrier gas pressure was measured with a Wallace-Tiernan absolute pressure gauge up to 25,000 Torr and above this pressure with a strain gauge-digital voltmeter combination. The strain gauge was calibrated with the Wallace-Tiernan up to 25,000 Torr and the calibration curve was extrapolated for use in the higher regions.

Although for N_2 it was not necessary to correct the pressure readings for gas compressibility, such a correction was necessary in the case of C_2H_4 and C_2H_6. For an ideal gas ($PV = nRT$)

$$E/P \propto E/N \qquad \text{(II-7)}$$

where P is the pressure in Torr and N is the number of molecules per cm^3 per Torr. For a compressible gas (PV = znRT)

$$E/P \propto E/N\,(1/z) \qquad \text{(II-8)}$$

where z is the compressibility factor. The compressibility factor approaches unity at low pressures and decreases with increasing pressure. In the present experiment the measured pressures P_M were divided by z to obtain the quantity $P' = P_M/z$ for which $E/P' \propto E/N$. The compressibility factor data were taken from Walters et al. (1954) for C_2H_4 and from Maxwell (1950) for C_2H_6.

All measurements were made at room temperature (298° K) and in all experiments the carrier gas pressures were much greater (by a factor of 3×10^2 to 2×10^7) than the attaching gas pressures. For this reason, the total pressures are referred to as carrier gas pressures.

Three high voltage power supplies provided the accelerating voltage. A Keithley 240 regulated high voltage supply was used for voltages ≤ 1 KV, a John Fluke 410 A supply for voltages 1-10 KV, and a John Fluke 430 A supply for voltages 10 KV-20 KV. The need for high fields in order to reach large values of E/P, especially for the highest pressures, demanded very careful filtering of the power supplies to reduce ripple. In many cases, corona and gas breakdown limited the value of E/P that one could achieve. This problem was particularly critical at the highest pressures.

II. DISTRIBUTION FUNCTIONS

1. General Theory

The electron energy distribution function $f(\epsilon, E/P)$ is a solution to the Boltzmann transport equation

$$\frac{\partial f}{\partial t} + \vec{v} \cdot \frac{\partial f}{\partial \vec{x}} + \frac{\vec{F}}{m} \frac{\partial f}{\partial \vec{v}} = \iint d\vec{v}_1 \, d\Omega \, g\sigma(g, \theta) [f' f_1' - f f_1] \qquad \text{(II-9)}$$

where $f(\vec{x}, \vec{v}, t)\, d\vec{x}\, d\vec{v}$ is defined to be the number of electrons having coordinates between $\vec{x}$ and $\vec{x} + d\vec{x}$ and velocities between $\vec{v}$ and $\vec{v} + d\vec{v}$. $\vec{F}$ is the external force ($= e\vec{E}$) acting on an electron of mass m in the external field $\vec{E}$. The right-hand side of Equation (II-9) is the Boltzmann collision term $(\partial f/\partial t)_c$ which represents the rate of change of f due to collisions with gas molecules. In the collision term, electrons of velocities $\vec{v}$ and $\vec{v}_1$ (relative velocity $|\vec{v} - \vec{v}_1| = g$) collide with molecules with the impact parameter b and the scattering angles θ, φ. $\sigma(g, \theta)d\Omega$ is the differential cross section for the scattering process while $f = f(\vec{x}, \vec{v}, t)$ and $f_1 = f(\vec{x}, \vec{v}_1, t)$. Primed quantities refer to velocities $\vec{v}$ and $\vec{v}_1$ after the collision. Details of the theory are found in Wu (1966) and in Present (1958).

In electron swarm experiments we deal with steady state conditions so that $\partial f/\partial t = 0$. For homogeneous gas mixtures $\vec{v} \cdot \partial f/\partial \vec{x} = 0$ so that Equation (II-9) becomes time and space independent. The Boltzmann transport equation is a nonlinear integro-differential equation which in

principle can be solved as an initial-value problem. It is difficult to solve exactly but several analytical and numerical methods have been developed. These methods are discussed by Chapman and Cowling (1952), by Allis (1956) and by Wu (1966).

When the system is in thermodynamic equilibrium, the Boltzmann transport equation has the well-known Maxwellian function

$$g(v)dv = \left(\frac{2}{\pi}\right)^{\frac{1}{2}} \left(\frac{m}{KT}\right)^{3/2} v^2 e^{-\frac{mv^2}{2KT}} dv \qquad \text{(II-10)}$$

as a solution. g(v) dv gives the fraction of electrons with velocities between v and v + dv. In Equation (II-10), T is the absolute temperature and k is Boltzmann's constant. In energy space we have

$$f(\epsilon)d\epsilon = \frac{2}{\pi^{\frac{1}{2}} (KT)^{3/2}} e^{-\epsilon/KT} \epsilon^{\frac{1}{2}} d\epsilon \qquad \text{(II-11)}$$

where $f(\epsilon)\, d\epsilon$ is the fraction of electrons in the energy interval ϵ to $\epsilon + d\epsilon$.

Electron energy distribution functions have been calculated for only a few molecules since experimental energy-loss data are not known for most gases. A comprehensive review of distribution functions and energy-loss data can be found in Massey and Burhop (1952), Loeb (1960), McDaniel (1964), and Christophorou (1971a).

2. Electron Distribution Functions Used in the Present Work

The electron energy distribution functions used in this work for N_2 were calculated by Engelhardt, Phelps, and Risk (1964) by solving the Boltzmann transport equation taking into account both elastic and inelastic collisions. Christophorou, Chaney, and Christodoulides (1969) recommended these distribution functions for N_2 after finding that the rates measured in N_2 mesh in a continuous fashion if the data of Engelhardt *et al.* are used.

The energy distribution functions $f(\epsilon, E/P)$ for electrons drifting in argon under the influence of a uniform electric field have been evaluated by Ritchie and Whitesides (1961). They considered a numerical treatment of the space and time independent Boltzmann equation for just elastic collisions, using the momentum transfer cross sections of Barbiere (1951). Barbiere's data ignored the Ramsauer-Townsend minimum at 0.28 eV [Ramsauer (1921), Townsend (1900)]. This minimum was subsequently taken into account by Nelson and Whitesides (1968) in their revised calculations on argon. These revised distribution functions were used in the present study.

A Maxwellian distribution function has been used for C_2H_4 since the system is essentially in thermal equilibrium at most E/P's of interest. Rates measured in C_2H_4 using a Maxwellian distribution mesh very well with rates obtained in N_2 in the region of overlapping energy, thereby validating this choide of $f(\epsilon, E/)$. The distribution function for C_2H_6 has not been measured; such a situation prohibits cross section analysis in ethane.

Electron energy distribution functions $f(\epsilon, E/P)$ are shown for the three carrier gases C_2H_4, N_2, and Ar in Figure II-3. One can observe that the distributions are broad with the half-width being of the same order of magnitude as the mean energy $\langle\epsilon\rangle$. By judicious choice of the carrier gas and E/P, one can investigate attachment in energy regions from thermal to ~ 10 eV.

III. ANALYTICAL METHODS

1. Attachment Rate Analysis

The absolute electron attachment rate αw(in sec^{-1} $Torr^{-1}$) is given by

$$\alpha w(E/P) = N_o \int_o^\infty v\, \sigma_a(v)\, g(v, E/P) dv \qquad \text{(II-12)}$$

or, in terms of energy,

$$\alpha w(\langle\epsilon\rangle) = N_o \left(\frac{2}{m}\right)^{\frac{1}{2}} \int_o^\infty \epsilon^{\frac{1}{2}} \sigma_a(\epsilon)\, f(\epsilon, E/P) d\epsilon \qquad \text{(II-13)}$$

where α is the electron attachment coefficient in units of cm^{-1} $Torr^{-1}$, σ_a is the attachment cross section, w is the electron swarm drift velocity in units of cm sec^{-1}, v and ϵ are the electron velocity and energy, respectively, and N_o ($= 3.24 \times 10^{16}$) is the number of attaching gas molecules per cm^3 per Torr at 298°K.

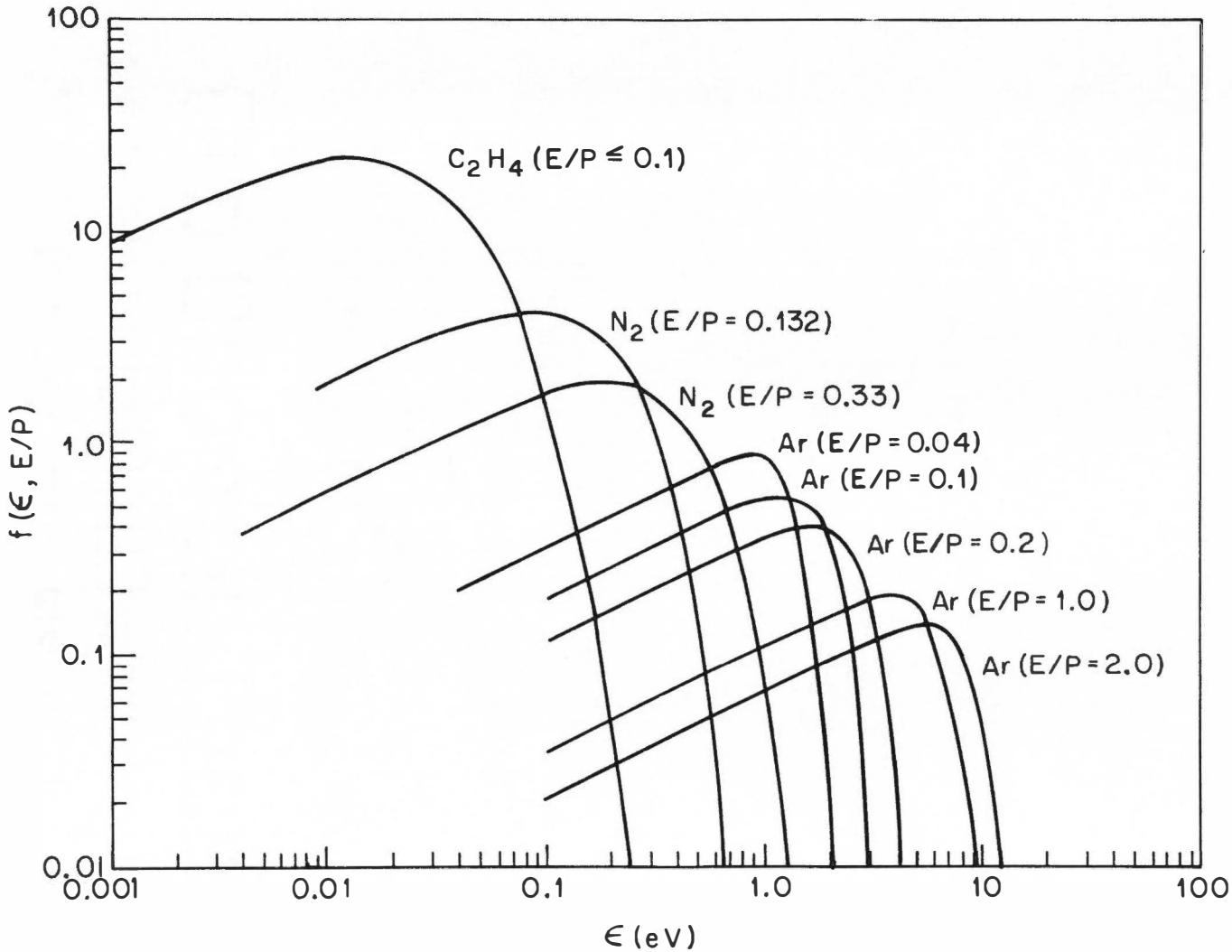

Figure II-3. Electron Energy Distribution Functions $f(\epsilon, E/P)$ for C_2H_4, N_2, and Ar.

It is desirable to be able to calculate both the magnitude and the energy dependence of the attachment cross section $\sigma_a(\epsilon)$, given experimental information on αw and $f(\epsilon, E/P)$. Previously, the swarm-beam method [see Christophorou (1971a)] was used to determine σ_a by combining the negative ion currents $I(\epsilon)$ obtained in beam experiments with attachment rates measured in swarm experiments. This procedure requires that attachment processes be the same in both the beam experiment and in the swarm and that the shape of the negative ion current be identical to the shape of the cross section. Details of this analysis were described by Christophorou et al. (1965). Another method for determining the magnitude and the energy dependence of $\sigma_a(\epsilon)$ is described by Christophorou et al. (1971b). This method is most useful for resonant attachment at thermal energies and assumes that σ_a can be represented by

$$\sigma_a(\epsilon) = \frac{A_\gamma}{\epsilon^\gamma} \quad . \tag{II-14}$$

The values γ and A_γ are determined through a least squares analysis.

2. Swarm Unfolding Technique

Christophorou, McCorkle and Anderson (1971) developed an unfolding procedure where the known swarm electron energy distribution function is used as a "smearing" function to unfold the monoenergetic rate from the experimentally determined rates. If we denote $R(\langle\epsilon\rangle_j)$ as the experimentally determined rate at the j^{th} value of the mean electron energy $\langle\epsilon\rangle$, $F(\langle\epsilon\rangle_j, \epsilon)$

as the electron energy distribution function corresponding to that mean energy and $M(\epsilon)$ as the monoenergetic rate at energy ϵ, then

$$R(\langle\epsilon\rangle_j) = \int_0^\infty M(\epsilon)\ F(\langle\epsilon\rangle_j, \epsilon)\ d\epsilon \quad . \tag{II-15}$$

The iterative solution for $M(\epsilon)$ starts by approximating $M(\epsilon)$ by $R_{exp}(\langle\epsilon\rangle)$. The initial form for $M(\epsilon)$ is introduced into Equation (II-15) and the right-hand side is evaluated at every mean energy $\langle\epsilon\rangle$. This integral will be denoted by $R_{cal}(\langle\epsilon\rangle_j)$. Relative weighting factors are then defined by

$$w(\langle\epsilon\rangle_j) \equiv \frac{R_{exp}(\langle\epsilon\rangle_j)}{R_{cal}(\langle\epsilon\rangle_j)} \tag{II-16}$$

with the auxilliary condition that $w(\langle\epsilon\rangle_j) = 1$ when $R_{cal}(\langle\epsilon\rangle_j) = 0$. The new value of $M(\epsilon)$ is determined through

$$M_{new}(\epsilon) = M_{old}(\epsilon)\ \frac{\sum_j w(\langle\epsilon\rangle_j) F(\langle\epsilon\rangle_j, \epsilon)}{\sum_j F(\langle\epsilon\rangle_j, \epsilon)} \quad . \tag{II-17}$$

The new value of $M(\epsilon)$ is introduced into Equation (II-15) and the procedure is repeated until the residuals defined by $\sum_j [R_{exp}(\langle\epsilon\rangle_j) - R_{cal}(\langle\epsilon\rangle_j)]^2$ are minimized. When the residuals reach a minimum value, the weighting factors $w(\langle\epsilon\rangle_j)$ approach unity and the function $M(\epsilon)$ does not change

with successive iterations. The number of iterations required for convergence is often large (> 3000) due to the large widths of the $F(\langle\epsilon\rangle, \epsilon)$ distribution functions. The ratio R defined by

$$R \equiv \frac{\sum_j [R_{exp}(\langle\epsilon\rangle_j) - R_{cal}(\langle\epsilon\rangle_j)]^2}{\sum_j [R_{exp}(\langle\epsilon\rangle_j)]^2} \qquad \text{(II-18)}$$

is a measure of the validity of the convergence and often was $\leq 1 \times 10^{-4}$ for calculations in this thesis. The final value of $M(\epsilon)$ is assumed to be close to the true monoenergetic rate of electron attachment, that is, the rate that would be measured had all the electrons in the swarm had the same energy. $M(\epsilon)$ can be used to calculate the attachment cross section $\sigma_a(\epsilon)$ from

$$\sigma_a(\epsilon) = \frac{M(\epsilon)}{N_o\left(\frac{2}{m}\right)\epsilon^{\frac{1}{2}}} \qquad \text{(II-19)}$$

where N_o is the number of attaching gas molecules per cm^3 per Torr at the temperature T, m is the electron mass, and $M(\epsilon)$ is in units of sec^{-1} $Torr^{-1}$. The swarm unfolding procedure has been found to be superior to all previous methods of calculation of $\sigma_a(\epsilon)$ and, for that reason, has been used throughout this thesis for the calculation of the attachment cross section.

CHAPTER III

ATTACHMENT OF SLOW ELECTRONS TO O_2 IN HIGH PRESSURE GASES

The O_2^{-*} negative ion is moderately short lived ($10^{-12} \leq \tau_a \leq 10^{-6}$ sec) and consequently can be collisionally stabilized in a high pressure swarm experiment. The nature and density of various stabilizing bodies has been found to have a profound effect on the attachment of electrons to O_2. These results will be discussed below and the high pressure rates will be extrapolated to yield approximate liquid state attachment rates.

I. ELECTRON ATTACHMENT TO O_2 IN HIGH DENSITIES OF N_2

Previous work on electron attachment to O_2 in a N_2 environment ($300 \leq P_{N_2} \leq 10,000$ Torr) has been discussed by McCorkle, Christophorou, and Anderson (1972) and by Christophorou (1972). The results obtained by these investigators have been scrutinized further and some of the early measurements have been repeated using more precise measurement techniques. Equipment modifications (see Chapter II) have also allowed an extension of this work up to N_2 pressures of 27,500 Torr ($\sim$ 36 atms). The attachment rates, $(\alpha w)_o$, extrapolated to zero O_2 pressure, P_{O_2}, are presented in Figure III-1. The function $\alpha w_o(\langle\epsilon\rangle)$ is seen to increase with increasing N_2 density and to become steeper at low energies with increasing P_{N_2}. The maximum value of αw is attained at thermal energies

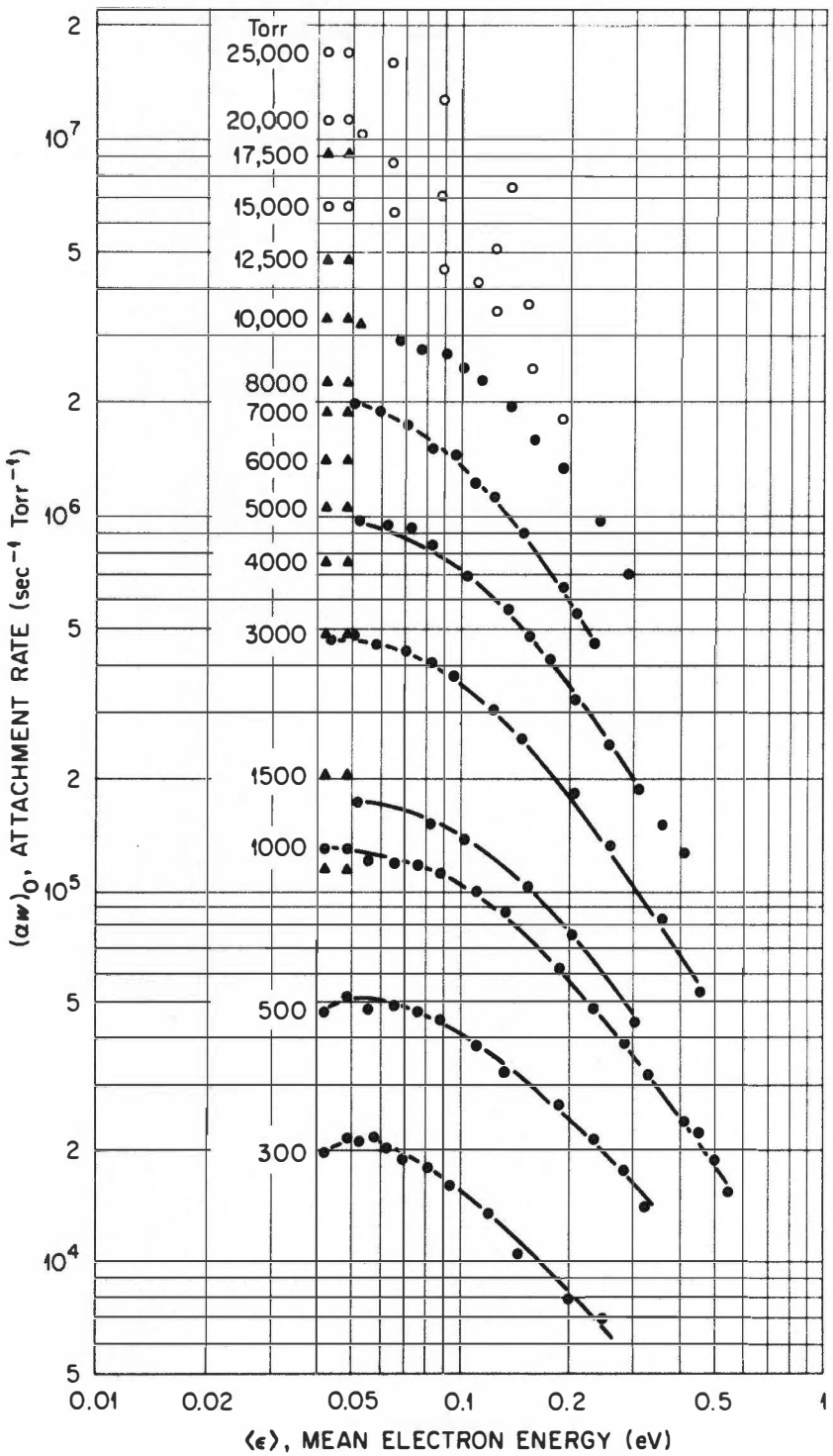

Figure III-1. Attachment Rate $(\alpha w)_o$ as a Function of Mean Electron Energy for O_2 in N_2.

(●) Data of McCorkle et al.; (▲) and (○) Present Results.

($\langle\epsilon\rangle \approx 0.04$ eV). In Figure III-2, the thermal attachment rate is presented and is seen to increase much faster than would be predicted on the basis of a pure three-body mechanism (see section IV).

McCorkle, et al. obtained the attachment rate cross section by unfolding attachment rate data using the swarm unfolding technique (see Chapter II, page 23). The cross sections $\sigma_a(\epsilon)$ determined in this manner showed two characteristic features: (i) a gradual shift of $\sigma_a(\epsilon)$ toward thermal energies with increasing P_{N_2} and (ii) structure in $\sigma_a(\epsilon)$ for $P_{N_2} \leq 1000$ Torr. The structure was attributed to electron attachment from the $v = 0$ vibrational level of O_2 to the $v' = 4$ and $v' = 5$ levels of O_2^-. The shift in $\sigma_a(\epsilon)$ toward thermal energies was ascribed to a perturbation of the O_2^- potential energy curve by N_2 during close collisions.

A sample calculation of $\sigma_a(\epsilon)$ was performed using the high pressure data at $P_{N_2} = 20{,}000$ Torr and is presented in Figure III-3. As in the previous work, the calculation was made using the swarm unfolding technique. The energy range over which $(\alpha w)_o$ can be measured is somewhat limited at the higher N_2 pressures. This restriction in the $\langle\epsilon\rangle$ range and the additional increase in experimental error (estimated to be $\pm$ 10% to $\pm$ 20%) at high P_{N_2} makes a determination of $\sigma_a(\epsilon)$ somewhat unreliable. Due to these difficulties, the cross section should be considered as only an estimate. However, it does support the earlier finding that $\sigma_a(\epsilon)$ is shifted to lower energies with increasing P_{N_2}.

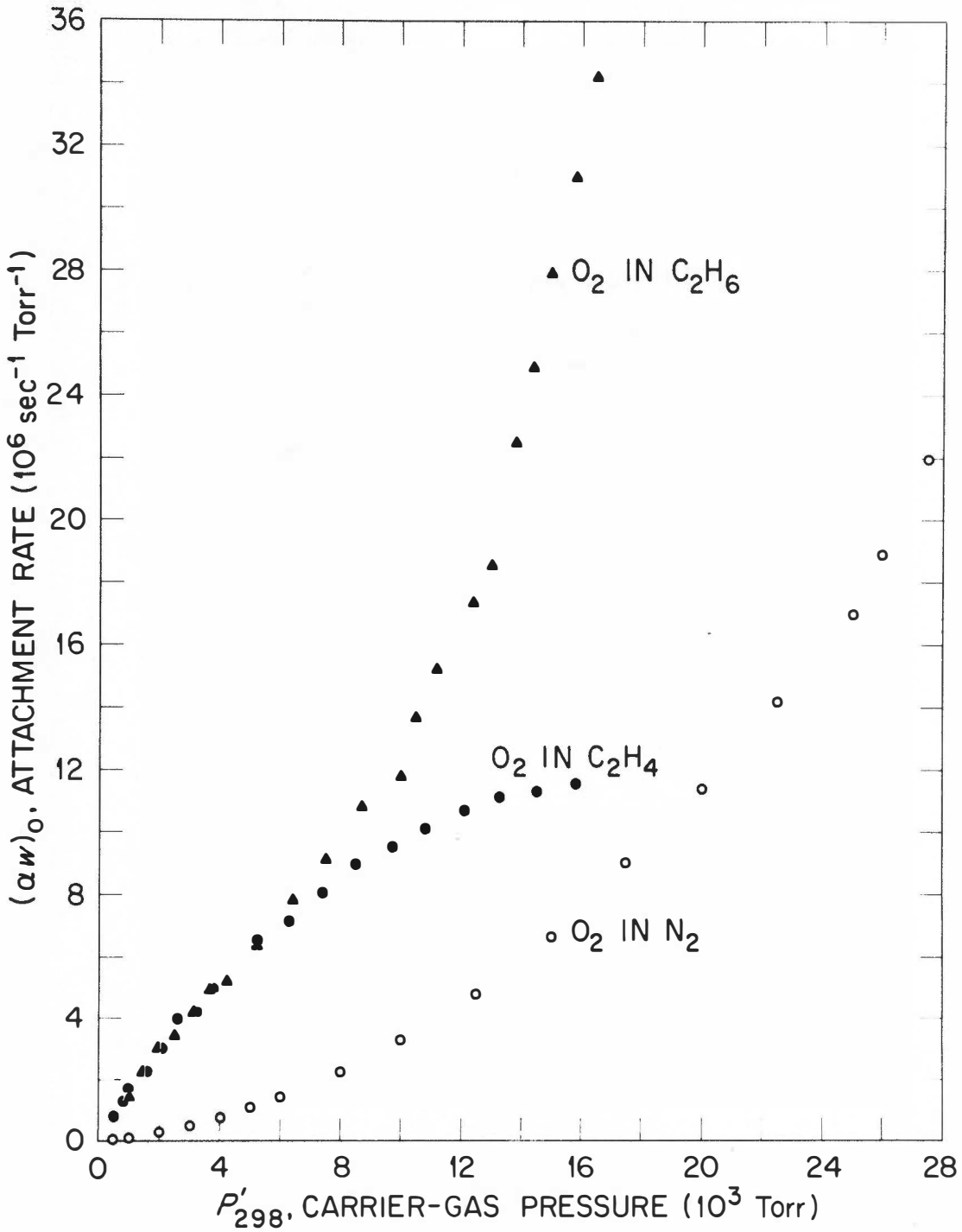

Figure III-2. Attachment Rate $(\alpha w)_o$ in N_2(○), C_2H_4 (•) and C_2H_6 (▲) as a Function of Carrier Gas Pressure.

The Data Plotted are for E/P_{298} Values Equal to 0.03 V cm^{-1} Torr^{-1} for N_2 and 0.1 V cm^{-1} Torr^{-1} for C_2H_4 and C_2H_6. These E/P Values Correspond to $\langle\epsilon\rangle$ = 0.05 eV.

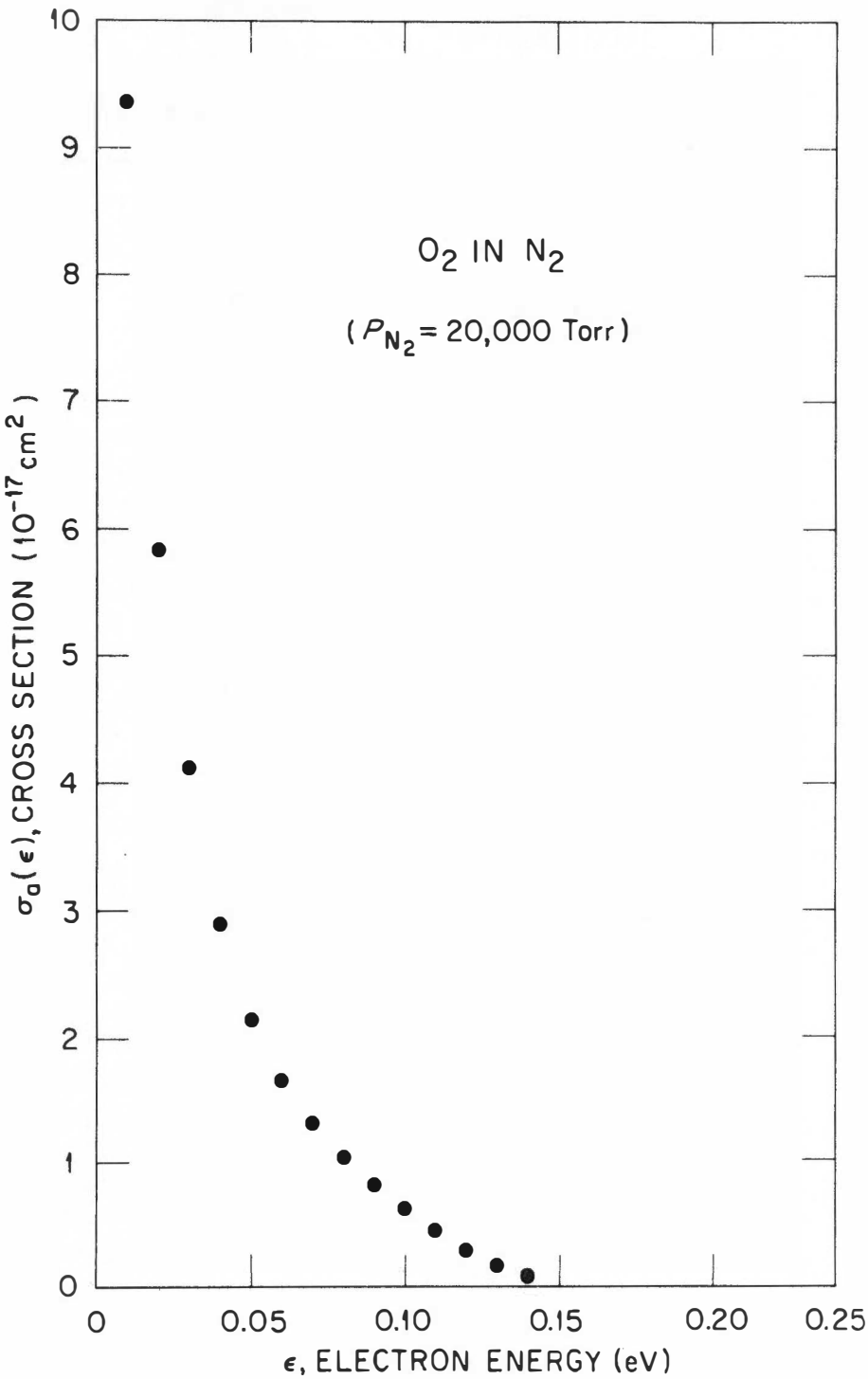

Figure III-3. Calculation of $\sigma_a(\epsilon)$ for O_2 in N_2 at P_{N_2} = 20,000 Torr.

II. ELECTRON ATTACHMENT TO O_2 IN HIGH DENSITIES OF C_2H_4

Electron attachment to O_2 in dense ethylene environments has been investigated over the pressure range $750 \leq P'_{C_2H_4} \leq 17,000$ Torr using the swarm technique. The pressure dependence of the thermal attachment rate is presented in Figure III-2, page 29, and is seen to be quite different from that for O_2 in gaseous N_2. Figure III-4A presents $(\alpha w)_o$, the attachment rate for $P_{O_2} \to 0$, as a function of E/P'_{298} and Figure III-4B shows the same quantity as a function of mean electron energy $\langle\epsilon\rangle$ for a number of total pressures P'_{298}. The kinetic equations which predict this behavior will be discussed in section IV. The energy scale has been calibrated by using $\langle\epsilon\rangle = \frac{3}{2} eD_L/\mu$ (ratio of lateral diffusion coefficient to electron mobility) obtained from the D_L/μ data of Walker (1973). These values replace the $\langle\epsilon\rangle = \frac{3}{2} e\, D/\mu$ data (ratio of longitudinal diffusion coefficient to electron mobility) of Wagner, et al. used previously by Christophorou (1971a). The two sets of data are shown in Figure III-5 as a function of E/P'_{298}.

There was no unfolding of the $\alpha w(\langle\epsilon\rangle)$ data because the electron distribution functions in C_2H_4 are not known experimentally. However, the change in the energy dependence of $(\alpha w)_o$ at low energies is consistent with the results for the O_2-N_2 mixtures which show that $\sigma_a(\epsilon)$ becomes sharper with increasing P_{N_2}.

In the case of C_2H_4 it was necessary to consider the pressure dependence of the electron drift velocity w, first noted by Huber (1969), in

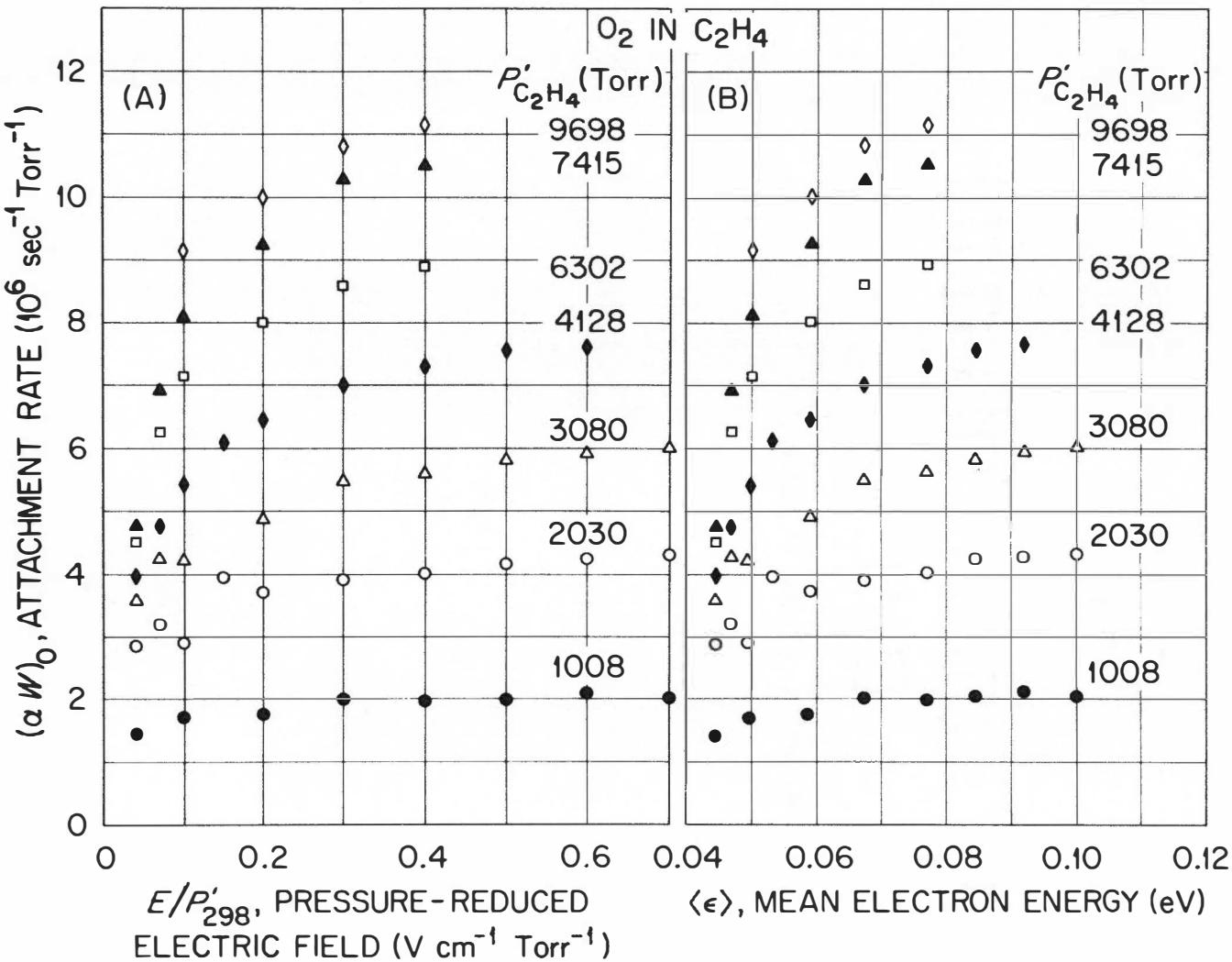

Figure III-4. (a) $(\alpha w)_o$ as a Function of E/P_{298} and (b) as a Function of $\langle \epsilon \rangle$ for O_2 in C_2H_4 Environments.

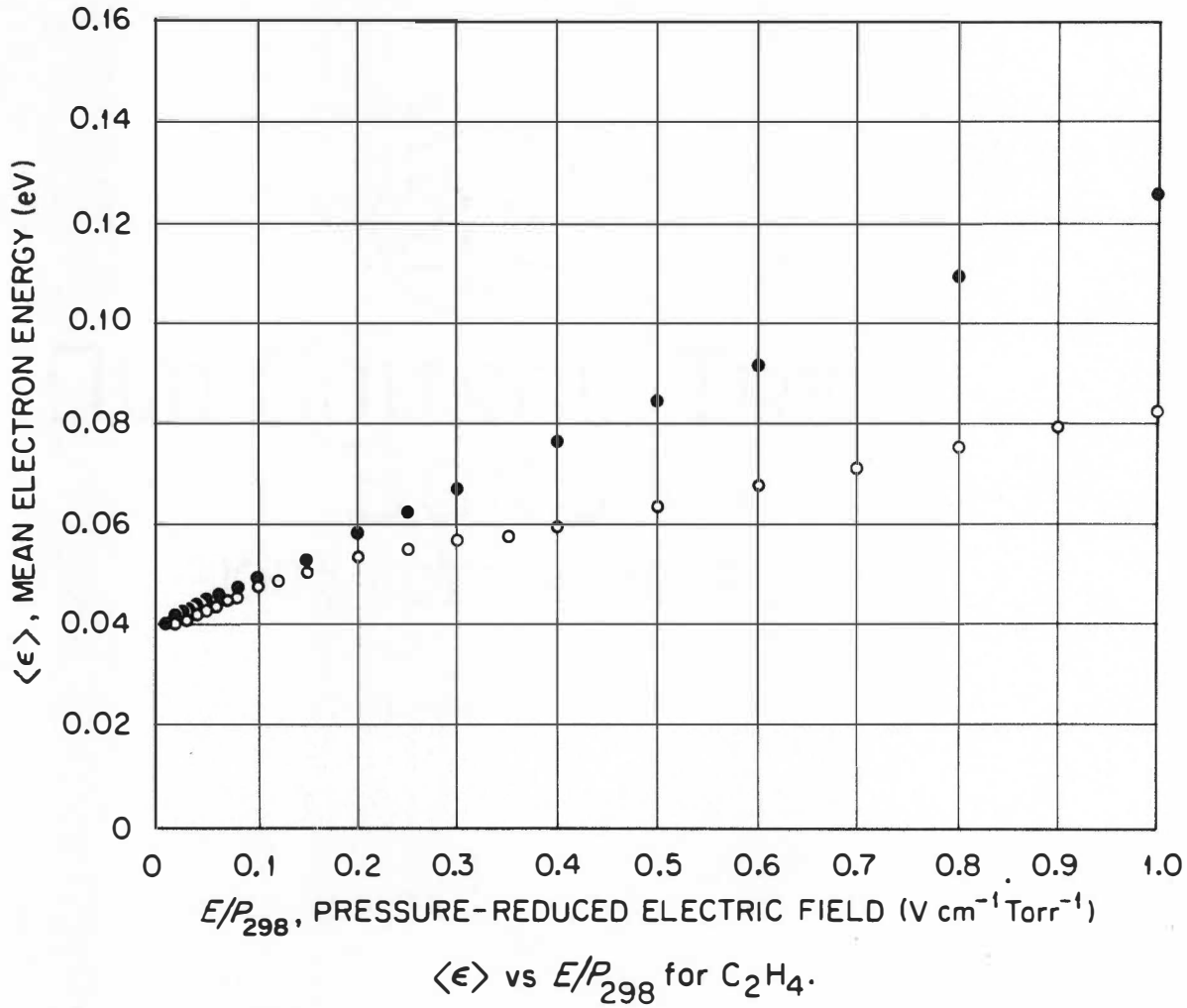

Figure III-5. w as a Function of E/P_{298} for C_2H_4.

(•) 3/2 D_L/μ Data of Walker. (○) 3/2 D_1/μ Data of Wagner et al.

the determination of $(\alpha w)_o$. Huber reported that w decreased slightly ($\sim 7\%$) over the pressure range from 455 to 6072 Torr. These decreases are just slightly above his experimental error ($\sim 5\%$) but they are real and have been confirmed by measurements at the Oak Ridge National Laboratory [Gant, Christophorou, and Pittman (1973)]. Huber's data were used over the range $455 \leq P'_{298} \leq 6072$ Torr and values obtained from a linear extrapolation were used for $P'_{298} \geq 6072$ Torr.

III. ELECTRON ATTACHMENT TO O_2 IN HIGH DENSITIES OF C_2H_6

Electron attachment to O_2 in a dense ethane environment has been investigated for ethane pressures in the range $750 \leq P'_{298} \leq 17,500$ Torr. In Figure III-2, page 29, the thermal attachment rate is presented as a function of ethane pressure. The rates in ethane are seen to be quite different, especially at high pressures, from those obtained for O_2-N_2 and for O_2-C_2H_4 mixtures. Figure III-6A presents $(\alpha w)_o$ as a function of E/P'_{298}, and Figure III-6B shows $(\alpha w)_o$ as a function of $\langle \epsilon \rangle$ for a number of ethane pressures. The energy scale was calibrated using the D_L/μ data of Walker (1965, 1973). The drift velocities used in the calculation of $(\alpha w)_o$ were those determined by Huber (1969). As for ethylene, $\sigma_a(\epsilon)$ could not be determined because $f(\epsilon, E/P)$ is unknown.

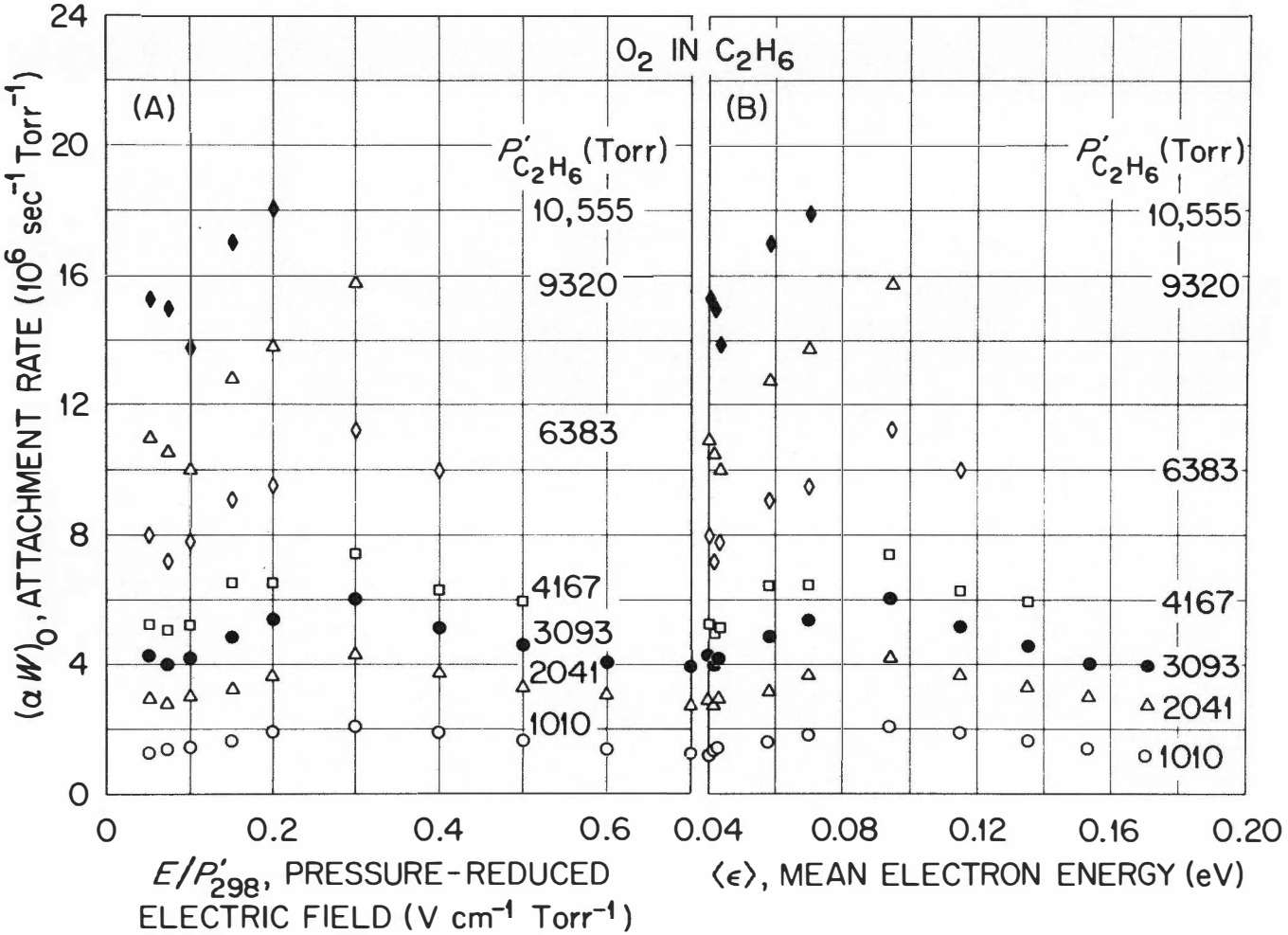

Figure III-6. Attachment Rate $(\alpha w)_o$ for O_2 in C_2H_6 as a Function of (a) E/P_{298} and (b) $\langle\epsilon\rangle$.

IV. REACTION SCHEMES FOR ELECTRON ATTACHMENT TO O_2 IN HIGH DENSITIES OF N_2, C_2H_4 and C_2H_6

From the previous discussion, it is evident that electron attachment to O_2 depends strongly on the nature and density of the gaseous environment. Kinetic mechanisms which are consistent with the experimental data will be outlined below.

1. O_2-N_2 Mixtures

The pressure dependence of the attachment rate has been explained by Christophorou (1972) in terms of a model whereby N_2 is assumed (i) to act as a stabilizing third body in distant collisions and (ii) to be involved in close collisions which seriously perturb the O_2^- potential energy curve. We can postulate two reaction mechanisms to account for these observations:

(i)
$$e + O_2 \xrightarrow{k_1} O_2^{-*} \qquad \text{(III-1)}$$

$$O_2^{-*} \xrightarrow{k_2} O_2 + e$$

$$O_2^{-*} + N_2 \xrightarrow{k_3} O_2^- + N_2 + \text{energy}$$

$$\xrightarrow{k_4} O_2 + N_2 + e$$

(ii) $$e + O_2 + N_2 \xrightarrow{k_5} [O_2^{-*} - N_2] \qquad \text{(III-2)}$$

$$[O_2^{-*} - N_2] \xrightarrow{k_6} O_2 + N_2 + e$$

$$N_2 + [O_2^{-*} - N_2] \xrightarrow{k_7} O_2^- + 2N_2 + \text{energy}$$

$$\xrightarrow{k_8} O_2 + 2N_2 + e \quad .$$

Mechanism (i) is identical to a three-body reaction whereby N_2 acts to stabilize O_2^{-*}. Mechanism (ii) postulates the formation of a transient complex $[O_2^{-*} - N_2]$ which can either autoionize or form O_2^{-*} upon collision with a second N_2 molecule. Using the above reaction scheme we have

$$(\alpha w)_o = k_1 \left\{ \frac{k_3 n_{N_2}}{k_2 + (k_3 + k_4) n_{N_2}} \right\} + \frac{k_5 n_{N_2} \{k_7 n_{N_2}\}}{k_6 + (k_7 + k_8) n_{N_2}} \qquad \text{(III-3)}$$

where k_i ($i = 1, \ldots 8$) are the rate constants for the processes considered and $n_{N_2} \propto P_{N_2}$ is the number density of N_2 molecules. In Equation (III-3), k_1 is the absolute rate of electron attachment to O_2 to form O_2^{-*} and $k_3 n_{N_2} / \{k_2 + (k_3 + k_4) n_{N_2}\}$ is the probability that the electron remains attached to the O_2 molecule. In the second term in Equation (III-3), $k_5 n_{N_2}$ is the rate for the formation of the complex and $k_7 n_{N_2} / \{k_6 + (k_7 + k_8) n_{N_2}\}$ is the probability that the electron remains on the O_2 molecule. Consideration of these processes together therefore gives Equation (III-3). Under

the assumption that $k_2 >> (k_3 + K_4)n_{N_2}$ and $k_6 >> (k_7 + k_8)n_{N_2}$ we have

$$(\alpha w)_o = A\ P_{N_2} + B\ P_{N_2}^{\ 2} \qquad \text{(III-4)}$$

or

$$\frac{(\alpha w)_o}{P_{N_2}} = A + B\ P_{N_2} \qquad \text{(III-5)}$$

where $A = k_1 k_3 / k_2$ and $B = k_5 k_7 / k_6$.

A plot of $(\alpha w)_o / P_{N_2}$ vs. P_{N_2} indicates good agreement with the predictions as exemplified by Equation (III-5). Such a plot is shown in Figure III-7 for the pressure range $300 \leq P_{N_2} \leq 25,000$ Torr. In this pressure range, the experimental data support the predictions of the proposed model. From a least squares fit to the data in Figure III-7 we obtained

$$A = 88.3\ \text{sec}^{-1}\ \text{Torr}^{-2} \qquad \text{(III-6)}$$

$$B = 0.025\ \text{sec}^{-1}\ \text{Torr}^{-3}$$

2. O_2-C_2H_4 Mixtures

Electron attachment to O_2 in ethylene environments has been analyzed on the basis of the following reaction scheme

$$e + O_2 \xrightarrow{k_1'} O_2^{-*} \qquad \text{(III-7)}$$

$$O_2^{-*} \xrightarrow{k_2'} O_2 + e$$

$$O_2^{-*} + C_2H_4 \xrightarrow{k_3'} O_2^{-} + C_2H_4 + \text{energy} \quad .$$

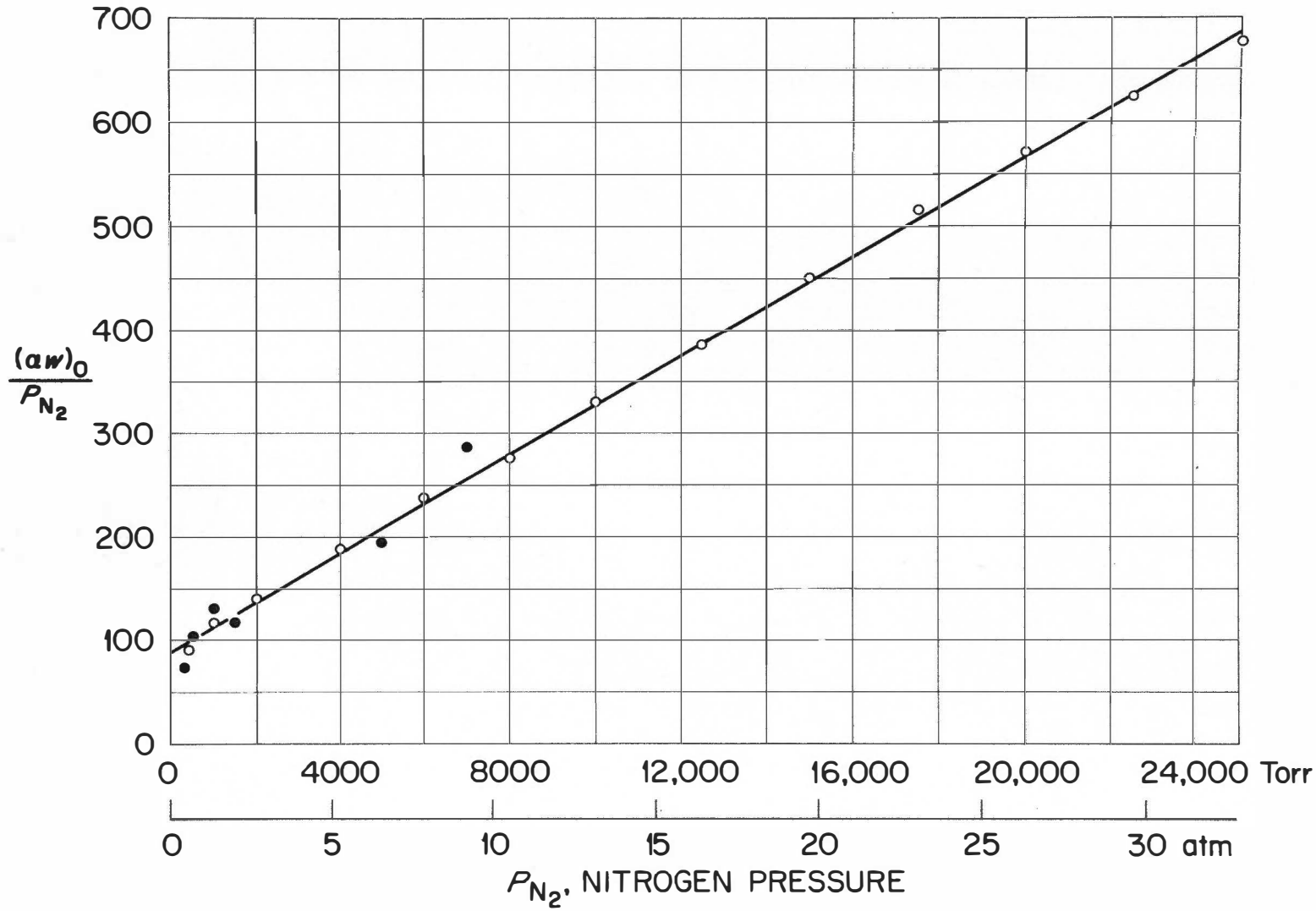

Figure III-7. $(\alpha w)_o/P_{N_2}$ for $\langle \epsilon \rangle$ = 0.05 eV.

Under the assumption that the probability of stabilization per collision is unity, we have

$$(\alpha w)_o = \frac{k_1' k_3' n_{C_2H_4}}{k_2' + k_3' n_{C_2H_4}} = \frac{k_1' k_3' P'_{C_2H_4}}{k_2' + k_3' P'_{C_2H_4}} \qquad \text{(III-8)}$$

where n_{N_2} is the ethylene number density, proportional to $P'_{C_2H_4}$. It is convenient to rewrite Equation (III-8) as

$$\frac{1}{(\alpha w)_o} = \frac{1}{k_1'} + \frac{k_2'}{k_1' k_3'} \frac{1}{P'_{C_2H_4}} \quad . \qquad \text{(III-9)}$$

The experimental data on $(\alpha w)_o$ vs. $P'_{C_2H_4}$ are plotted in the manner suggested by Equation (III-9) in Figure III-8 for $E/P'_{298} = 0.1$ Vcm^{-1} Torr^{-1}. The results are seen to be consistent with Equation (III-9). From a least squares fit to six such plots in the E/P'_{298} range from 0.1 to 0.5 Vcm^{-1} Torr^{-1} (corresponding to $0.048 \leq \langle \epsilon \rangle \leq 0.064$ eV) we obtained

$$1/k_1' = 0.43 \times 10^{-7} \text{ sec Torr}$$

$$k_2'/k_1' k_3' = 0.46 \times 10^{-3} \text{ sec Torr}^2$$

whereby $k_1' = 2.33 \times 10^7$ sec^{-1} Torr^{-1} and $k_2'/k_3' = 1.07 \times 10^4$ Torr .

3. O_2-C_2H_6 Mixtures

The reaction scheme discussed in the previous section for O_2-C_2H_4 mixtures can be assumed to be operative for the O_2-C_2H_6 mixtures

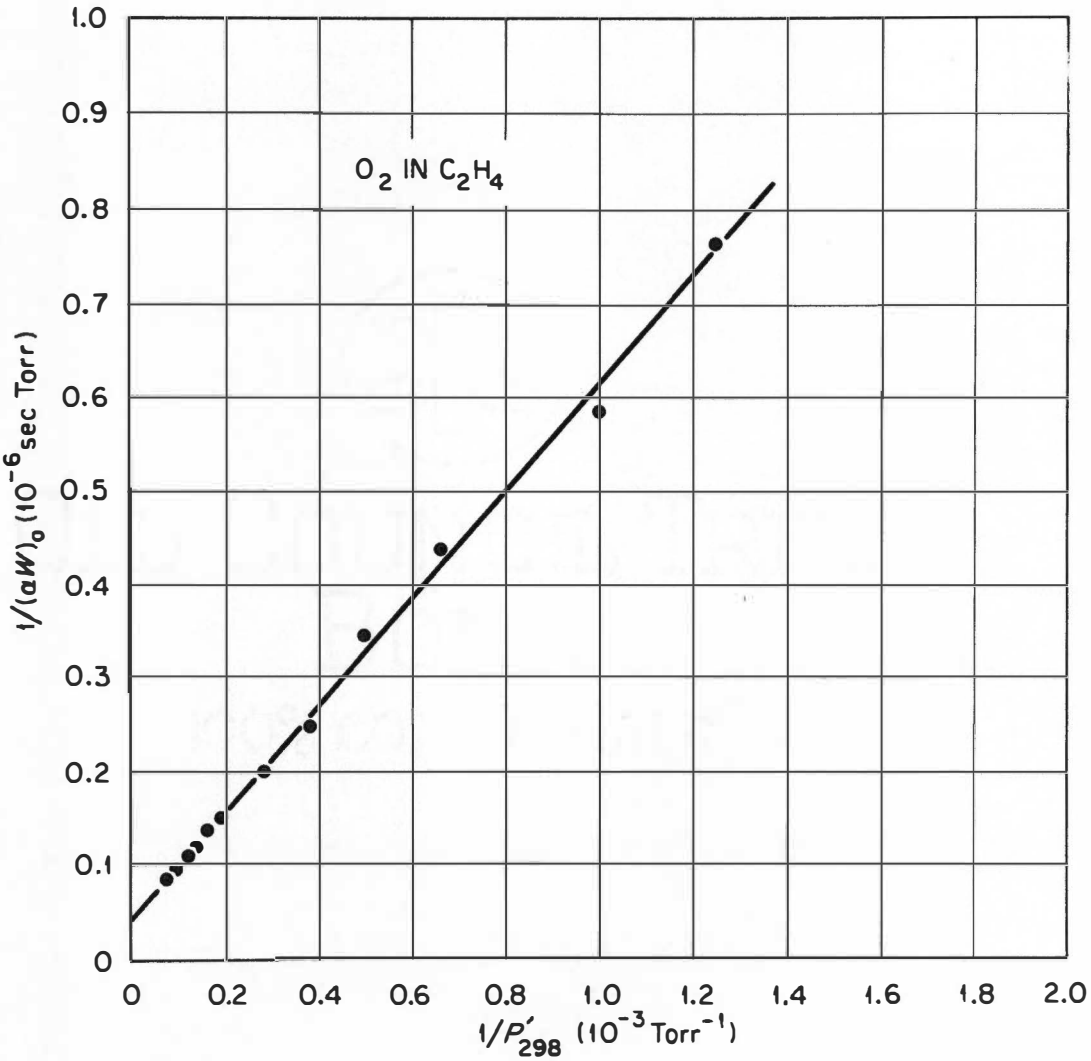

Figure III-8. $1/(\alpha w)_o$ as a Function of $1/P_{298}$ for O_2 in C_2H_4. The Data are for $E/P_{298} = 0.1$ V cm^{-1} $Torr^{-1}$.

also. Hence

$$e + O_2 \xrightarrow{k_1''} O_2^{-*} \qquad \text{(III-10)}$$

$$O_2^{-*} \xrightarrow{k_2''} O_2 + e$$

$$O_2^{-*} + C_2H_6 \xrightarrow{k_3''} O_2^{-} + C_2H_6 + \text{energy}$$

whereby we have

$$\frac{1}{(\alpha w)_o} = \frac{1}{k_1''} + \frac{k_2''}{k_1'' k_3''} \frac{1}{P'_{C_2H_6}} \quad . \qquad \text{(III-11)}$$

Figure III-9 shows a plot of $1/(\alpha w)_o$ vs. $1/P'_{C_2H_4}$ for $E/P'_{298} = 0.1$ Vcm^{-1} Torr^{-1}. The experimental results are consistent with Equation (III-11) for $P'_{C_2H_6} \leq 5000$ Torr, but for $P'_{C_2H_6} \geq 5000$ Torr the rates are seen to increase faster then predicted by Equation (III-11). The data in Figure III-9 have been fitted by a least squares analysis yielding

$$1/k_1'' = 3.2 \times 10^{-8} \text{ sec Torr}$$

$$k_2''/k_1'' k_3'' = 6.4 \times 10^{-4} \text{ sec Torr} \quad .$$

Using these values, we calculated the rates $(\alpha w)_o$ that would be predicted from the mechanism shown in Equation (III-10) and subtracted these rates from the measured ones to yield a residual rate $(\alpha w)_{ox}$. The residual rates are plotted as a function of $P'_{C_2H_6}$ in Figure III-10. From a least squares analysis of the residual rates in Figure III-10 we obtained a slope of 4.7.

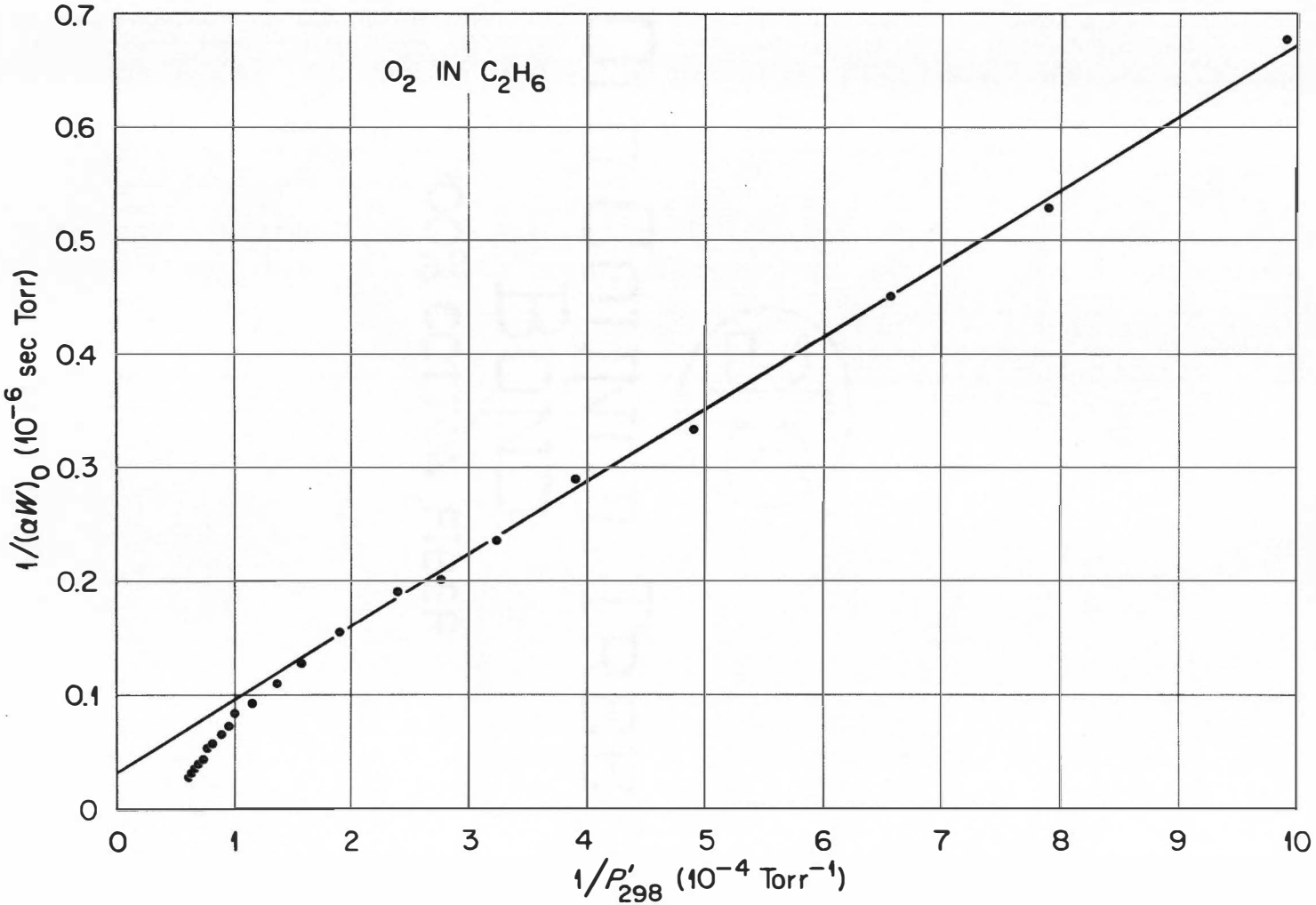

Figure III-9. $1/(\alpha w)_o$ as a Function of $1/P_{298}$ for O_2 in C_2H_6.

The Data are for E/P_{298} = 0.1 V cm^{-1} Torr^{-1}.

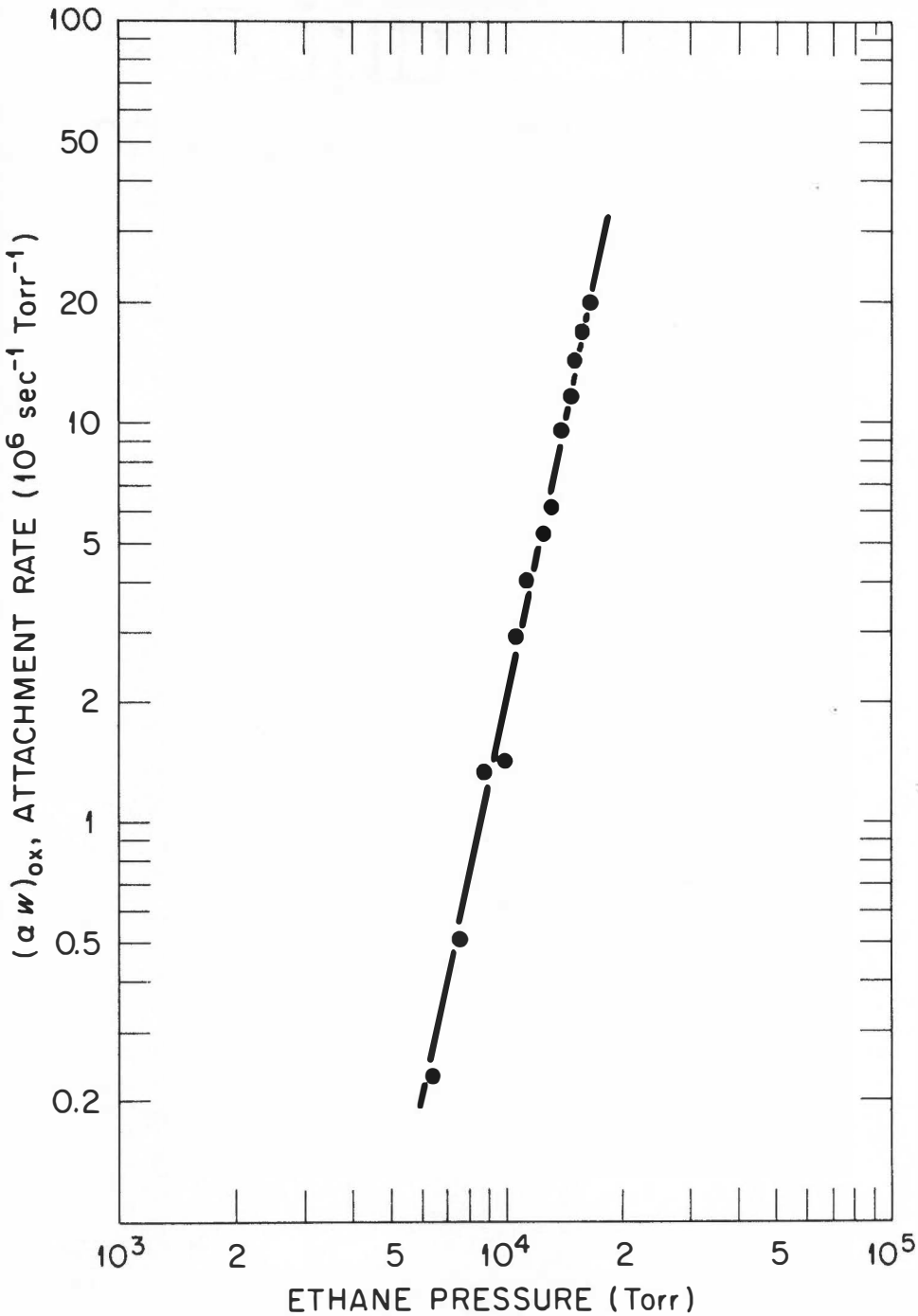

Figure III-10. The Residual Attachment Rates, $(\alpha w)_{ox}$, vs. $P_{C_2H_6}$.

It is evident that electron attachment to O_2 in ethane cannot be explained entirely by the reaction scheme in Equation (III-10) but must require one which depends more strongly on $P'_{C_2H_6}$. One possible explanation of the rate dependence could be due to electron clustering, i. e.

$$e + (C_2H_6)_x + O_2 \rightarrow O_2^- + x\, C_2H_6 \qquad \text{(III-12)}$$

which, on the basis of the slope of Figure III-10, must involve four to five C_2H_6 molecules.

V. AUTOIONIZATION LIFETIME OF O_2^{-*}

The analysis in section IV-2 provides an excellent method for determining the absolute rate of electron attachment, k_1, and the critical pressure, $P_c = k_2/k_3$, at which the rate for autoionization is equal to the rate for stabilization. The latter quantity is useful in determining the lifetime $\tau(O_2^{-*})$ of the negative ion and can be found from the inverse plots even if the critical pressure were not reached in the experiment. If we have the general stabilization reaction with the negative ion X^{-*} and the stabilizing body S, then

$$X^{-*} + S \rightarrow X^- + S + \text{energy} \quad . \qquad \text{(III-13)}$$

If we assume that the probability of stabilization of X^{-*} per collision is unity, we can estimate the rate of stabilization at the critical pressure P_c of the stabilizing body S. The frequency of collisions ν_c between X^{-*} and S is

$$\nu_c = v \, \sigma_L^c \, n_c \qquad \text{(III-14)}$$

where v is the relative velocity of X^{-*} and S, n_c is the number density of S at the critical pressure, and σ_L^c is the classical Langevin cross section for spiraling collisions between X^{-*} and S given by

$$\sigma_L^c = \frac{2\pi}{v} \frac{(e^2\alpha)}{M_r}^{1/2} \qquad \text{(III-15)}$$

In Equation (III-15), α is the static polarizability of S, e is the electronic charge, and M_r is the reduced mass of X^- and S. From Equations (III-14) and (III-15) we have for the average lifetime between collisions

$$\tau_c = \nu_c^{-1} = \frac{1}{2\pi n_c} \frac{(M_r)}{e^2\alpha}^{1/2} \qquad \text{(III-16)}$$

From Equation (III-16) we can approximate the lifetime of X^{-*}, $\tau(X^{-*})$, by $\tau(X^{-*}) \approx \tau_c$. If the quantum mechanical expression for spiraling collisions, $\sigma_L^q = 4\pi/v \ (e^2\alpha)^{1/2}/M_r$ [Vogt and Wannier (1954)], is used, then the lifetime is one half that calculated on the basis of Equation (III-16).

For the O_2^{-*}-C_2H_4 system we calculated a lifetime $\tau_c(O_2^{-*})$ of 1.9×10^{-12} sec using $\alpha_{C_2H_4} = 42.6 \times 10^{-25}$ cm^3, taken from the work of Landolt and Bornstein (1951), and $P_c = 10{,}700$ Torr. Therefore, $\tau(O_2^{-*}) = k_2'^{-1} = 1.9 \times 10^{-12}$ sec. This value is in agreement with an earlier estimate by Christophorou (1972) and with a value deduced recently by Linder and Schmidt (1971) using electron scattering methods.

VI. EXTRAPOLATION TO THE LIQUID STATE

1. O_2-N_2 Mixtures

At 25,000 Torr the N_2 density is 0.04 gm/cm^3 which is a factor of ~ 20 lower than the density of liquid nitrogen. If it is assumed that the model proposed in section IV is valid over the entire density range up to the liquid regime we find that

$$(\alpha w)_o \; (\epsilon \approx 0.04 \text{ eV}) = 0.74 \times 10^{10} \text{ sec}^{-1} \text{ Torr}^{-1}$$

for O_2 in liquid N_2. This value compares favorably with $(\alpha w)_o = \sigma_a v = 1.1 \times 10^{10}$ sec^{-1} Torr^{-1} obtained from using $\sigma_a = \pi \lambda\!\!\!^{-2}$, where $\lambda = 2\pi\lambda\!\!\!^{-}$ is the de Broglie wavelength for a 0.04 eV electron. This observation may indicate that the proposed model holds reasonably well over the entire range of N_2 densities up to that of the liquid.

2. O_2-C_2H_4 Mixtures

The analysis in Figure III-8, page 41 , is an excellent way to predict liquid density behavior from attachment studies in the high pressure gas phase. The lowest data point in Figure III-8 is very close to the y axis and the intercept of the straight line can thereby be determined quite precisely, giving $(\alpha w)_o$ for $P_{C_2H_4} \to \infty$. From an extrapolation of the gas data one obtains $[(\alpha w)_o]_{\text{intercept}} = 2.3 \times 10^7$ sec^{-1} Torr^{-1} $= 4.3 \times 10^{11}$ sec^{-1} M^{-1}. At the density of liquid ethylene Equation (III-9) predicts that $[(\alpha w)_o]_{\text{liquid}} = 3.3 \times 10^{11}$ sec^{-1} M^{-1}.

There appear to be no data on the attachment of electrons to O_2 in liquid ethylene but Bakale and Schmidt (1973) have reported a rate of 5×10^{11} sec^{-1} M^{-1} for O_2 in neopentane and a rate of 5.2×10^{11} sec^{-1} M^{-1} for O_2 in neohexane, both at 296°K. Richards and Thomas (1971) have reported a rate of 1.5×10^{11} sec^{-1} M^{-1} for O_2 in n-hexane at 193°K. These values are in reasonable agreement with the one we predicted for O_2 in liquid C_2H_4. This agreement may indicate that the process of thermal electron capture by O_2 in C_2H_4 is well understood over the entire density range. The ethylene molecule simply acts as a stabilizing third body over the density range from the low pressure gas to the liquid regime.

3. O_2-C_2H_6 Mixtures

The simplicity of the ethylene behavior is not evident for the case of ethane and it was not possible to formulate a model to describe the behavior of $(\alpha w)_o$ in high densities of C_2H_6. Because of this, it was not possible to predict $(\alpha w)_o$ for O_2 in liquid ethane.

VII. THREE-BODY RATE COEFFICIENTS

The three-body coefficients for the reactions

$$e + O_2 + N_2 \rightarrow O_2^- + N_2 + \text{energy} \qquad \text{(III-17)}$$

$$e + O_2 + C_2H_4 \rightarrow O_2^- + C_2H_4 + \text{energy} \qquad \text{(III-18)}$$

$$e + O_2 + C_2H_6 \rightarrow O_2^- + C_2H_6 + \text{energy} \qquad \text{(III-19)}$$

have been determined from the linear portions of the $(\alpha w)_o$ vs. P'_x ($x = N_2$, C_2H_4, and C_2H_6) graphs for a number of mean energies $\langle\epsilon\rangle$. These coefficients as well as the ones determined earlier by McCorkle et al. (1972) for the reaction

$$e + O_2 + O_2 \rightarrow O_2^- + O_2 + \text{energy} \qquad \text{(III-20)}$$

are plotted in Figure III-11 as a function of $\langle\epsilon\rangle$. The energy scale for reactions (III-17) and (III-20) was established by determining $\langle\epsilon\rangle$ from the known distribution functions for N_2 [see Christophorou (1971a)]. The energy calibration for (III-18) and (III-19) has been discussed earlier in sections II and III. In Figure HI-11 the solid curves are the early results of Chanin et al. (1962). McCorkle et al. (1972) argued that the energy scale used by Chanin et al. was in error and replotted (broken curve in Figure III-11) this data using mean energies obtained from the known electron distribution functions in N_2. The replotted data are seen to be in good agreement with the results of McCorkle et al. and on the basis of this agreement it was suggested that a similar correction might be necessary in the case of Equation (III-20). However, no correction was made because the distribution functions for pure O_2 are not known.

From the analysis of the three-body coefficients one can conclude that C_2H_4 and C_2H_6 have comparable efficiencies in stabilizing O_2^{-*}. No other information on the three-body coefficients for reactions (III-18) and (III-19) exist as a function of $\langle\epsilon\rangle$. Thermal ($\sim$ 300°K) values equal to

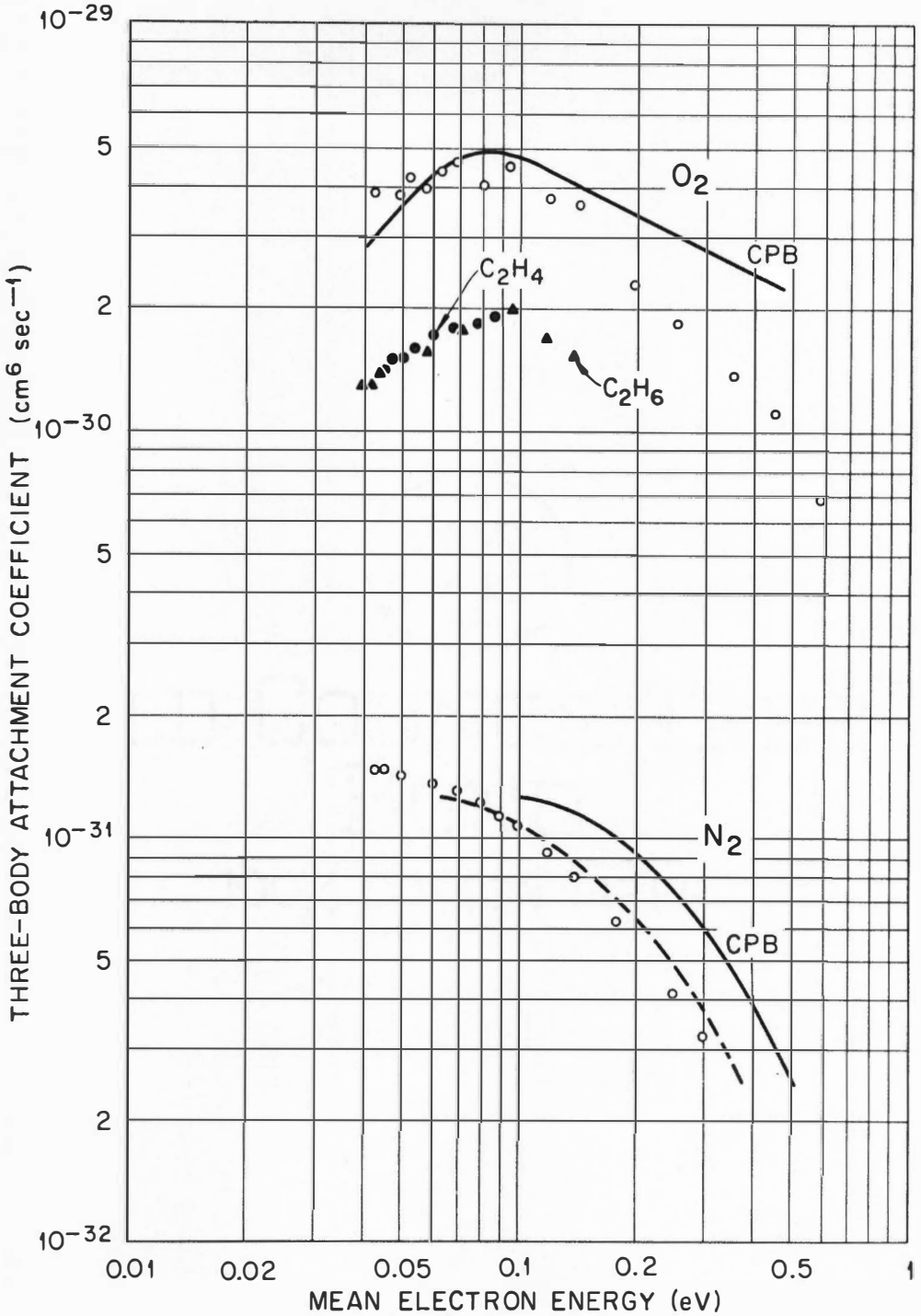

Figure III-11. Three-body Attachment Coefficients as a Function of $\langle \epsilon \rangle$ for $e + O_2 + O_2 \rightarrow O_2^- + O_2 + \text{energy}$; $e + O_2 + N_2 \rightarrow O_2^- + N_2 + \text{energy}$; $e + O_2 + C_2H_4 \rightarrow O_2^- + C_2H_4 + \text{energy}$; $e + O_2 + C_2H_6 \rightarrow O_2^- + C_2H_6 + \text{energy}$.

See Text for Explanation of Symbols.

3.1×10^{-30} cm^6 sec^{-1} [Stockdale et al. (1967)], 1.7×10^{-30} cm^6 sec^{-1} [Bouby et al. (1967)], and 2.5×10^{-30} cm^6 sec^{-1} [Bouby et al. (1970)] have been reported but these values probably correspond to $\langle \epsilon \rangle \gtrsim 0.05$ eV. From the present data in Figure III-11 it is seen that the three-body coefficient has a value of 1.54×10^{-30} cm^6 sec^{-1} at $\langle \epsilon \rangle = 0.05$ eV.

CHAPTER IV

ATTACHMENT OF SLOW ELECTRONS TO C_6H_6 IN HIGH PRESSURE GASES

I. INTRODUCTION

An extensive series of experiments have been performed using the high pressure swarm apparatus to determine whether benzene (C_6H_6) attaches slow electrons (≤ 0.3 eV) in the gas phase at moderate carrier-gas densities ($2000 \leq P \leq 10,000$ Torr). Previously, Compton et al. (1966) discovered a compound negative ion resonance state (CNIR) in C_6H_6 using slow electrons with $\epsilon \sim 1.4$ eV. Christophorou and Blaunstein (1969) also examined electron attachment to C_6H_6 at 400 Torr in a swarm experiment and placed an upper limit of $\sim 1 \times 10^3$ sec^{-1} $Torr^{-1}$ to the attachment rate at 400 Torr. The benzene negative ion has been observed to exist in the liquid state by several investigators [Tuttle and Weissman (1966), Hoijtink and Zandstra (1960), Gardner (1966), and Giling and Kloosterboer (1973)]. In view of these findings, it seemed desirable to examine the possibility that C_6H_6 attaches slow electrons in the gas phase at moderate densities.

II. EXPERIMENTAL DIFFICULTIES

Benzene has been found to attach slow (≤ 0.3 eV) electrons in dense N_2 environments over the range $2000 \leq P_{N_2} \leq 10,000$ Torr. In order to confirm these results and to clear up certain experimental difficulties,

additional experiments using Ar, C_2H_4, and a mixture of N_2 and C_2H_4 as carrier gases were also performed. These experiments will be described later in this chapter. Benzene is very difficult to study because of its low attachment rate ($\sim 10^3$ sec^{-1} Torr^{-1}) and because of the possibility that this rate might arise from impurities contained in the sample. The measurement of such low rates, however, is well within the capability of the experimental system (see Chapter II). Because of this reason and because of the fact that no other investigators have observed $C_6H_6^-$ in the gas phase, we felt that it would be prudent to examine the possibility that contaminants could contribute significantly to the attachment rate.

Oxygen is always a suspect as a contaminant because the liquid benzene initially contains dissolved O_2. Before beginning measurements on C_6H_6, O_2 is removed from the sample by freezing the solution to $\sim$ -70°C in a dry-ice-acetone bath and pumping until there is a vacuum of 1×10^{-6} Torr above the liquid. C_6H_6 is then frozen at liquid N_2 temperatures until a vacuum of $\sim 5 \times 10^{-7}$ Torr is attained. Measurements on samples prepared in this way agree within $\pm$ 20% from sample to sample. In view of these precautions it seems unlikely that O_2 contributes significantly to the attachment rate. This contention is supported by the observation that the rates for attachment to C_6H_6 are much different from those measured previously for attachment to O_2 (see Chapter III).

It also seemed desirable to examine the possibility that electron attaching contaminants could be introduced from the walls of the chamber and from the tubing leading from the sample container to the chamber. These hypotheses were tested by leaving the benzene in the tubing and the chamber for three to five hours before initiating the experiment. Rates measured following this procedure were entirely consistent with those obtained in the usual manner. It seems very unlikely that contaminants could be introduced from the walls since the system is pumped out to $\sim 1 \times 10^{-8}$ Torr at the conclusion of each experiment and the outgas rate is < 0.2 μ/hr.

The benzene samples used were obtained from James Hinton and Company and were of a quoted purity of 99.999%. Additional experiments were performed to test whether the 0.001% impurity contributed measurably to the rate. The sample was heated to various temperatures in the range from 25°C to 70°C under the hypothesis that the impurity would have a different partial pressure at each temperature and would presumably cause a temperature dependence to the attachment rate. The results of these experiments were entirely consistent with the results at room temperature. In order for a 0.001% impurity to cause a measured rate of $\sim 1 \times 10^{3}$ sec^{-1} $Torr^{-1}$ it must have an attachment rate of $\sim 1 \times 10^{8}$ sec^{-1} $Torr^{-1}$ at 2000 Torr. In view of the pressure dependence of the attachment rate (see Figure IV-1) the process would have to be a nondissociative one. It seems unlikely that a nondissociative process could have such a high rate

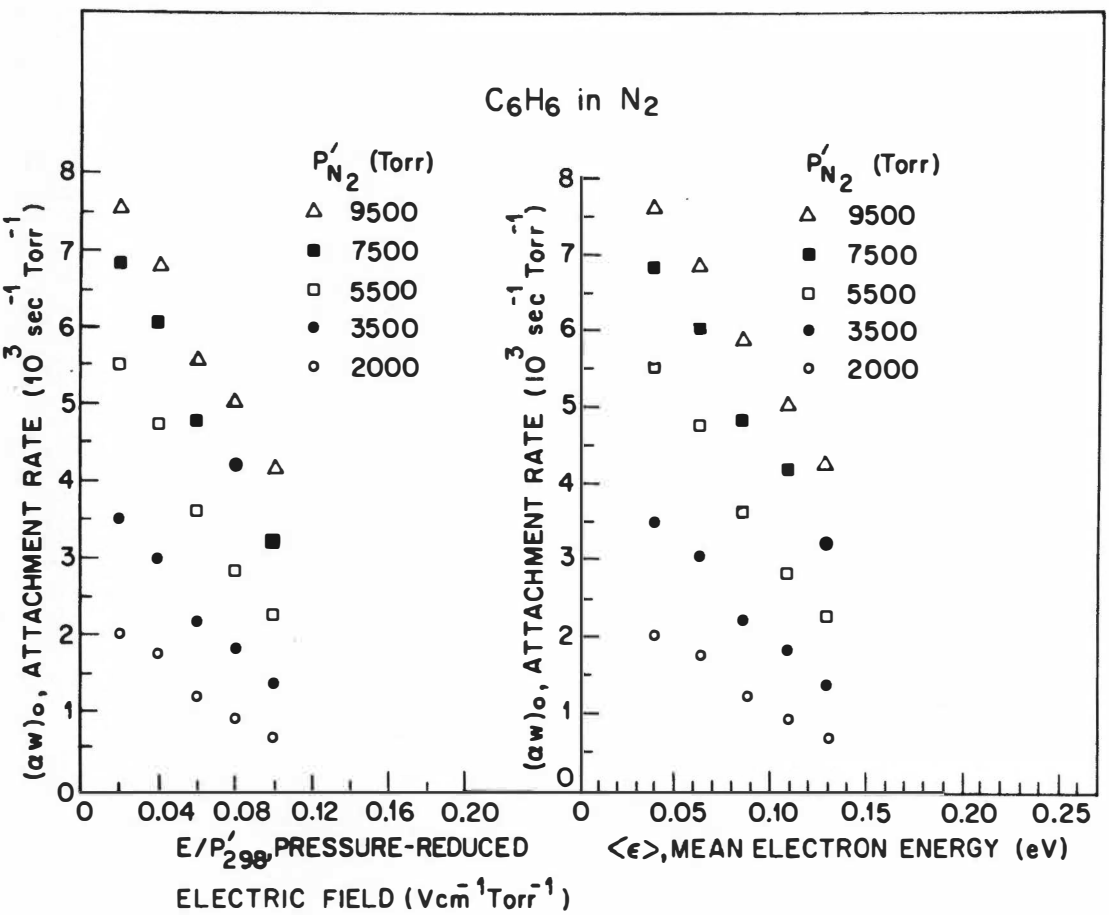

Figure IV-1. Attachment Rate $(\alpha w)_o$ for C_6H_6 in N_2 as a Function of (a) E/P_{298} and (b) $\langle \epsilon \rangle$, at the Indicated N_2 Pressures.

($\sim 1 \times 10^{8}$ sec^{-1} Torr^{-1}) and such a short lifetime ($\sim 10^{-13}$ sec) as estimated in section IV. In view of these findings we concluded that benzene is indeed the attaching species.

III. EXPERIMENTAL RESULTS

1. C_6H_6 in N_2

A. Absolute Rate of Electron Attachment to C_6H_6 in High Densities of N_2

The attachment of slow electrons (≤ 0.3 eV) to C_6H_6 has been observed in C_6H_6-N_2 mixtures for $5 \leq P_{C_6H_6} \leq 10$ Torr and $P_{N_2} > 2000$ Torr. Figure IV-1 presents the attachment rate $(\alpha w)_o$ for $P_{C_6H_6} \to 0$, as a function of the pressure-reduced electric field, E/P_{298}, and the mean electron energy $\langle \epsilon \rangle$. The rates were found to be independent of $P_{C_6H_6}$ within experimental error. The rates in Figure IV-1 are seen to increase with increasing P_{N_2} and to reach their maximum at a given P_{N_2} at thermal ($\simeq 0.04$ eV) energies. Figure IV-2 shows $(\alpha w)_o$ as a function of P_{N_2}. The rates are seen to increase linearly with P_{N_2} for $P_{N_2} < 6000$ Torr and to increase at a less than linear rate for $P_{N_2} > 6000$ Torr. Furthermore, the higher the $\langle \epsilon \rangle$, the higher the N_2 range over which $(\alpha w)_o$ increases linearly with P_{N_2}. This is a result of the fact that the lifetime, $\tau(C_6H_6^{-*})$, of $C_6H_6^{-*}$ decreases with $\langle \epsilon \rangle$. The calculation of $\tau(C_6H_6^{-*})$ will be discussed in section IV.

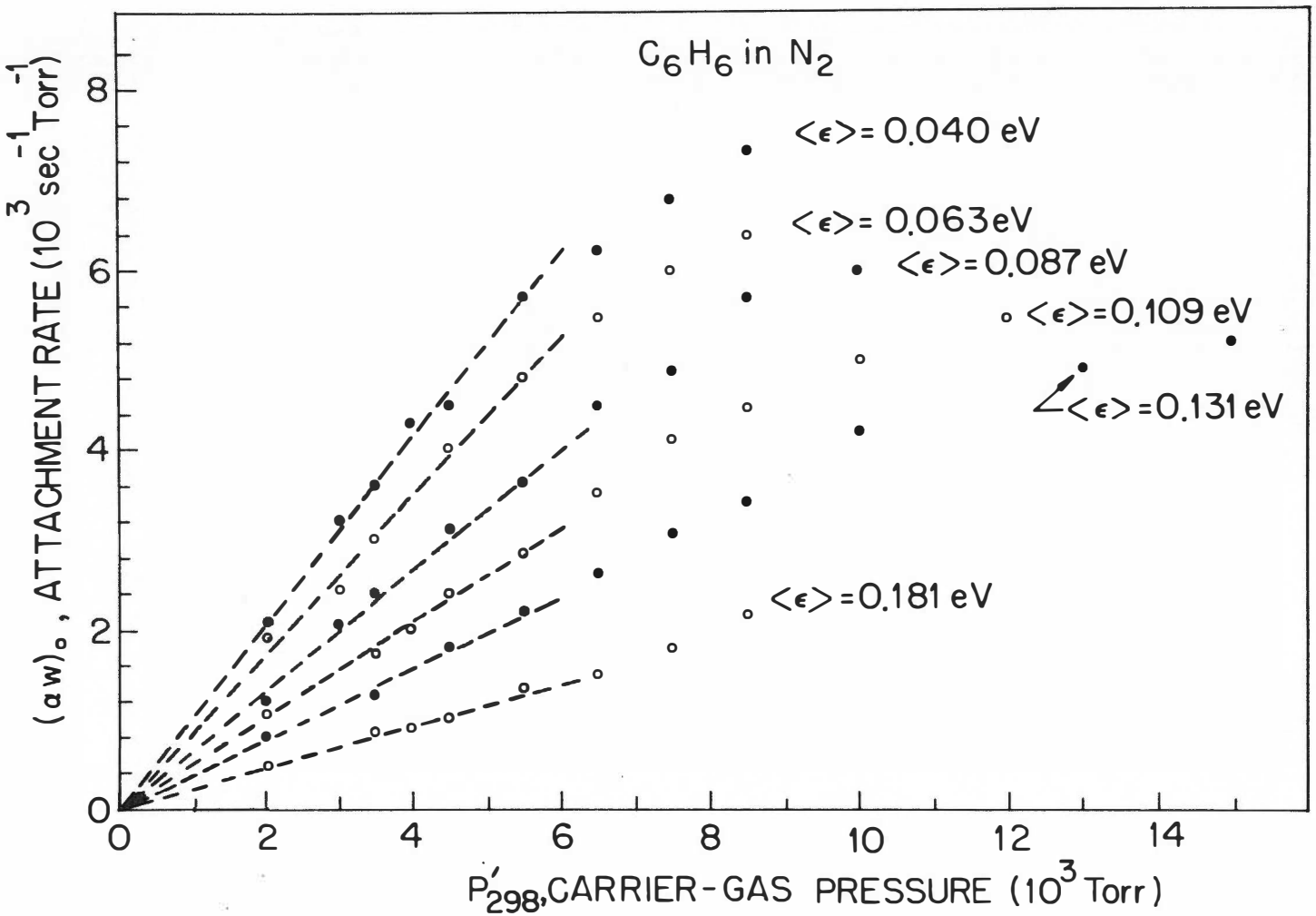

Figure IV-2. Attachment Rate $(\alpha w)_o$ for C_6H_6 as a Function of P_{N_2} for the Indicated $\langle \epsilon \rangle$.

The Broken Lines are a Linear Least-Squares Fit to the Data for $P_{298} \leq$ 6000 Torr.

B. Electron Attachment Cross Sections

Absolute cross sections, $\sigma_a(\epsilon)$, for the attachment of electrons to C_6H_6 to form $C_6H_6^{-*}$ have been calculated using the swarm unfolding technique discussed in Chapter II. The results are presented in Figure IV-3 for P_{N_2} = 2000 Torr and for P_{N_2} = 9500 Torr. Results similar to these were obtained at intermediate pressures. The peak energy ($\sim$ 0.04 eV) is relatively pressure independent. The full width at half maximum varies from 0.026 eV at 2000 Torr to 0.042 eV at 9500 Torr with some indication that it increases with increasing P_{N_2}.

C. Three-Body Rate Coefficients

The three-body rate coefficients for the reaction

$$e + C_6H_6 + N_2 \rightarrow C_6H_6^{-} + N_2 + \text{energy} \qquad \text{(IV-1)}$$

have been determined from the linear portion of the $(\alpha w)_o$ vs. P_{N_2} curves in Figure IV-2 (dotted lines). These values are energy dependent and are presented in Figure IV-4.

2. C_6H_6 in C_2H_4, in Ar, and in C_2H_4-N_2 Mixtures

In order to verify the attachment results for C_6H_6-N_2 mixtures, electron attachment studies were undertaken with C_6H_6 in C_2H_4 for $P'_{C_2H_4} \leq 13{,}000$ Torr. However, it was impossible to detect any attachment in such mixtures. In view of the results presented for C_6H_6 in high densities of N_2, this was entirely unexpected. Additional experiments on

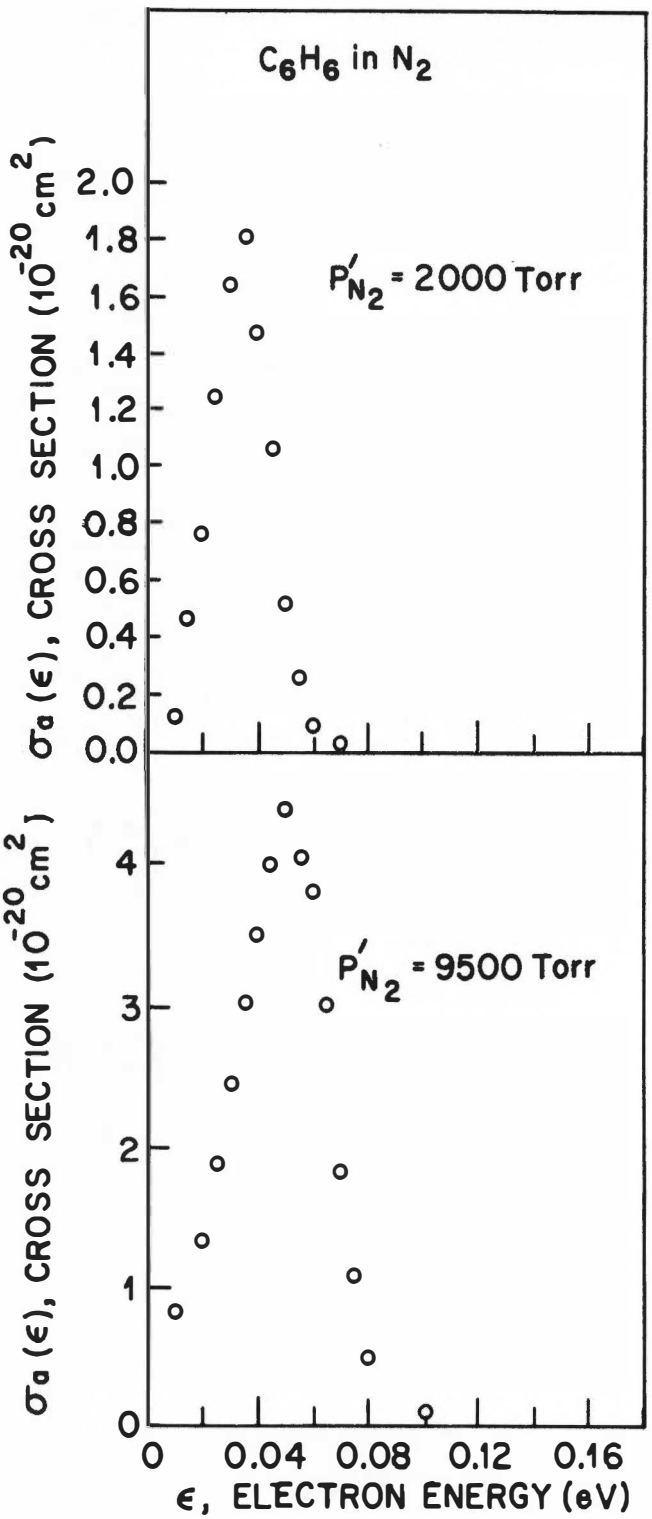

Figure IV-3. $\sigma_a(\epsilon)$ as a Function of $\langle\epsilon\rangle$ for C_6H_6 in N_2 for P_{N_2} = 2000 Torr and P_{N_2} = 9500 Torr.

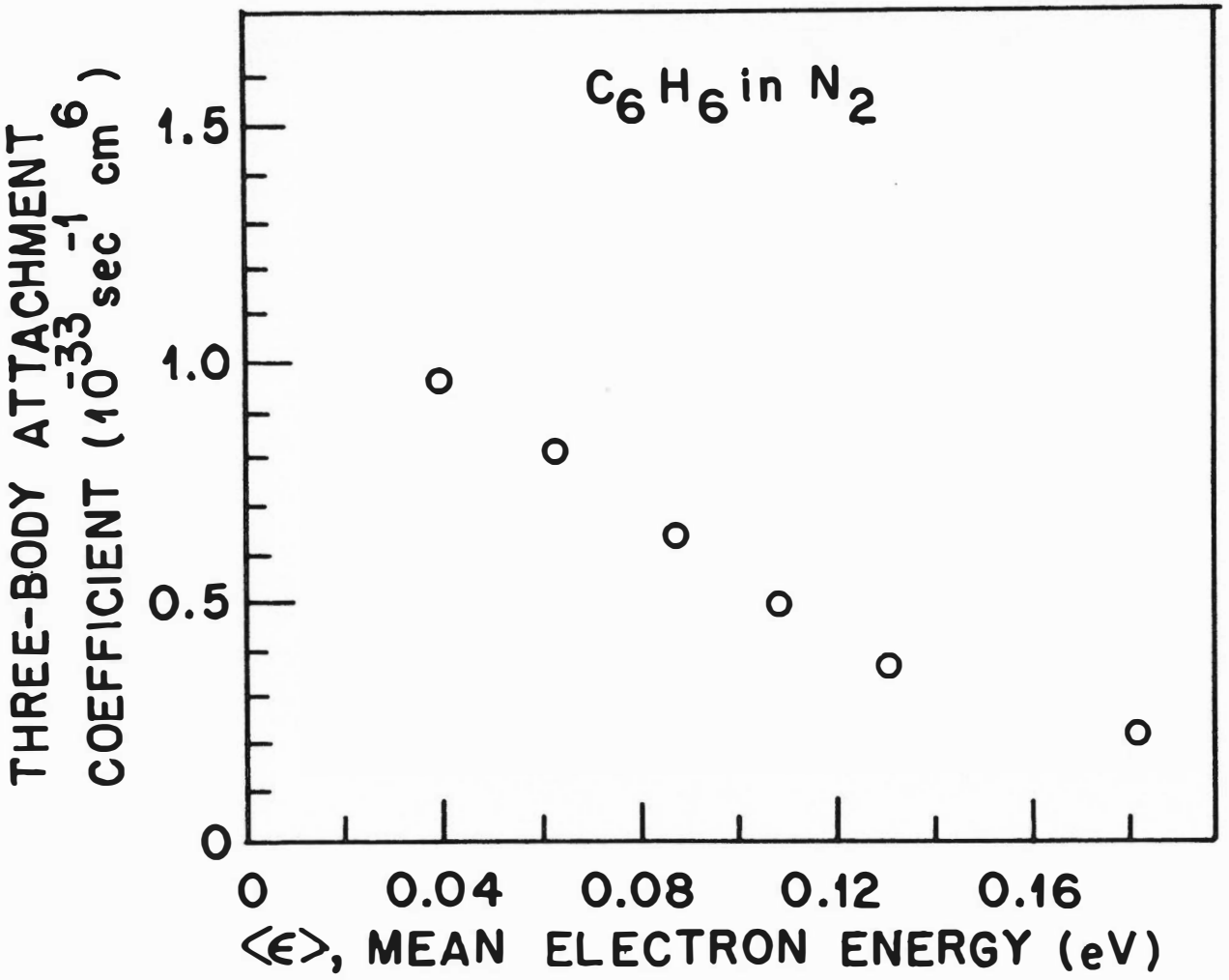

Figure IV-4. Three-body Attachment Coefficients as a Function of $\langle \epsilon \rangle$ for $e + C_6H_6 + N_2 \rightarrow C_6H_6^- + N_2 + \text{energy}$.

C_6H_6 in argon and in N_2-C_2H_4 mixtures were then performed to resolve the question of electron attachment to benzene.

Figure IV-5 shows the attachment coefficient, α, as a function of $P_{C_6H_6}/P_{Ar}$ for P_{Ar} = 5000 Torr and 10,000 Torr. Results are presented for $0.002 \leq E/P_{298} \leq 0.005$. These E/P's correspond [Christophorou (1971a)], to mean energies of 0.25, 0.31, 0.35, and 0.38 eV, respectively. The marked decrease in α with increasing $P_{C_6H_6}/P_{Ar}$ indicates that C_6H_6 causes a severe perturbation in the argon distribution functions. The data in Figure IV-5 will be considered to be very approximate and will not be analyzed further. These data do, however, provide concrete verification that C_6H_6 attaches low energy electrons.

Figure IV-6 shows the results of an experiment on the attachment of electrons to C_6H_6 to form $C_6H_6^{-*}$ in a mixture of C_2H_4 and N_2. In this study, $P_{C_6H_6}$ = 8 Torr, P_{total} = 5000 Torr and $100 \leq P_{C_2H_4} \leq 500$ Torr. The data in Figure IV-6 were taken at an E/P_{298} of 0.022 V cm^{-1} $Torr^{-1}$. At this E/P_{298}, the drift belocity of electrons in C_2H_4 is equal to that for electrons in N_2 within experimental error ($w_{N_2} = 1.94 \times 10^5$ cm sec^{-1}), and hence no correction is needed as the partial pressure $P_{C_2H_4}/P_{N_2}$ is changed. The distribution function for electrons in N_2 and in C_2H_4 is approximately Maxwellian at this E/P, thereby requiring no correction for mixture composition.

The results in Figure IV-6 indicate that C_6H_6 does attach electrons in C_2H_4-N_2 mixtures but that $(\alpha w)_{mix}$ is a sharply decreasing function of

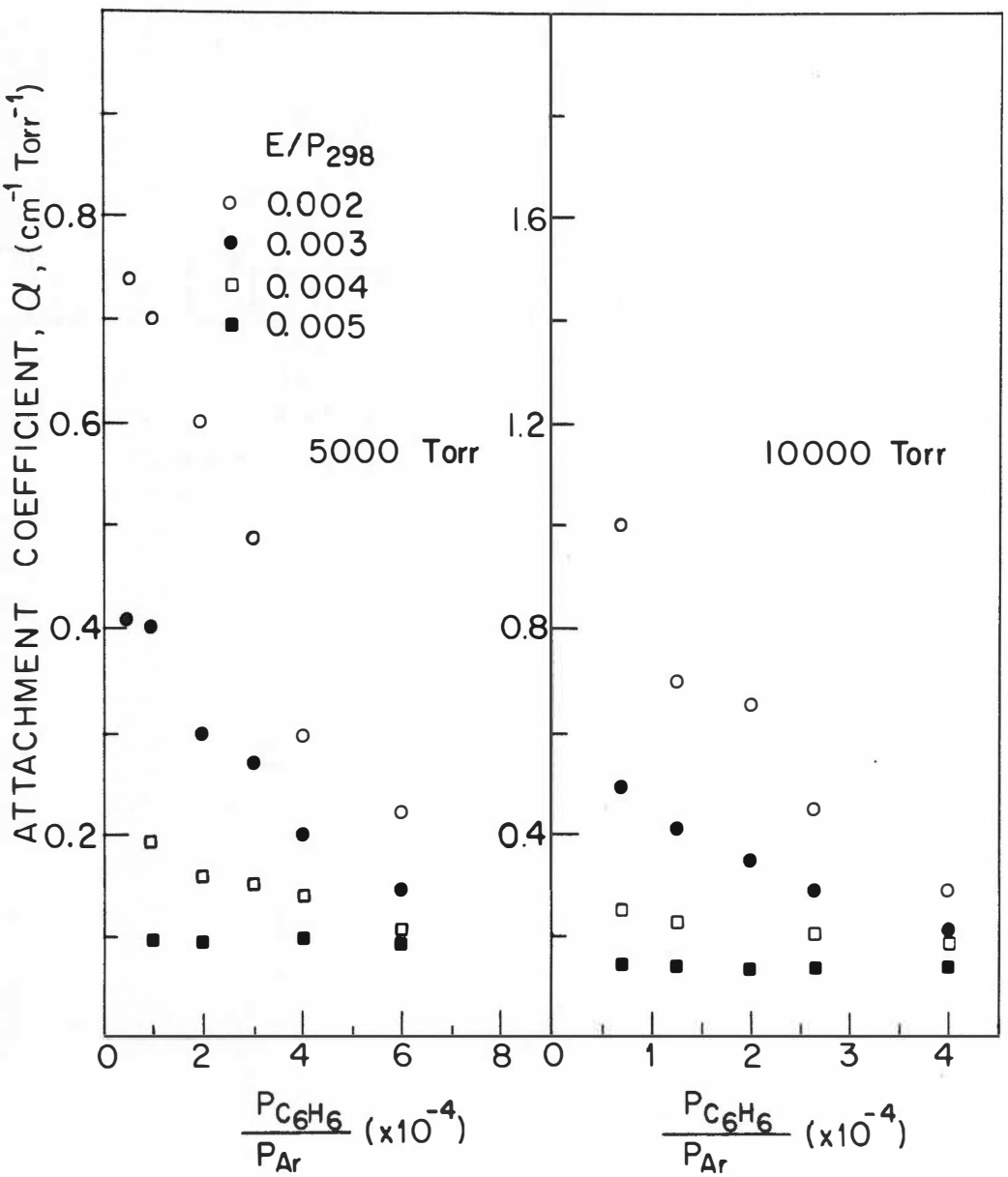

Figure IV-5. Attachment Coefficient α as a Function of $P_{C_6H_6}/P_{Ar}$ for Total Pressures of 5 and 10×10^3 Torr and E/P_{298} Values 2, 3, 4, and 5×10^{-3} V cm^{-1} Torr^{-1}.

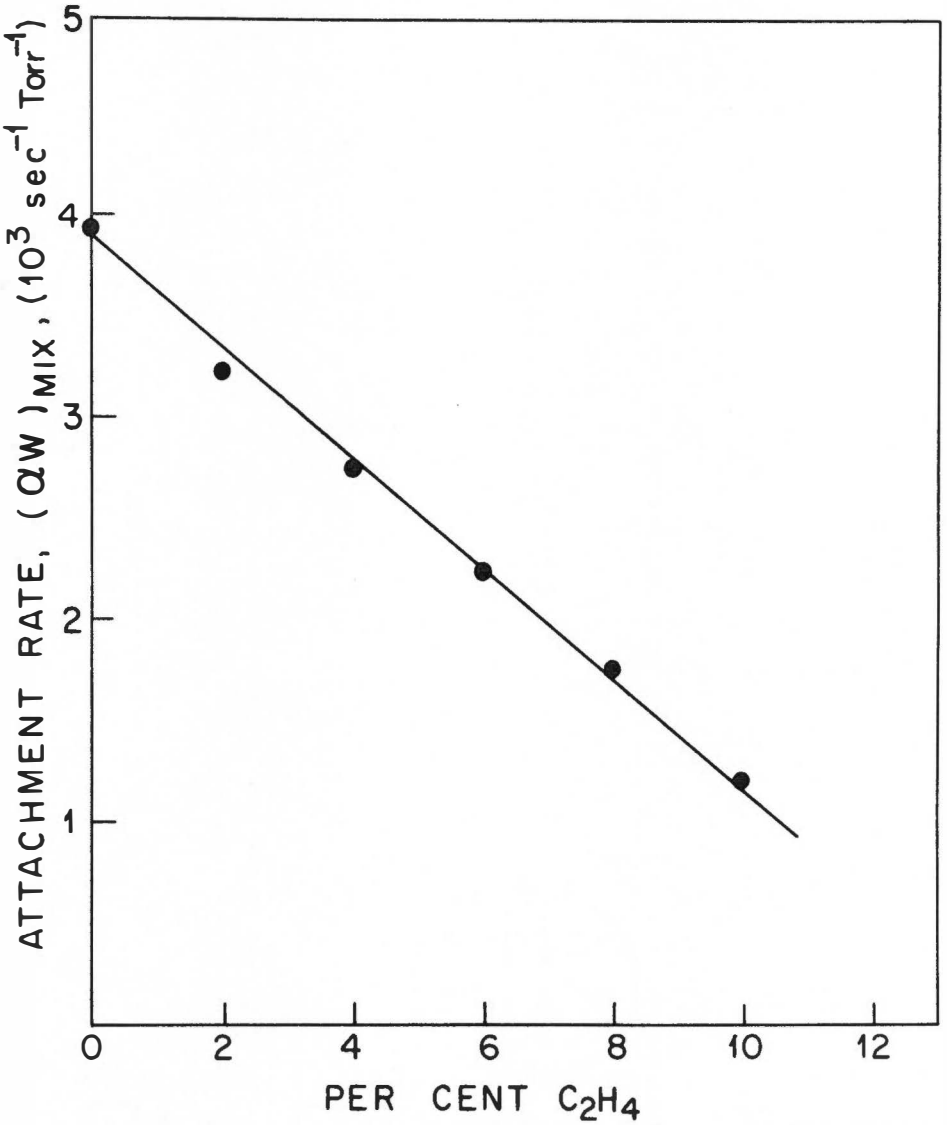

Figure IV-6. Attachment Rate as a Function of Percent of C_2H_4 in a Mixture of C_6H_6, C_2H_4, and N_2 at a Total Pressure of 5000 Torr and an E/P_{298} of 0.022 V cm^{-1} $Torr^{-1}$.

The C_6H_6 Pressure was Fixed at 8 Torr.

$P_{C_2H_4}/P_{N_2}$. A mechanism which explains this decrease will be described in the next section.

IV. DISCUSSION

1. Reaction Scheme for Electron Attachment to C_6H_6 in High Densities of N_2

It is possible to explain the results on C_6H_6-N_2 mixtures in terms of the following model:

$$e + C_6H_6 \xrightarrow{k_1} C_6H_6^{-*} \qquad \text{(IV-2)}$$

$$C_6H_6^{-*} \xrightarrow{k_2} C_6H_6 + e \qquad \text{(IV-3)}$$

$$C_6H_6^{-*} + N_2 \xrightarrow{k_3} C_6H_6^{-} + N_2 + \text{energy} \qquad \text{(IV-4)}$$

whereby

$$(\alpha w)_o = \frac{k_1 k_3 n_{N_2}}{k_2 + k_3 n_{N_2}} \qquad \text{(IV-5)}$$

where n_{N_2} is the nitrogen density, proportional to P_{N_2}. Equation (IV-5) can be put into the form

$$\frac{1}{(\alpha w)_o} = \frac{1}{k_1} + \frac{k_2}{k_3}\frac{1}{P_{N_2}} \; . \qquad \text{(IV-6)}$$

The C_6H_6 attachment data have been plotted in Figure IV-7 in the manner

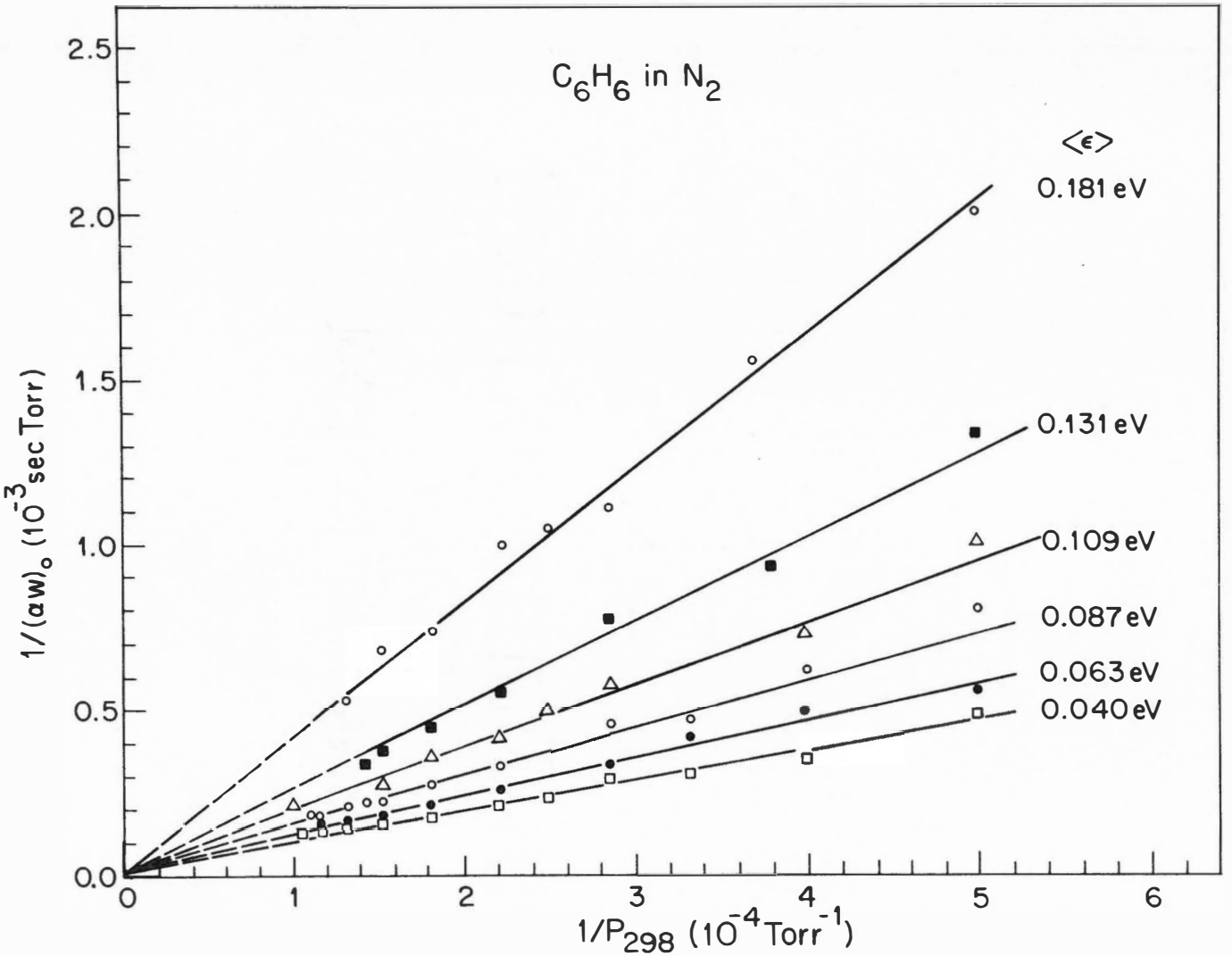

Figure IV-7. $1/(\alpha w)_o$ as a Function of $1/P_{298}$ for C_6H_6 in N_2 for the Indicated Values of ⟨ϵ⟩.

suggested by Equation (IV-6) and it is seen that the data are consistent with the proposed model. The intercept ($1/k_1$) is seen to be independent of $\langle\epsilon\rangle$ and the slope k_2/k_3 is seen to increase with increasing $\langle\epsilon\rangle$. A least squares fit to the data in Figure IV-7 yields $k_1 = 5 \times 10^4$ sec^{-1} Torr^{-1} and the values k_2/k_3 that are presented in Table IV-1.

2. Autodetachment Lifetime

The analysis in the previous section is an excellent way to obtain the critical pressure $P_c = k_2/k_3$ at which the rate of autoionization equals the rate of stabilization. P_c can be determined from the least squares fit without actually having been reached experimentally. This is fortunate since it is impossible to obtain reliable data in the ultrahigh pressure regime. From Table IV-1, P_c is seen to vary from 44,000 Torr to 200,000 Torr. In order to estimate the autodetachment lifetime we calculate the average time, τ_c, between collisions of $X^{-*}(C_6H_6^{-*})$ and S (N_2) as given in Equation (III-16). Using Equation (III-16), the values of P_c in Table IV-1, and the assumption that the probability of stabilization per collision, p, is unity, we determined the lifetimes listed in column 4 of Table IV-1. These are seen to lie in the pico and subpicosecond range. $\tau(C_6H_6^{-*})$ is found to be energy dependent as is shown in Figure IV-8. If $p < 1$, the average time for stabilizing $C_6H_6^{-*}$ in collisions with N_2 will be greater than τ_c; therefore

$$\tau(C_6H_6^{-*})_{p<1} > \tau(C_6H_6^{-*})_{p=1} \qquad \text{(IV-7)}$$

The lifetimes in Table IV-1 are seen to be lower limit estimates.

Table IV-1

Values of k_1, k_2/k_3 ($\equiv P_c$) and $\tau_a(C_6H_6^{-*})$ at various $\langle\epsilon\rangle$

$\langle\epsilon\rangle$	k_1	k_2/k_3 ($\equiv P_c$)	$\tau_a(C_6H_6^{-*})$
(eV)	(sec^{-1} $Torr^{-1}$)	(Torr)	(sec)
0.040	5×10^4	4.4×10^4	10.4×10^{-13}
0.063	5×10^4	5.5×10^4	8.3×10^{-13}
0.087	5×10^4	7.0×10^4	6.5×10^{-13}
0.109	5×10^4	9.2×10^4	5.0×10^{-13}
0.131	5×10^4	1.25×10^5	3.6×10^{-13}
0.181	5×10^4	2.0×10^5	2.3×10^{-13}

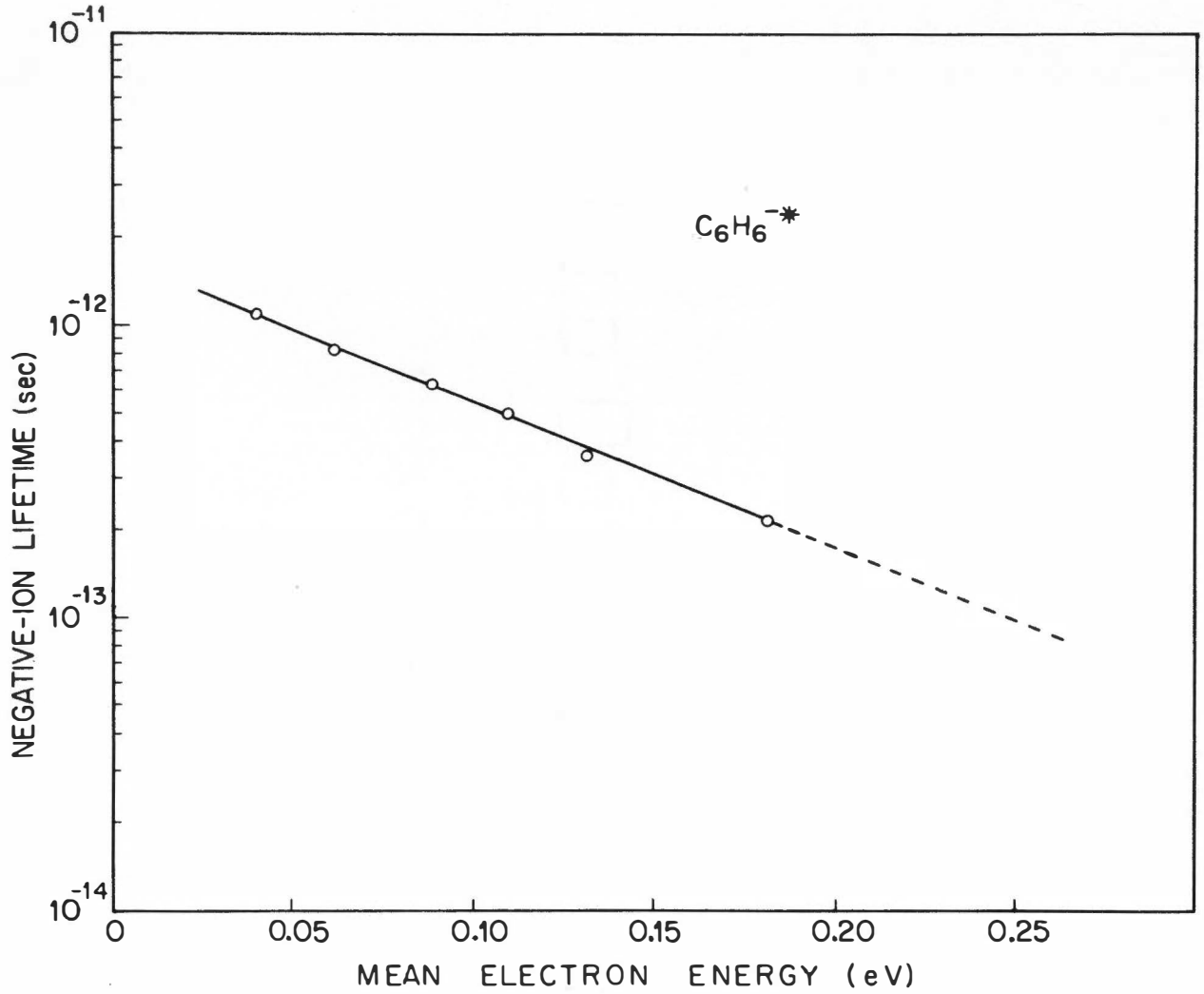

Figure IV-8. Variation of the Autodetachment Lifetime of $C_6H_6^{-*}$ with Mean Electron Energy $\langle\epsilon\rangle$.

3. Extrapolation to the Liquid State

The analysis in part 2 is also seen to be an excellent way to determine k_1, the absolute rate of electron attachment to C_6H_6 in the limit $P_{N_2} \rightarrow \infty$. k_1 is the attachment rate that would be measured if the N_2 density were great enough so that every negative ion were stabilized. This rate should be very close to that expected for electron attachment in the liquid state, that is

$$[(\alpha w)_o]_{\text{intercept}} \approx [(\alpha w)_o]_{\text{liquid}} \quad . \tag{IV-8}$$

For liquid N_2 and $\langle \epsilon \rangle = 0.04$ eV we have $[(\alpha w)_o]_{\text{liquid}} = k_1 = 5 \times 10^4$ sec^{-1} Torr^{-1} $= 1 \times 10^9$ sec^{-1} M^{-1}. No measurements have been made of the rate of attachment of electrons to C_6H_6 in liquid nitrogen but a thermal attachment rate $\leq 1 \times 10^9$ sec^{-1} M^{-1} has been reported by Bakale *et al.* (1972) for C_6H_6 in liquid n-hexane. This value is in good agreement with the present finding.

4. Importance of the Experimental Results with C_2H_4

The drastic decrease in the attachment rate, $(\alpha w)_{mix}$, with increasing $P_{C_2H_4}$ (Figure IV-6, page 63) indicates that collisional detachment is an important mechanism to consider in the model presented earlier. In order to include collisional detachment we must have, in addition to Equations (IV-2)-(IV-4), the reactions:

$$C_6H_6^{-*} + N_2 \xrightarrow{k_7} C_6H_6 + N_2 + e \tag{IV-9}$$

$$C_6H_6^{-*} + C_2H_4 \xrightarrow{k_3'} C_6H_6^- + C_2H_4 + \text{energy} \qquad \text{(IV-10)}$$

$$C_6H_6^{-*} + C_2H_4 \xrightarrow{k_7'} C_6H_6 + C_2H_4 + \text{energy} + e \quad . \qquad \text{(IV-11)}$$

Consideration of Equations (IV-2) to (IV-4) and (IV-9) to (IV-11) gives for the attachment of electrons to C_6H_6 in N_2-C_2H_4 mixtures:

$$(\alpha w)_{mix} = k_1 \frac{\{k_3 P_{N_2} + k_3' P_{C_2H_4}\}}{k_2 + (k_3 + k_7) P_{N_2} + (k_3' + k_7') P_{C_2H_4}} \quad . \qquad \text{(IV-12)}$$

Under the assumption that $k_3 P_{N_2} >> k_3' P_{C_2H_4}$ we have:

$$\frac{(\alpha w)_{N_2}}{(\alpha w)_{mix}} \approx 1 + \frac{k_7' P_{C_2H_4}}{k_2 + (k_3 + k_7) P_{N_2}} \qquad \text{(IV-13)}$$

where $(\alpha w)_{N_2}$ is the rate for the C_6H_6-N_2 system and $(\alpha w)_{mix}$ is the rate for the C_6H_6-N_2-C_2H_4 system. The previous assumption is valid since, experimentally, the rates for attachment to C_6H_6 in N_2 environments are much larger than those in C_2H_4 environments. At P_{total} = 5000 Torr, the rates for the C_6H_6-N_2 system are still well within the three-body region so that $k_2 >> (k_3 + k_7) P_{N_2}$. Therefore,

$$\frac{(\alpha w)_{N_2}}{(\alpha w)_{mix}} \approx 1 + \frac{k_7'}{k_2} P_{C_2H_4} \quad . \qquad \text{(IV-14)}$$

Figure IV-9 shows the data plotted in the manner suggested by Equation (IV-14). It can be seen that the data provide good agreement with the revised model. A linear least squares fit to the data in Figure IV-9 gives $k_7'/k_2 = 2.8 \times 10^{-3}$ $Torr^{-1}$. Therefore, at 1000 Torr total pressure, collisional detachment is 2.8 times as probable as autoionization. If we take $\tau_a (= k_2^{-1}) = 4 \times 10^{-13}$ sec, then $k_7' = 7.0 \times 10^9$ sec^{-1} $Torr^{-1}$. The rate for collisional detachment is very high and is indicative of the importance of this mechanism in C_2H_4.

The analysis on electron attachment to C_6H_6 in N_2 was performed under the assumption that collisional detachment is unimportant in that system ($k_3 >> k_7$). In view of the magnitude of k_7' it might be necessary to revise those results taking collisional detachment into consideration. However, the importance of such a process seems to be a function of the stabilizing body and also perhaps of the metastable ion itself since detachment was not observed to be significant in O_2-N_2 and in O_2-C_2H_4 mixtures (see Chapter III). Actually, in the case of O_2^{-*}, C_2H_4 was found to be more efficient in stabilizing the negative ion than was N_2.

5. The Electron Affinity of C_6H_6

Many theoretical estimates have been made of the electron affinity, EA_B, of benzene; these calculations justify the commonly accepted value of

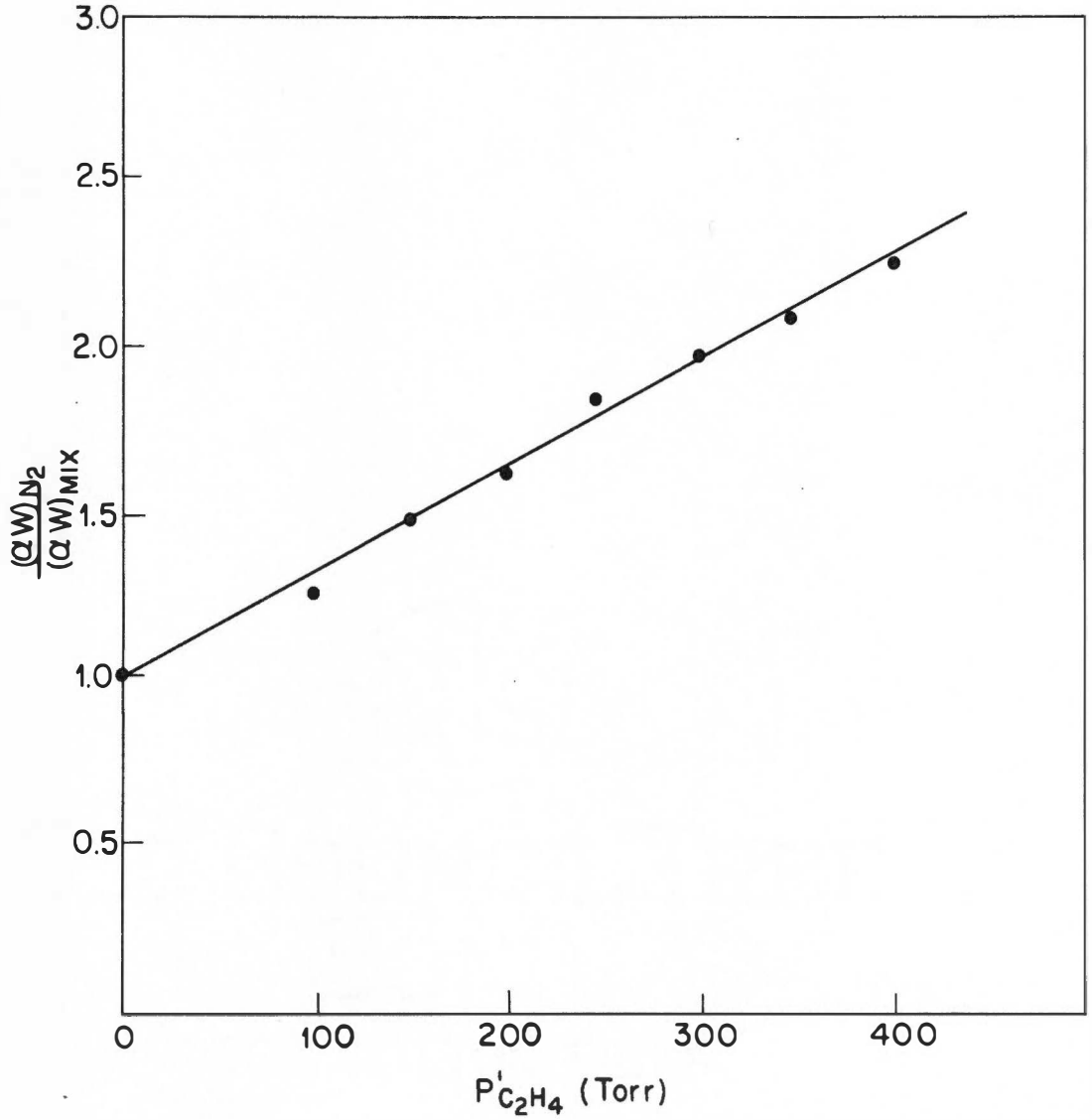

Figure IV-9. $(\alpha w)_{N_2}/(\alpha w)_{mix}$ vs. $P_{C_2H_4}$ in a Mixture of C_6H_6, C_2H_4, and N_2 at a Total Pressure of 5000 Torr.

The C_6H_6 Pressure was kept Constant at 8 Torr.

-1.4 eV (see Table IV-2). Compton, Christophorou, and Huebner (1966) observed a compound negative ion resonance (CNIR) in C_6H_6 with an onset at $\sim$ 0.9 eV and a maximum at $\sim$ 1.4 eV. In view of these findings $EA_B \geq -0.9$ eV. Considering the present result which indicates that $C_6H_6^-$ exists in the gas phase, we must conclude that $EA_B > 0$ eV. We would expect EA_B to be very small in light of the small lifetime estimated for $C_6H_5^{-*}$ in section 2. The value of - 1.4 eV may correspond to the vertical attachment energy. This quantity is defined [see Christophorou (1971a)] as the energy difference between the neutral molecule in its ground rotational, vibrational, and electronic states plus an electron at rest at infinity and the molecular negative ion formed without a change in internuclear separation. Since many of the theoretical estimates of EA_B yield values close to the vertical attachment energy it would seem that their calculations neglected nuclear relaxation. In light of the finding that $EA_B > 0$ we must conclude that the potential energy surface of $C_6H_6^-$ lies below that of C_6H_6 with its minimum at considerably greater internuclear separations.

Table IV-2

Literature Values for the Electron Affinity of Benzene;

Threshold of Lowest CNIR State of Benzene

Electron Affinity	Reference and Method	Threshold of Lowest CNIR State
(eV)		(eV)
-1.63	1[a]	0.9 ± 0.3
-1.62	2[a]	0.95
-1.59	3	
-1.42	4[a]	
-1.4	5-7[a]	
-0.36	8[b]	
-0.06	9[a]	

[a]Theory.

[b]Kinetics of electrode processes.

1. R. M. Hedges and F. A. Matsen, J. Chem. Phys. 28, 250 (1958).

2. S. Ehrenson, J. Phys. Chem. 66, 706 (1962).

3. A. F. Gains, J. Kay, and F. M. Page, Trans. Faraday Soc. 62, 874 (1966).

4. D. R. Scott and R. S. Becker, J. Phys. Chem. 66, 2713 (1962).

5. J. R. Hoyland and L. Goodman, J. Chem. Phys. 36, 21 (1962).

6. N. S. Hush and J. A. Pople, Trans. Faraday Soc. 51, 600 (1955).

7. G. L. Caldow, Mol. Phys. 18, 183 (1970).

Table IV -2 (continued)

8. L. E. Lyons, Nature 166, 193 (1950).

9. T. L. Kunii and H. Kuroda, Theoret. Chim. Acta (Berl.) 11, 97 (1968).

CHAPTER V

ATTACHMENT OF LOW ENERGY ELECTRONS TO C_2H_5Br IN HIGH DENSITIES OF N_2 AND Ar

I. INTRODUCTION

Continuing our effort to link together knowledge on electron attachment in dilute gases and in condensed media we investigated low energy (< 3 eV) electron attachment to bromoethane (C_2H_5Br) in mixtures with N_2 for $P_{N_2} \leq 25,000$ Torr (~ 33 atm) and in mixtures with argon for $P_{Ar} \leq 42,500$ Torr (~ 56 atm). Dissociative electron attachment to C_2H_5Br has been investigated previously by Christodoulides and Christophorou (1971) using swarm techniques at relatively low total pressures (≤ 1.3 atm) and by Collins, Christophorou and Carter (1970) using a time-of-flight mass spectrometer. These results were discussed within the framework of the resonance-scattering theory of dissociative electron attachment to diatomic molecules [see Bardsley, Herzenberg and Mandl (1964, 1966), Bardsley and Mandl (1968), and O'Malley (1966)] and provided evidence that dissociative electron attachment proceeds via a short-lived compound negative ion state. Since Br^- was the only ion observed in the mass spectrometer, it was reasonable to consider C_2H_5Br as a diatomic-like molecule R-Br as far as dissociative attachment is concerned.

In the present study C_2H_5Br has been found to capture slow (< 3 eV) electrons in high densities of N_2 and Ar with a cross section which increases with increasing carrier gas density. The dependence of the attachment rate on carrier gas density has been studied in detail and a model is presented which accounts for the experimental results. In addition, certain differences between the present study and the previous ones [Christodoulides et al. (1971), and Collins et al. (1970)] will be presented and discussed.

II. EXPERIMENTAL RESULTS

The bromoethane used in this study was purchased from Matheson, Coleman and Bell, Inc. and was of a quoted purity of 99.9%. The ratio of the nitrogen carrier gas pressure, P_{N_2}, to the sample gas pressure, $P_{C_2H_5Br}$, was in the range $1 \times 10^5 \leq P_{N_2}/P_{C_2H_5Br} \leq 5 \times 10^6$. The ratio of the argon carrier gas pressure, P_{Ar}, to the sample gas pressure was in the range $1 \times 10^5 \leq P_{Ar}/P_{C_2H_5Br} \leq 1 \times 10^7$. All measurements were made at room temperature (298°K). Neither argon nor nitrogen pressures were corrected for compressibility because the correction is small even at the highest pressures used.

The dependence of the attachment rate, $(\alpha w)_o$, on the pressure-reduced electric field, E/P_{298}, and the mean electron energy, $\langle\epsilon\rangle$, is shown in Figure V-1 for the indicated N_2 pressures. The values of the drift velocity, w, and the mean electron energy, $\langle\epsilon\rangle$, were taken from Christophorou (1971a). As in earlier studies, $(\alpha w)_o$ designates the value of

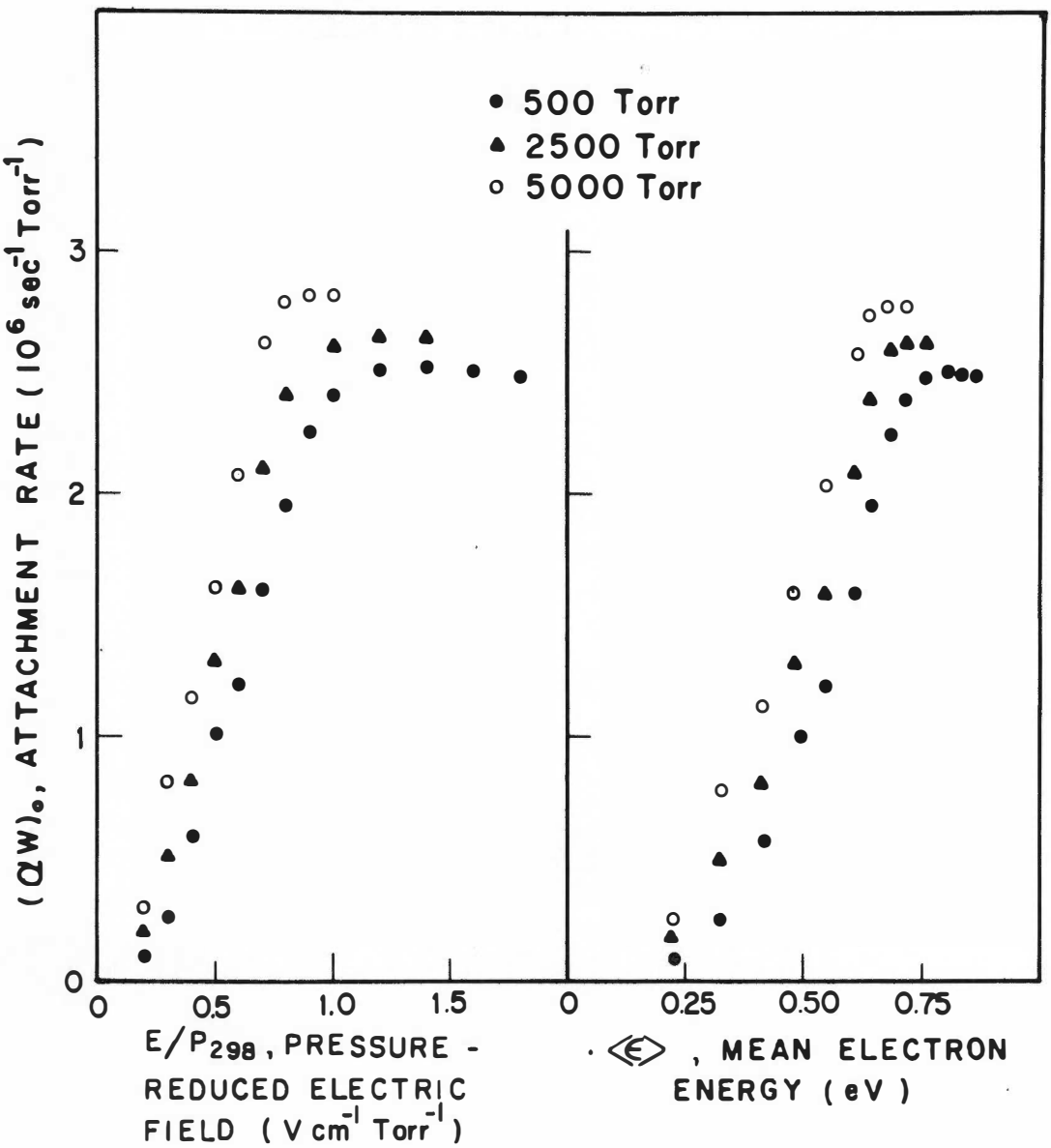

Figure V-1. Attachment Rate, $(\alpha w)_o$, as a Function of E/P_{298} and $\langle\epsilon\rangle$ for C_2H_5Br in N_2 for the Indicated N_2 Pressures.

αw as $P_{C_2H_5Br} \rightarrow 0$. However, in the experiments with N_2, there was no observable partial pressure dependence to αw. In Figure V-2 we show $(\alpha w)_o$ as a function of both E/P_{298} and $\langle \epsilon \rangle$ for argon as a carrier gas. Care was taken to keep the sample pressure low ($\leq$20 μ) so that the argon distribution functions are not disturbed appreciably. Figure V-3 presents the partial pressure dependence of the rate at a total pressure of 500 Torr. This case was selected because it shows the most drastic partial pressure dependence for low $\langle \epsilon \rangle$. For high P_{Ar} and for $\langle \epsilon \rangle \geq 1$ eV, αw is independent of $P_{C_2H_5Br}$, but at low $\langle \epsilon \rangle$ and low P_{Ar}, there is a significant partial pressure dependence. The rates presented in this chapter for each P_{Ar} are those extrapolated to $P_{C_2H_5Br} = 0$ Torr.

The data for electron attachment to C_2H_5Br in N_2 and Ar media indicate that the attachment rates increase with increasing carrier gas pressure. In Figures V-4 and V-5 $(\alpha w)_o$ is presented as a function of P_{N_2} and P_{Ar}, respectively, for a number of $\langle \epsilon \rangle$. It is seen that, initially, $(\alpha w)_o$ increases linearly with P_x ($x = N_2, Ar$), but as P_x increases further, $(\alpha w)_o$ shows a less than linear dependence on P_x. At the highest values of P_x, $(\alpha w)_o$ is seen to be virtually pressure independent. These results will be discussed further in section III where a model will be proposed to account for the observed rates.

In Figure V-6, the attachment rates extrapolated to zero total pressure for both the present work and the earlier study [Christodoulides and Christophorou (1971)] are shown. From these data, it is evident that

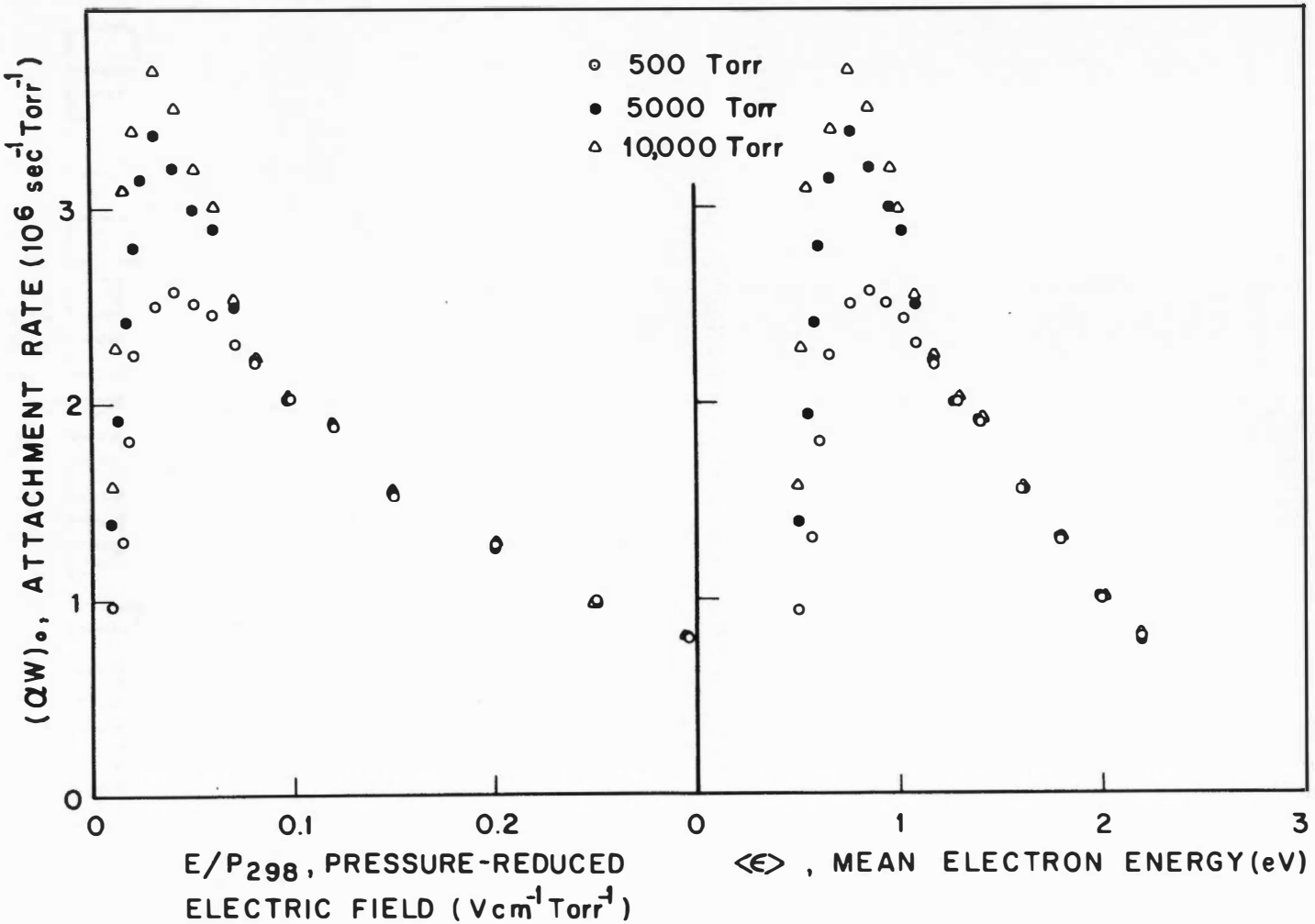

Figure V-2. Attachment Rate, $(\alpha w)_o$, as a Function of E/P_{298} and $\langle\epsilon\rangle$ for C_2H_5Br in Ar.

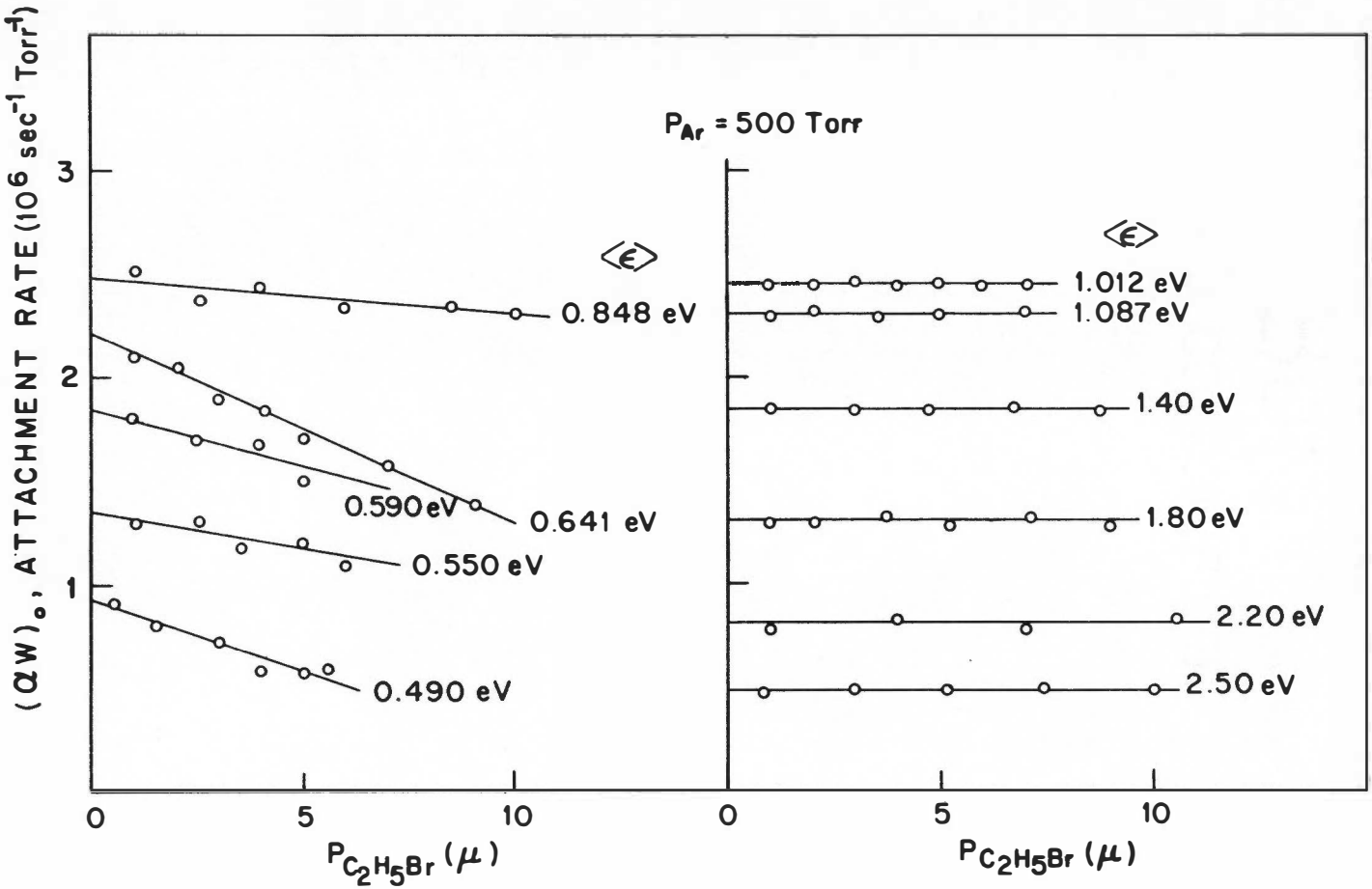

Figure V-3. The Partial Pressure Dependence of $(\alpha w)_o$ for C_2H_5Br in Ar at P_{Ar} = 500 Torr.

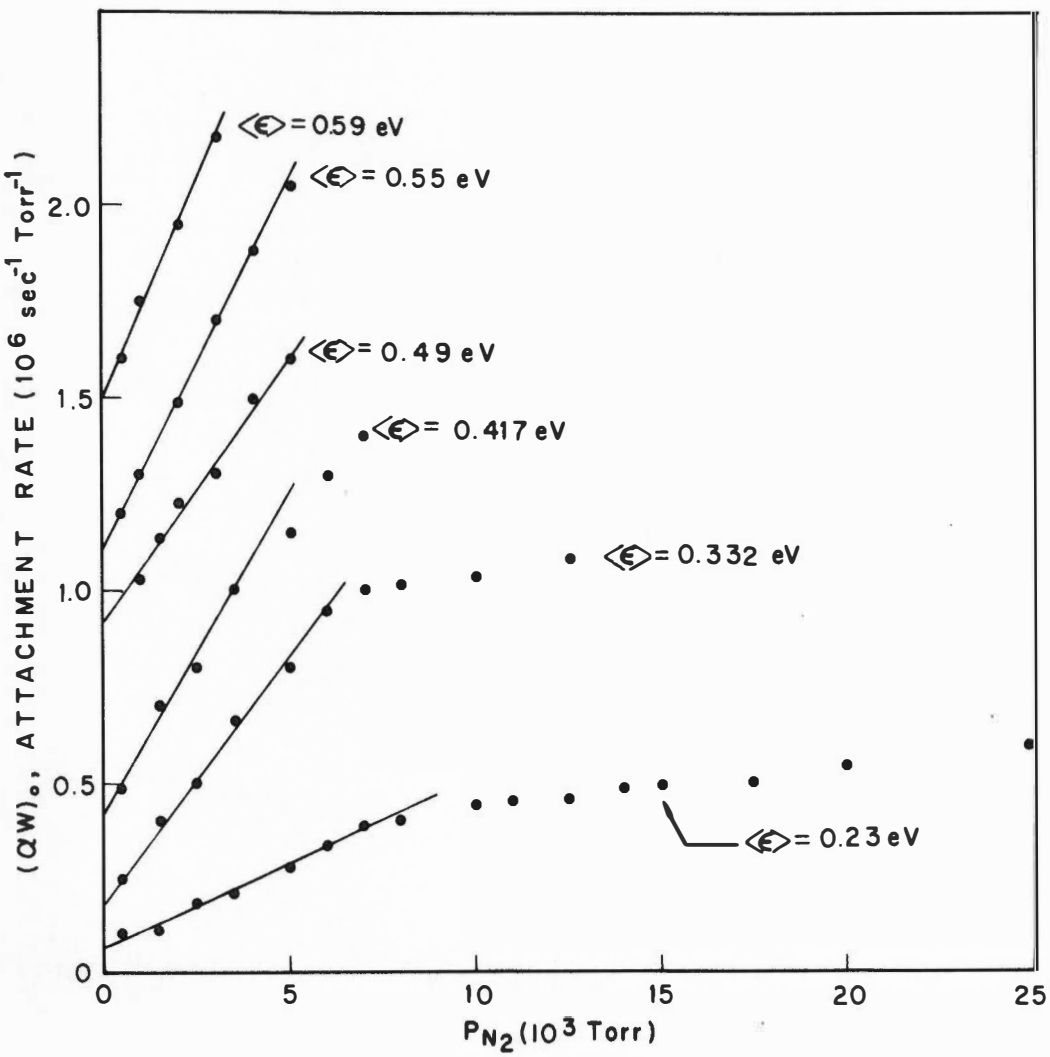

Figure V-4. The Attachment Rate, $(\alpha w)_o$, for C_2H_5Br in N_2 as a Function of P_{N_2} for Several $\langle\epsilon\rangle$.

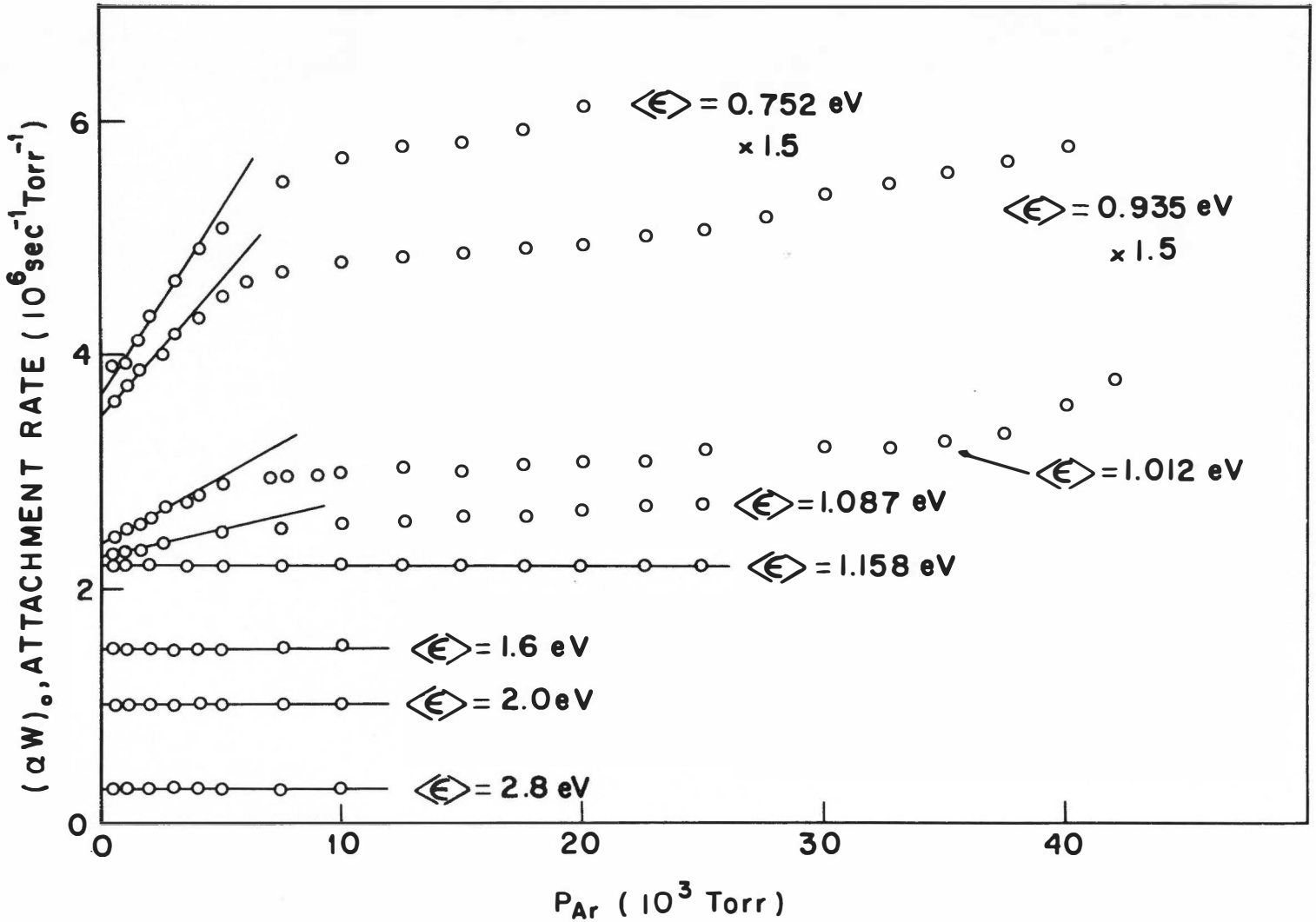

Figure V-5. The Attachment Rate, $(\alpha w)_o$, for C_2H_5Br in Ar as a Function of P_{Ar} for Several $\langle\epsilon\rangle$.

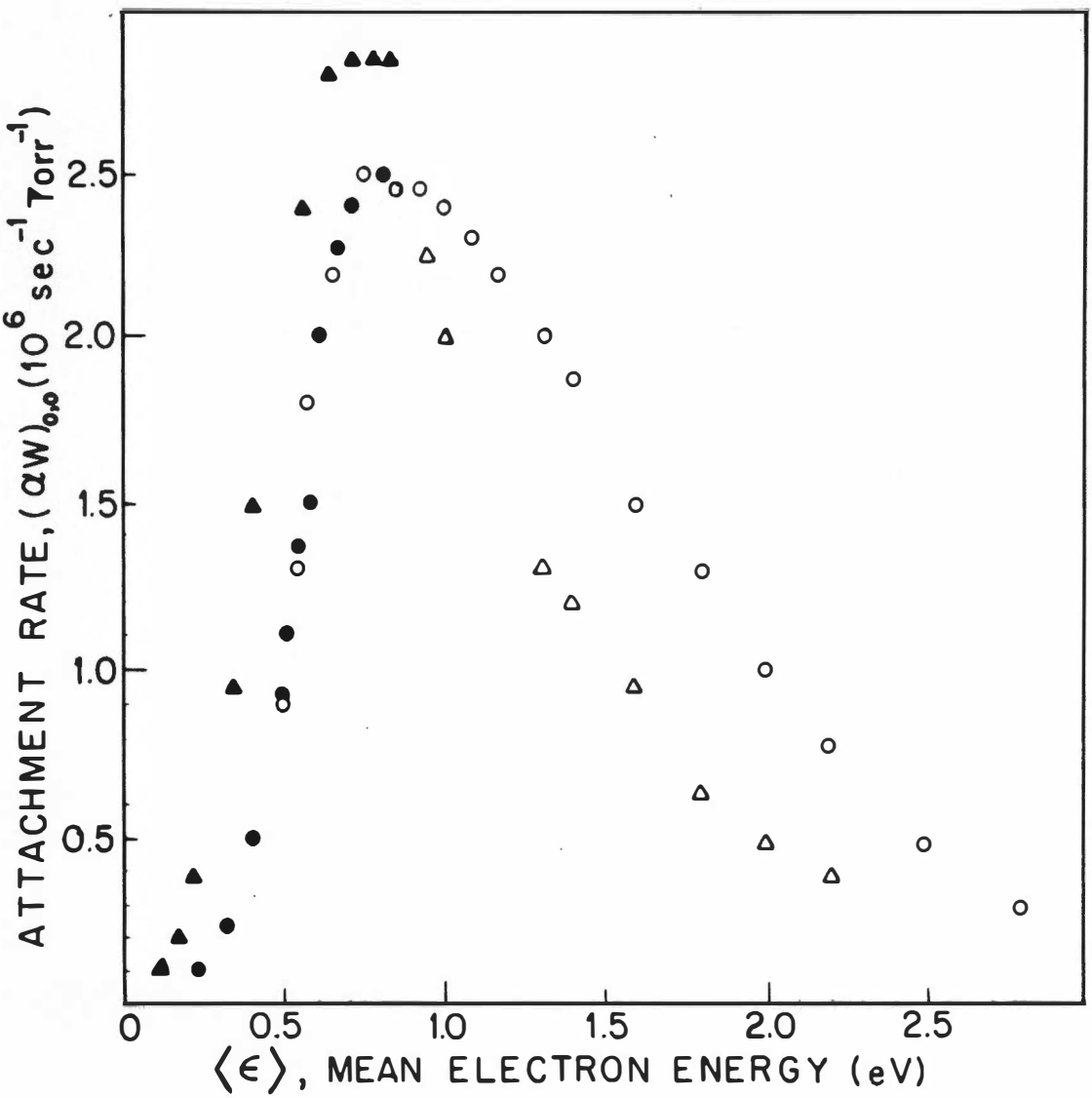

Figure V-6. The Attachment Rates Extrapolated to Zero Total Pressure for the Present Work and the Work of Christodoulides and Christophorou.

(●) - Present Data for N_2; (○) - Present Data for Ar; (▲) - Previous Data for N_2; (△) - Previous Data for Ar.

there is a considerable discrepancy between the two experiments. The magnitude of αw agrees rather well (within 14% at the peak), but the shape (and hence the cross section) is quite different. Efforts to resolve these differences have failed and for this reason, both sets of data are shown for purposes of comparison. In Figure V-6, the solid circles are the present data using N_2 and the open circles are the present data using argon. The solid triangles represent the N_2 data and the open triangles represent the argon data of Christodoulides and Christophorou (1971).

The swarm unfolding technique (see Chapter II) has been applied to the present data in Figure V-6 to obtain absolute attachment cross sections, $\sigma_a(\epsilon)$, as a function of electron energy ϵ. These functions [for N_2 data (•) alone, for Ar data (▲) alone, and for N_2-Ar data (○)] are presented in Figure V-7 and are seen to be very consistent in both magnitude and shape. A calculation of $\sigma_a(\epsilon)$ by Christodoulides and Christophorou (1970) [using the swarm-beam technique (see Chapter II)] is also presented in Figure V-7 for purposes of comparison. A comparison of the results of the two calculations shows that there is a discrepancy both in the position of the peak of $\sigma_a(\epsilon)$ [ϵ_{max} = 1.1 eV for the present study; ϵ_{max} = 0.76 eV for the work of Christodoulides and Christophorou (1970)] and in the magnitude of the cross section [$\sigma_{max} \sim 1 \times 10^{-17}$ cm^2 for the present work; $\sigma_{max} \sim 0.4 \times 10^{-17}$ cm^2 for the previous study]. The full-width at half maximum (FWHM) for the data of Christodoulides and Christophorou is seen to be much wider (FWHM $\sim$ 0.5 eV) than that in the present study (FWHM $\sim$ 0.15 eV). The swarm-beam

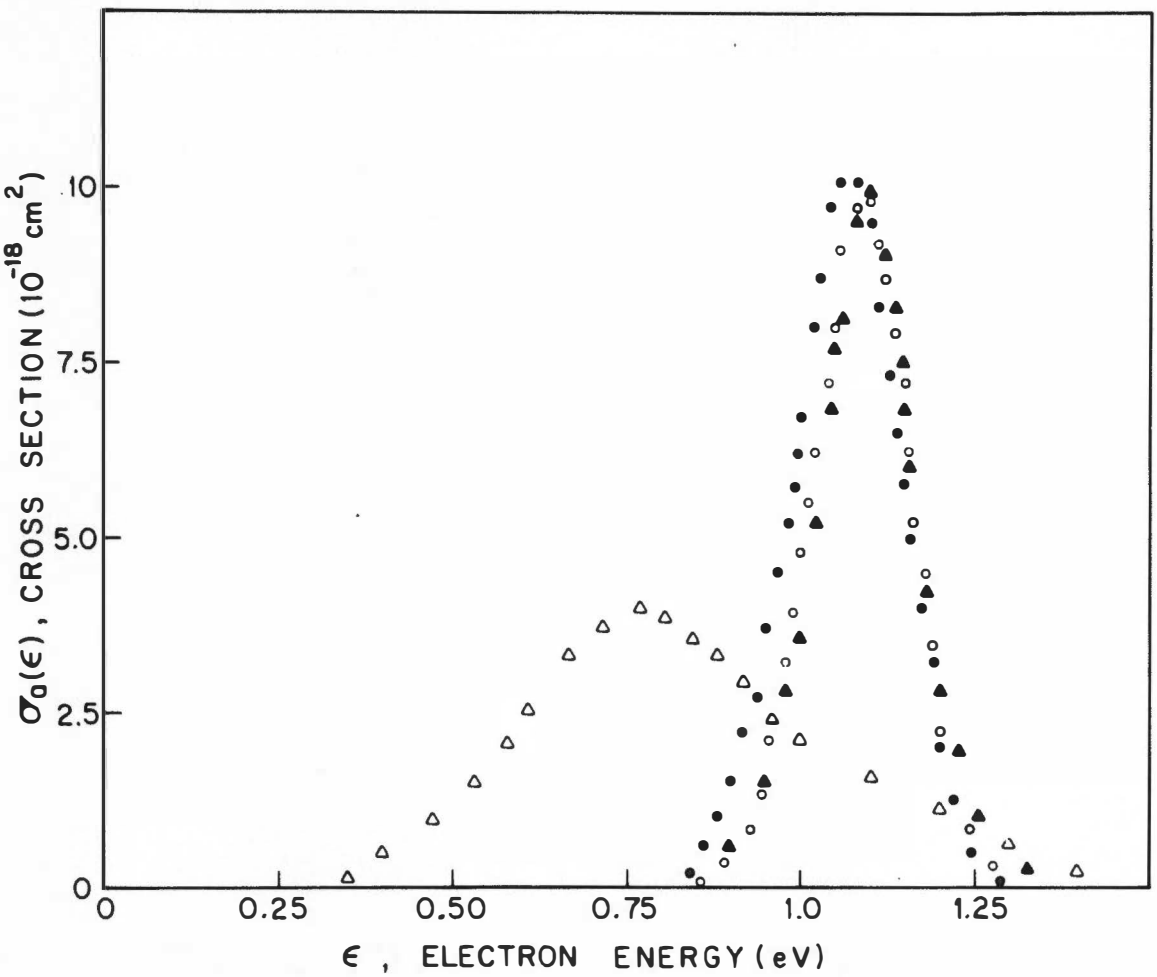

Figure V-7. $\sigma_a(\epsilon)$ Calculated Using the Data of Figure V-6 for the Present Work and the Previous One by Christodoulides et al.

(●) - N_2 Data; (o) - Ar Data; (▲) - N_2, Ar Data; (Δ) - Swarm Unfolding of Christodoulides' Data.

calculation assumes that the negative ion yield $I(\epsilon)$ is proportional to the attachment cross section, thereby giving a relative cross section spectrum. The resulting $\sigma_a(\epsilon)$ calculated in this way has the same shape and width as $I(\epsilon)$. In the swarm unfolding technique, both the magnitude and the shape of $\sigma_a(\epsilon)$ are allowed to change during the calculation. These differences in the assumptions made in the calculation of $\sigma_a(\epsilon)$ contribute to part of the discrepancy between the two cross section functions. An unfolding calculation of $\sigma_a(\epsilon)$ using the data of Christodoulides and Christophorou (1970) shows very high residuals with most of the discrepancy being in the argon data. From this analysis, it appears that the argon rates of Christodoulides and Christophorou (1970) fall off too rapidly since the calculated rates (R_{cal} in Chapter II) are considerably higher than the experimental ones. However, the swarm unfolding procedure is quite sensitive to the shape and the magnitude of αw and often, small changes in αw will give rise to large changes in $\sigma_a(\epsilon)$. Because of the substantial improvements made in the electronics system, we feel that the measurement techniques used in this work are somewhat more precise than those used previously and we therefore place greater confidence in the present rates.

The swarm unfolding technique has also been applied to obtain attachment cross sections at higher pressures. Figure V-8 shows an example of this calculation for P_x = 5000 Torr and 10,000 Torr. Similar cross section functions were obtained for pressures between these two values.

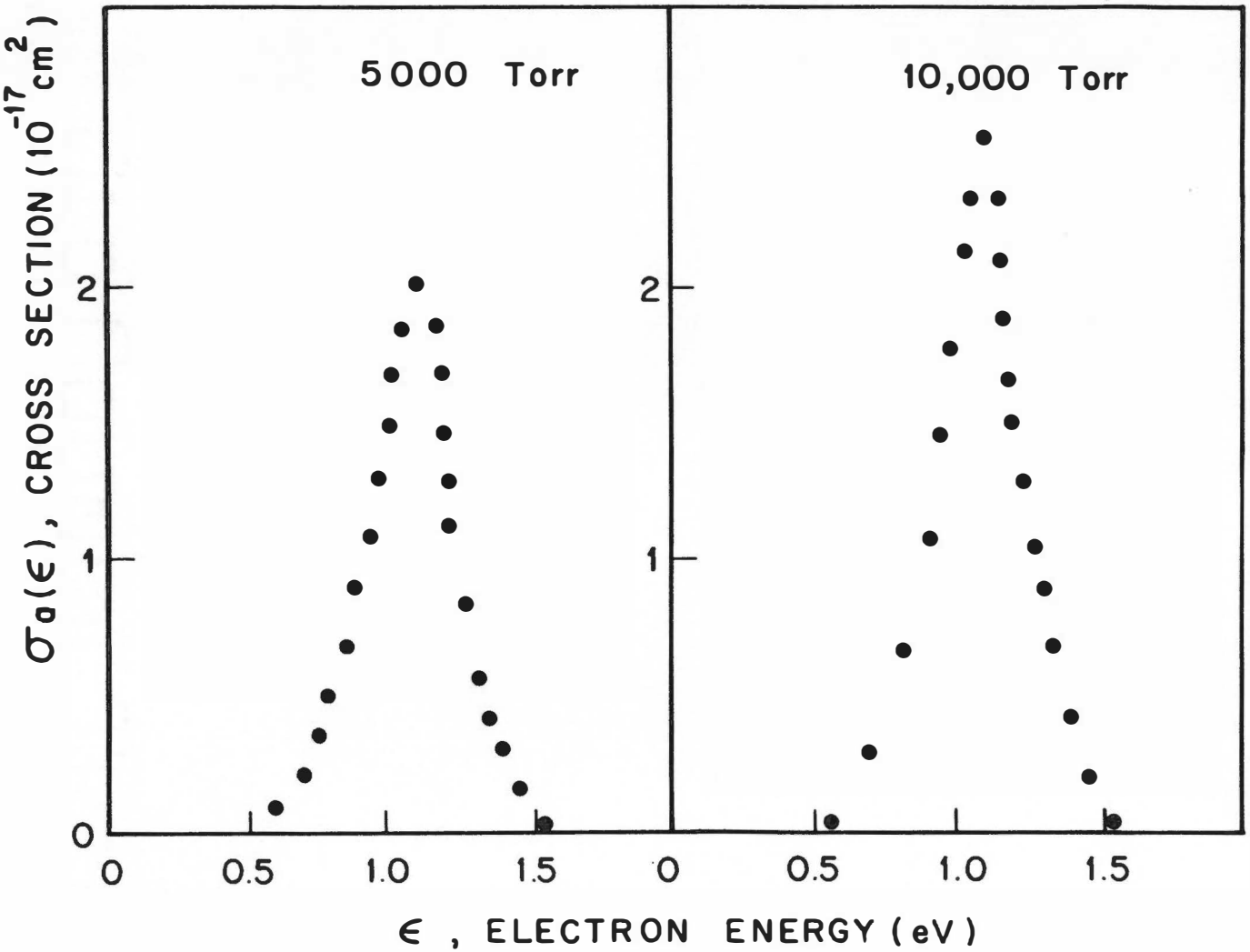

Figure V-8. $\sigma_a(\epsilon)$ Calculated Using Attachment Data at P_x = 5000 Torr and 10,000 Torr.

III. DISCUSSION

1. Reaction Scheme for Electron Attachment to C_2H_5Br in High Densities of N_2 and Ar

The data in Figures V-1, V-2, V-4, and V-5, pages 78, 80, 82, and 83, respectively, will be analyzed on the basis of the following reaction scheme:

$$e + C_2H_5Br \xrightarrow{k_1} C_2H_5Br^{-*} \qquad (V\text{-}1)$$

$$C_2H_5Br^{-*} \xrightarrow{k_2} C_2H_5 + Br^- \qquad (V\text{-}2)$$

$$C_2H_5Br^{-*} \xrightarrow{k_3} C_2H_5Br + e \qquad (V\text{-}3)$$

$$X + C_2H_5Br^{-*} \xrightarrow{k_{4x}} C_2H_5Br^- + X + \text{energy} \qquad (V\text{-}4)$$

where X = N_2 or Ar. Analysis of Equations (V-1) to (V-4) gives

$$(\alpha w)_o = \frac{k_1 \{k_2 + k_{4x} n_x\}}{k_2 + k_3 + k_{4x} n_x} \qquad (V\text{-}5)$$

where n_x is the number density of x, proportional to P_x. Equation (V-5) can be written as

$$(\alpha w)_o = \frac{k_1 k_2 + k_1 k_{4x} P_x}{k_2 + k_3 + k_{4x} P_x} \quad . \qquad (V\text{-}6)$$

In the limit where $P_x \to 0$, Equation (V-6) reduces to

$$(\alpha w_o)_{P_x \to 0} = \frac{k_1 k_2}{k_2 + k_3} \qquad \text{(V-7)}$$

which is the usual expression for a pure dissociative process requiring no stabilization. These rates were presented earlier in Figure V-6, page 84, as a function of the mean electron energy $\langle \epsilon \rangle$. The "stabilization rate," $\alpha w_{st} = (\alpha w)_o - (\alpha w)_{P_x \to 0}$, is shown in Figure V-9 for two pressures (P_x = 2,500 Torr and 10,000 Torr). In Figure V-10, a comparison is presented between $(\alpha w)_o$ and $(\alpha w)_{st}$ at P_x = 10,000 Torr. In this figure, $(\alpha w)_{st}$ has been normalized to $(\alpha w)_o$ at the peak energy ($\langle \epsilon \rangle$ = 0.75 eV). The two curves are seen to be similar for $\langle \epsilon \rangle < 0.9$ eV; they differ at higher energies because $(\alpha w)_o$ is pressure independent (and hence $\alpha w_{st} \to 0$) for $\langle \epsilon \rangle \geq 1.1$ eV. The similarity of these two curves lends support to the hypothesis that there is just one compound negative ion state involved in the reaction scheme (V-1) to (V-4).

The dissociation rate, Equation (V-7), can be subtracted from Equation (V-6) to give

$$(\alpha w)_{st} = \frac{\left(\frac{k_1 k_3}{k_2 + k_3}\right) k_{4x} P_x}{k_2 + k_3 + k_{4x} P_x} \qquad \text{(V-8)}$$

which can be rewritten as

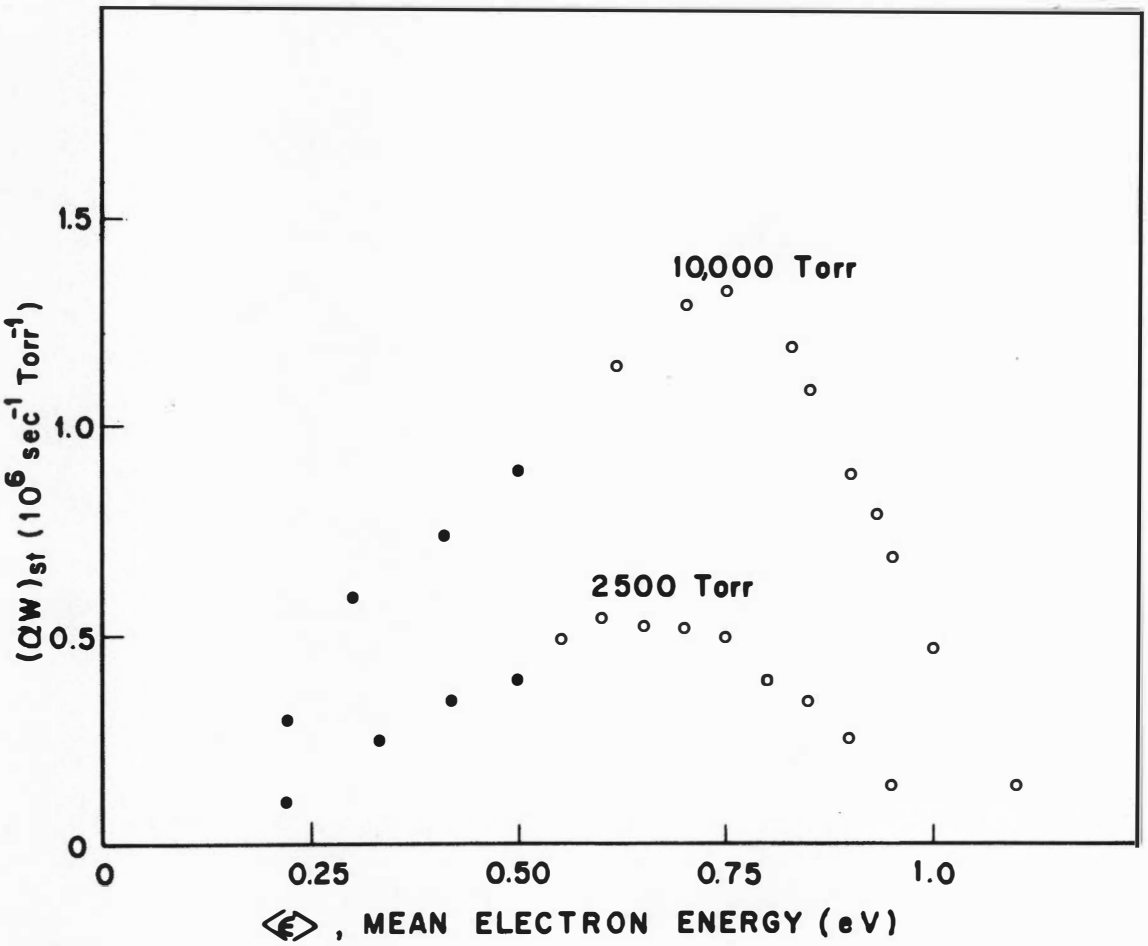

Figure V-9. The Stabilization Rate, $(\alpha w)_{st}$, as a Function of $\langle \epsilon \rangle$ for P_x = 2500 Torr and 10,000 Torr.

(•) - N_2 Data; (o) - Ar Data.

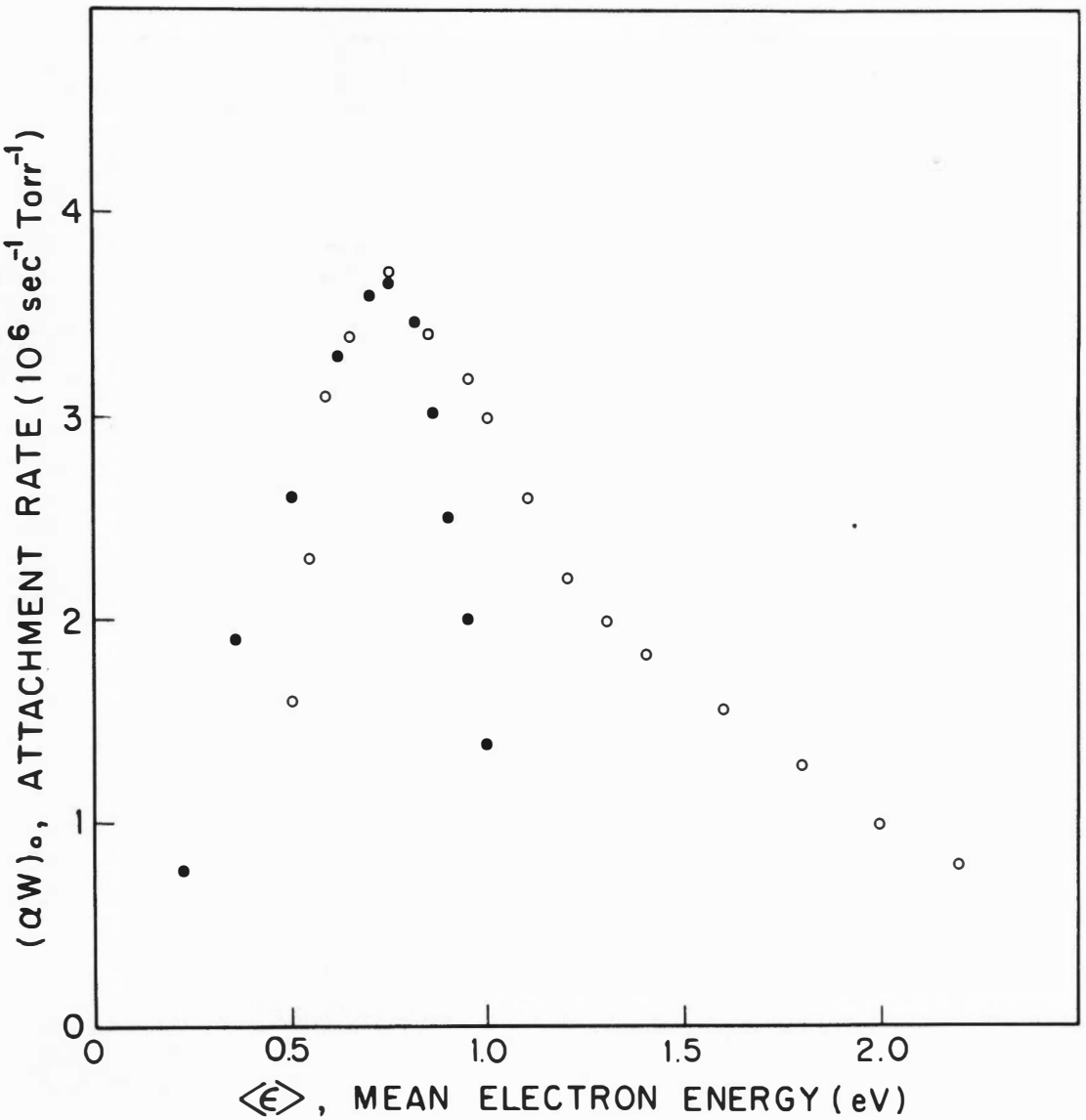

Figure V-10. A Comparison Between $(\alpha w)_o$ and $(\alpha w)_{st}$ at P_x = 10,000 Torr.

$(\alpha w)_{st}$ has been Normalized to $(\alpha w)_o$ at the Peak Energy $\langle \epsilon \rangle$ = 0.75 eV. (o) = $(\alpha w)_o$; (●) = $(\alpha w)_{st}$.

$$\frac{1}{(\alpha w)_{st}} = A + \frac{B}{P_x} \qquad (V\text{-}9)$$

where $A = k_2 + k_3/k_1k_3$ and $B = (k_2 + k_3)/k_1k_3k_4^2$. The experimental data on $(\alpha w)_o$ vs. P_x are plotted in the manner suggested by Equation (V-9) in Figure V-11 for several mean energies and they are seen to be consistent with Equation (V-9) for $P_x \leq 25,000$ Torr. Beyond this point ($1/P = 0.4 \times 10^{-4}$ Torr^{-1}) the data diverge from the model. From a linear least squares fit to the data in Figure V-11, the constants A and B can be obtained. These are presented in Table V-1.

2. Determination of the Three Body Coefficients

The three body coefficients for the reaction

$$e + C_2H_5Br + X \xrightarrow{k_{3b}} C_2H_5Br^- + X + \text{energy} \qquad (V\text{-}10)$$

($X = N_2$ or Ar) have been determined by a least squares fit to the data in Figure V-4, page 82, and Figure V-5, page 83, for $P_x \leq 5,000$ Torr. In this region $(\alpha w)_o$ varies linearly with P_x ($k_2 + k_3 \gg k_{4x}P_x$) and k_{3b} is found to be equal to $k_1k_{4x}/(k_2 + k_3)$. These rate constants are small and depend strongly on the electron energy as is shown in Figure V-12.

3. Rate Constant Analysis

From the previous analysis we have determined $(\alpha w)_{p_x \to 0} = k_1k_2/(k_2 + k_3)$ and $k_{3b} = k_1k_{4x}/(k_2 + k_3)$. Dividing the dissociation rate,

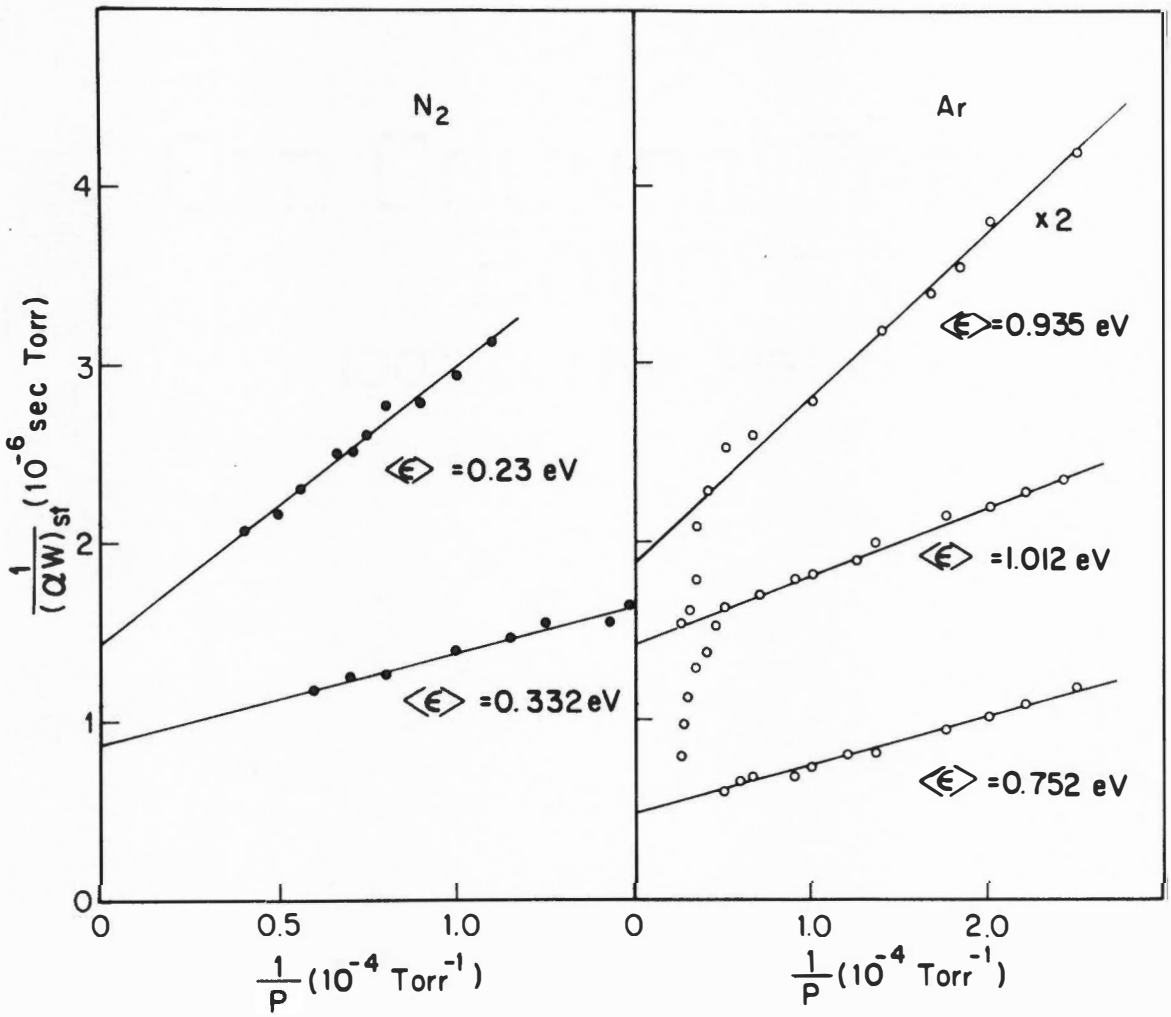

Figure V-11. $1/(\alpha w)_{st}$ vs. $1/P_x$ for C_2H_5Br in N_2 and Ar.

Table V-1

Values of A and B

$\langle\epsilon\rangle$ (eV)	A (sec Torr) $\times 10^{-6}$	B (sec Torr^2) $\times 10^{-2}$
0.23	1.40	1.55
0.33	0.86	0.54
0.49	0.73	0.50
0.55	0.68	0.43
0.65	0.60	0.35
0.75	0.50	0.38
0.85	0.56	0.40
0.93	1.00	0.42
1.012	1.40	0.48

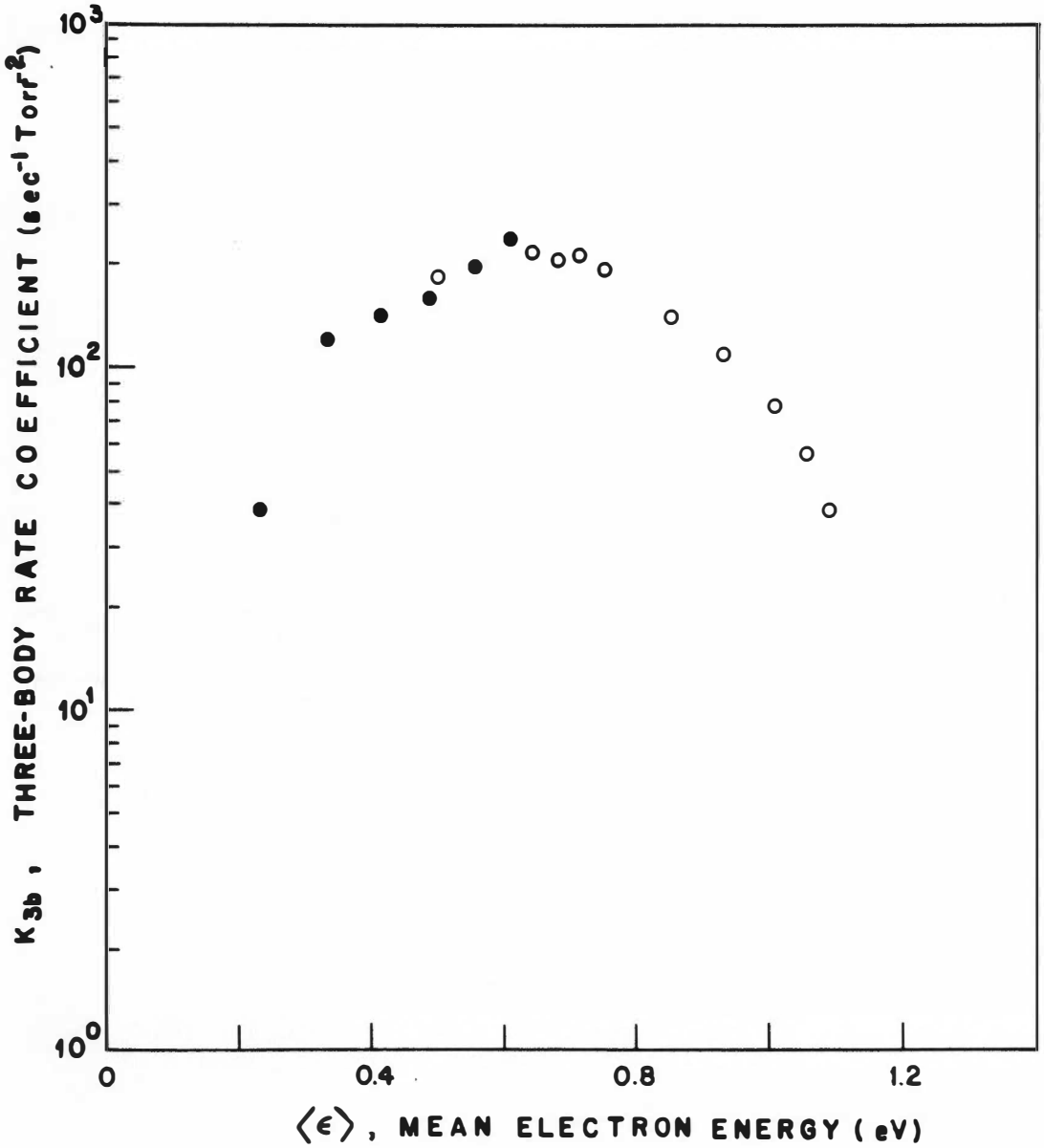

Figure V-12. Three-body Rate Coefficients for the Reaction $e + C_2H_5Br + X \rightarrow C_2H_5Br^- + X + \text{energy}$ (X = N_2 or Ar).

$(\alpha w)_{P_x \to 0}$, by k_{3b} gives k_3/k_{4x} as a function of $\langle\epsilon\rangle$. This ratio is plotted in Figure V-13 (closed circles are N_2 data; open circles are Ar data) and is seen to increase with increasing $\langle\epsilon\rangle$. From the $(\alpha w)_{P_x \to 0}$ plot and the inverse plot (Figure V-11, page 94) we can determine $k_2/k_3 = (\alpha w)_{P_x \to 0} \times A$ and therefore the ratio $k_2/(k_2 + k_3)$. $k_2/(k_2 + k_3)$ is the probability that $C_2H_5Br^{-*}$ will dissociate as compared to the competing process of autoionization. The quantities k_2/k_3 and $k_2/(k_2 + k_3)$ are plotted in Figure V-14 as a function of $\langle\epsilon\rangle$ and also are listed in Table V-2. It can be seen from Figure V-14 that, as the electron energy increases, dissociation becomes much more probable than autoionization (at $\langle\epsilon\rangle$ = 1.087 eV, k_2 = 4.23 k_3 and $k_2/k_2 + k_3$ = 0.81). The ratio k_3/k_{4x} can also be determined from $(k_2/k_{4x})/(k_2/k_3)$. This quantity is plotted in Figure V-15 as a function of mean energy $\langle\epsilon\rangle$.

The absolute rate of electron attachment, k_1, for $P_{x \to \infty}$ can be determined from the ratio $(\alpha w)_{P_x \to 0}/k_2/(k_2 + k_3)$. This quantity is plotted in Figure V-16 as a function of $\langle\epsilon\rangle$. The open circles are values calculated in the manner above; the dark circles represent values of $(\alpha w)_{P_x \to 0}$ for $\langle\epsilon\rangle \geq$ 1.1 eV. As can be seen from Figure V-5, page 83, $(\alpha w)_o$ is pressure independent for $\langle\epsilon\rangle \geq$ 1.1 eV. The pressure independence of $(\alpha w)_o$ for $\langle\epsilon\rangle \geq$ 1.1 eV can be attributed to the fact that, in this range $k_2/k_{4x}P_x \gg 1$ (see Figure 13) and that $k_2/k_3 \gg 1$ (see Figure V-14). Under these conditions we have

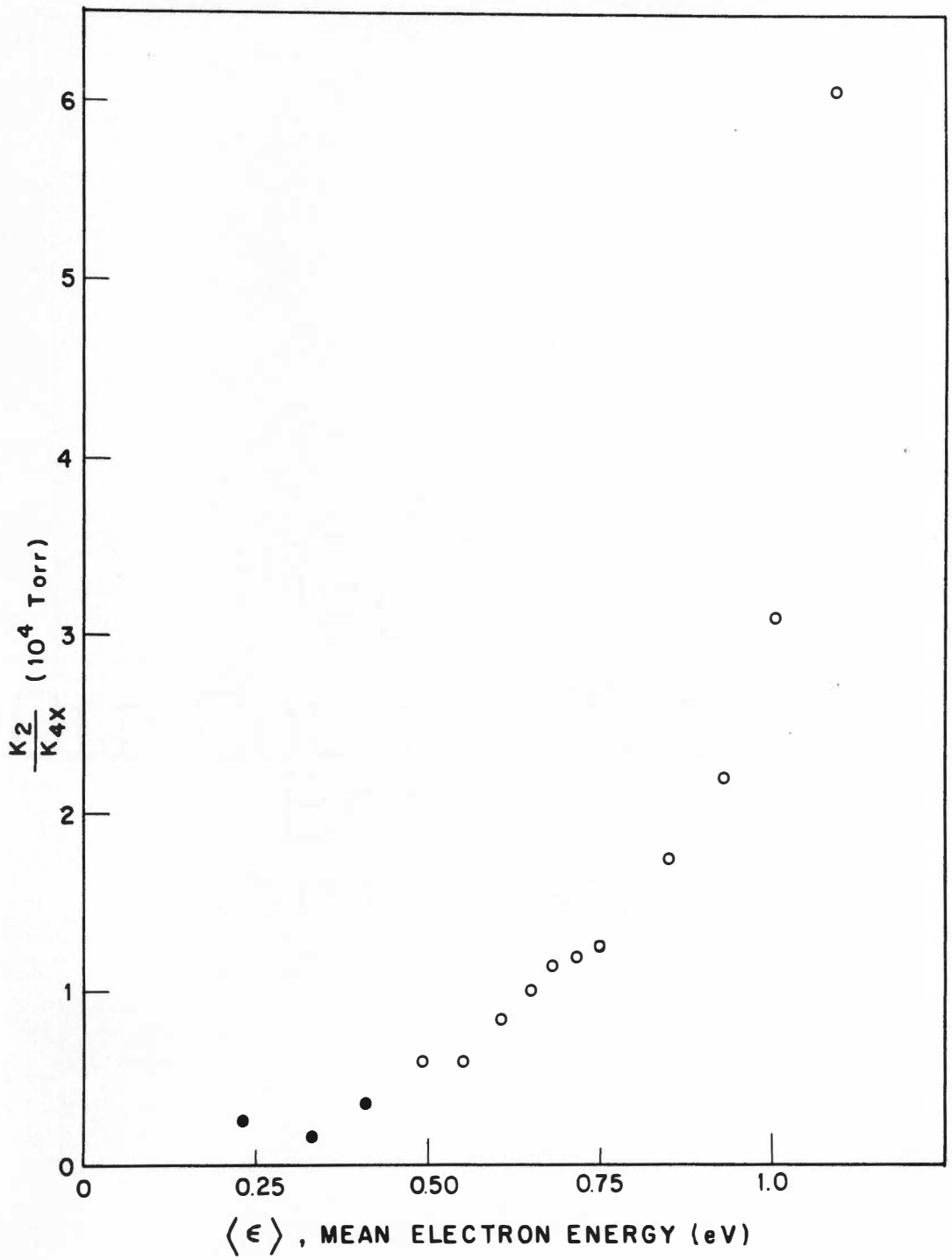

Figure V-13. k_2/k_{4x} as a Function of $\langle\epsilon\rangle$.

Closed Circles are N_2 Data; Open Circles are Ar Data.

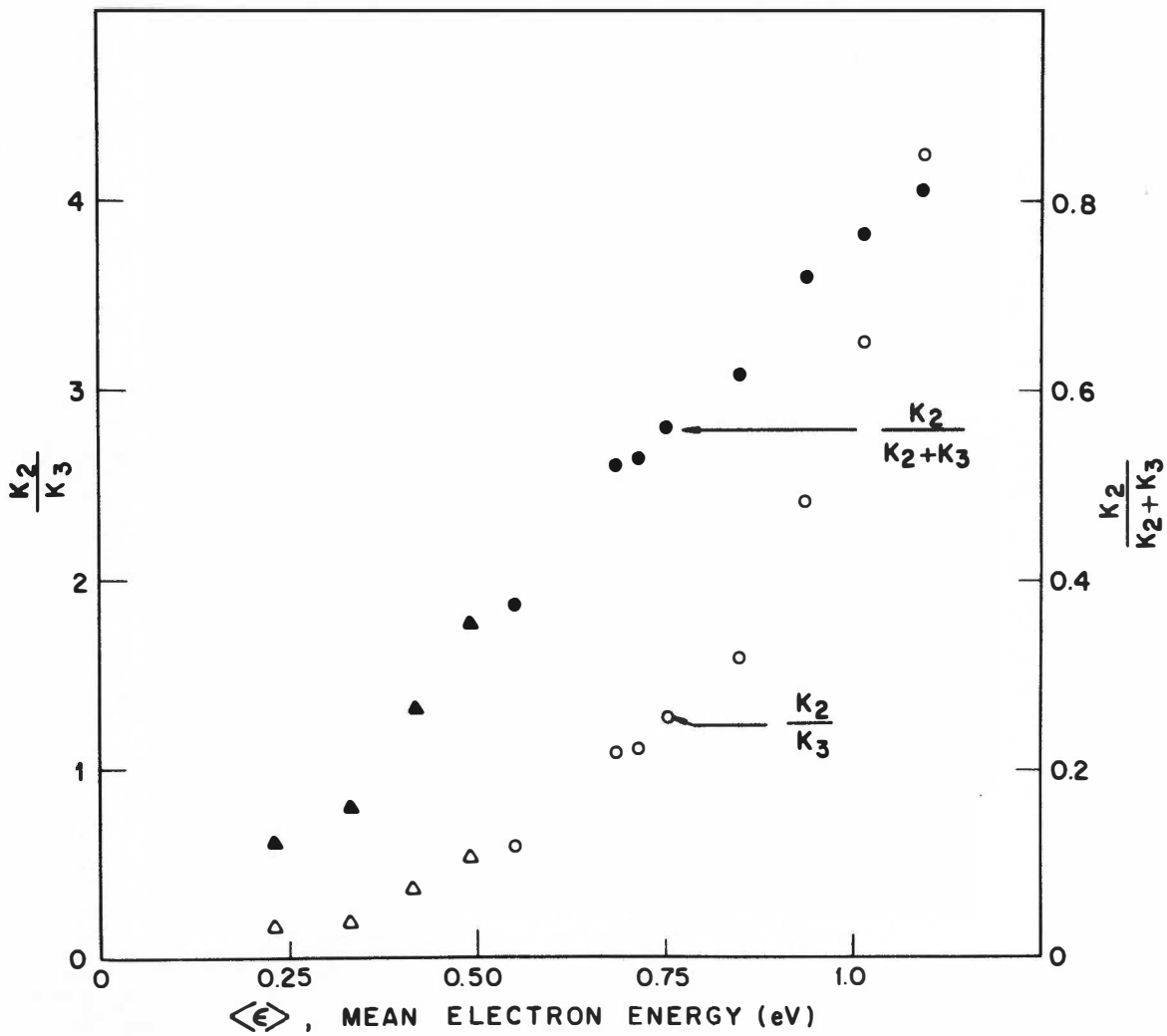

Figure V-14. k_2/k_3 and $k_2/(k_2 + k_3)$ as a Function of $\langle\epsilon\rangle$.

(▲, Δ) N_2 Data; (o, ●) Ar Data.

Table V-2

Values of k_2/k_3 and $k_2/k_2 + k_3$

$\langle \epsilon \rangle$ (eV)	k_2/k_3	$k_2/k_2 + k_3$
0.23	0.14	0.12
0.33	0.19	0.16
0.42	0.36	0.26
0.49	0.53	0.35
0.55	0.60	0.37
0.68	1.08	0.52
0.72	1.11	0.53
0.85	1.37	0.58
0.94	2.42	0.71
1.012	3.26	0.76
1.095	4.23	0.81

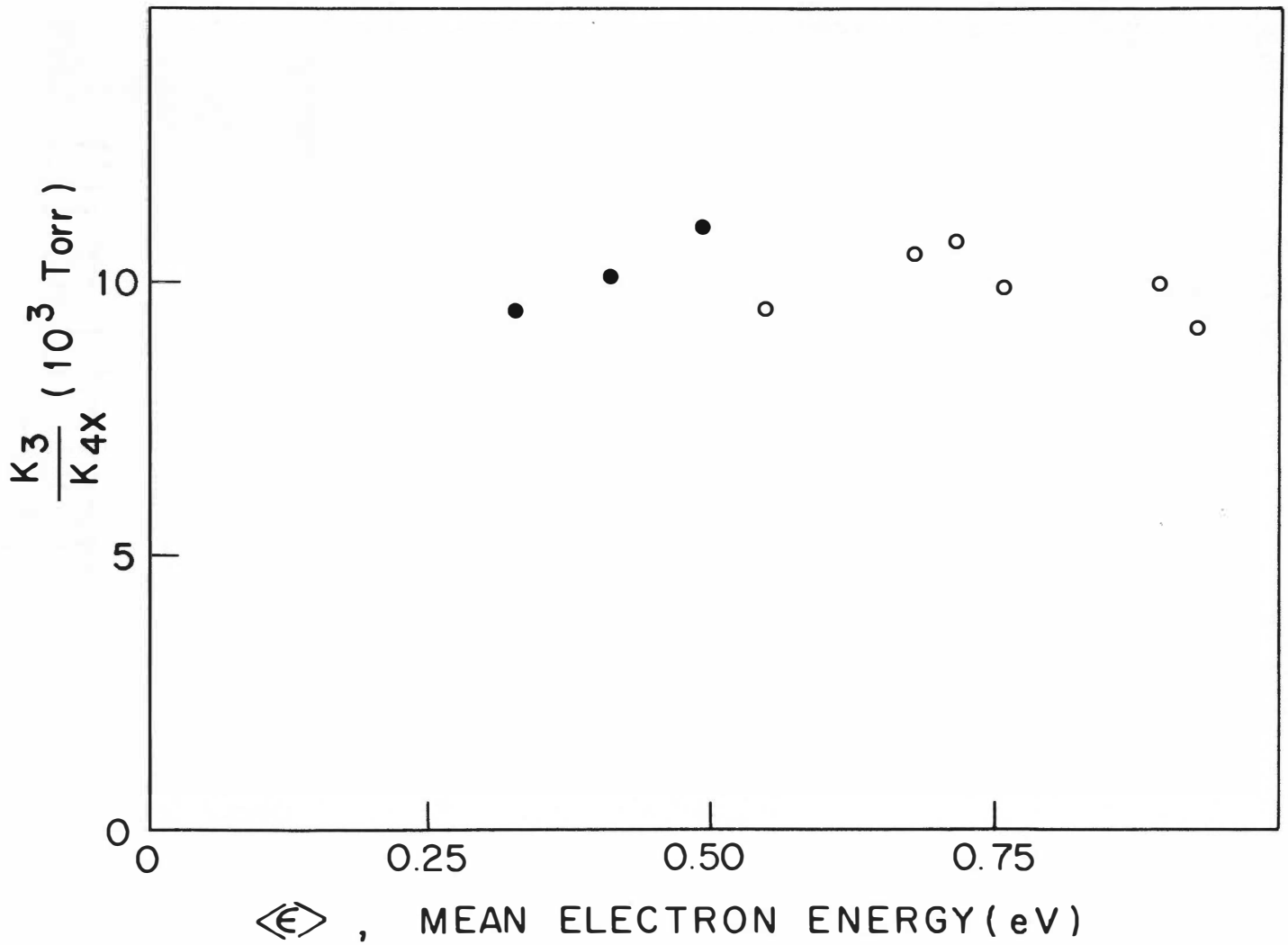

Figure V-15. k_3/k_{4x} as a Function of $\langle\epsilon\rangle$.

Closed Circles are N_2 Data; Open Circles are Ar Data.

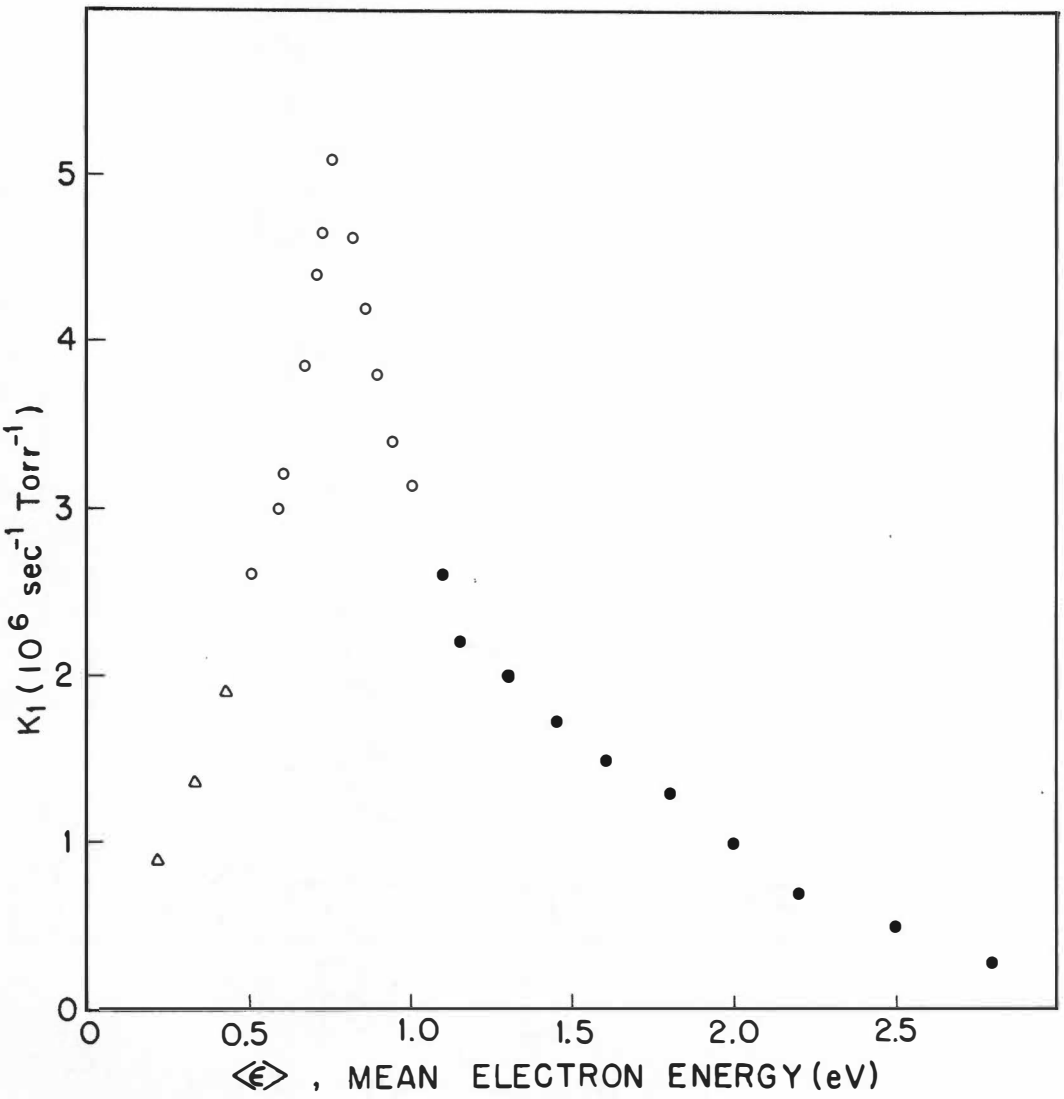

Figure V-16. The Absolute Rate of Electron Attachment, k_1, as a Function of $\langle\epsilon\rangle$.

(Δ) - N_2 Data; (o) - Ar Data; ($\bullet$) - $(\alpha w)_o$ for $\langle\epsilon\rangle \geq 1.1$ eV.

$$(\alpha w)_{P_x \to 0} = \frac{k_1 \{k_2 + k_{4x} P_x\}}{k_2 + k_3 + k_{4x} P_x} \approx k_1 \quad . \qquad \text{(V-11)}$$

These inequalities also show that $k_{3b} \to 0$ for $\langle \epsilon \rangle \geq 1.1$ eV.

4. Autodetachment Lifetime of $C_2H_5Br^{-*}$

Previously, Christodoulides and Christophorou (1971) attributed the values of $(\alpha w)_o$ to a dissociative electron attachment process involving a short-lived ($\leq 10^{-13}$ sec) compound negative ion state of $C_2H_5Br^{-*}$ and a pressure-dependent process, involving a longer-lived state, which could be either dissociative or nondissociative. In the notation used in this chapter, the short-lived dissociative process corresponds to the rate $(\alpha w)_{P_x \to 0} = k_1 k_2/(k_2 + k_3)$ and the longer-lived pressure dependent process corresponds to $(\alpha w)_{st} = (\alpha w)_o - (\alpha w)_{P_x \to 0}$. Although two states may be involved, considering the similarity between $(\alpha w)_o$ and $(\alpha w)_{st}$ as evidenced in Figure V-10, page 92, one may postulate the existence of just one compound negative ion state which has several modes of decay. These decay channels include dissociation (rate = k_2), autoionization (rate = k_3) and collisional stabilization (rate = $k_{4x} P_x$). The reaction scheme (V-1) to (V-4) was derived under this assumption and the experimental data support the model.

In Chapter III, a method was presented for finding the critical pressure, P_c, for which the rate of autoionization of the negative ion M^{-*}

was equal to the rate of stabilization of M^{-*} by a third body X. Assuming that the pressure dependent process is just the stabilization chennel, the lifetime of this channel (k_3^{-1}) can be determined using the methods of Chapter III. There is obviously competition between the processes of dissociation and autoionization which is equivalent to having the probability of stabilization, p, less than unity. Such a determination using Equation (III-16) [see also Equation (IV-7)] will yield a lower limit to k_3^{-1}. The results of such a calculation show that $k_3^{-1} \sim 5.6 \times 10^{-12}$ sec using $P_c = k_3/k_{4x}$.

The results obtained above can be used to determine a lower limit to the lifetime (k_2^{-1}) of the dissociative channel. We have $k_2^{-1} = k_3^{-1}(k_3/k_2)$ and, since the last factor is known as a function of $\langle\epsilon\rangle$, we can determine a lower limit to k_2^{-1} as a function of $\langle\epsilon\rangle$. The results of this calculation are shown in Figure V-17. It is evident that $k_2^{-1} < k_3^{-1}$ over the range where $k_2 > k_3$ and $k_2^{-1} > k_3^{-1}$ over the range where $k_2 < k_3$.

The calculations above have yielded values of k_2^{-1} and k_3^{-1} which are lower limits to the lifetimes of the processes of dissociation and autoionization, respectively. The lifetime of the compound negative ion state would be expected to be somewhat shorter than k_2^{-1} and k_3^{-1} because if a given quantum mechanical state has decay channels k_i ($i = 1, \ldots N$), then the total rate $k = \sum_i k_i$ and the lifetime is $\tau_a = k^{-1} = (\sum_i k_i)^{-1}$. However, it is difficult to place a lower limit to τ_a in this case because the values of k_2^{-1}

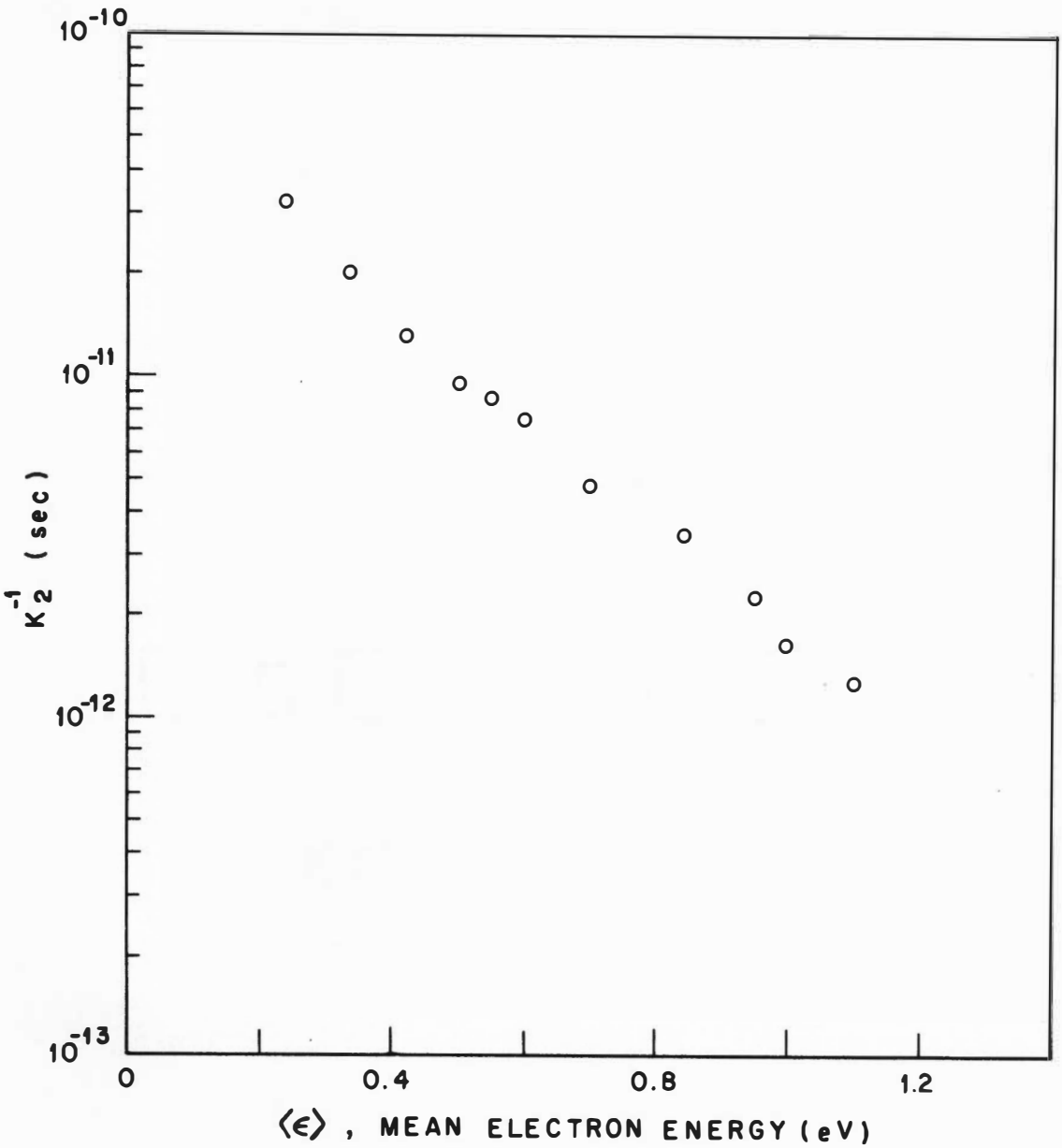

Figure V-17. k_2^{-1} as a Function of ⟨ϵ⟩.

and k_3^{-1} are only lower limits. Because of this fact, we will not attempt to calculate the lifetime of $C_2H_5Br^{-*}$ further.

5. Deviation of the Experimental Results from the Proposed Model

Figures V-4, V-5, and V-11, pages 82, 83, and 94, indicate that the experimental rates are in agreement with the proposed model for $P_{Ar} < 20,000$ Torr, but for $P_{Ar} > 20,000$ Torr, the rates are higher than predicted by Equations (V-1) to (V-4). Because of the many experimental difficulties at the higher pressures, it was feasible to take data for only a few E/P's. The results for $\langle \epsilon \rangle = 0.935$, 1.012, and 1.087 eV in Figures V-4, page 82, and V-5, page 83, show the small magnitude of this deviation. Figure V-18 shows a log plot of the residual attachment rate $\alpha w_{res} = (\alpha w)_o - (\alpha w)_{model}$ as a function of pressure. $(\alpha w)_{model}$ is the attachment rate that would be measured had the reaction scheme (V-1) to (V-4) been the only one responsible for electron attachment. These values were then subtracted from the experimental rates at each P_{Ar} and the rates $(\alpha w)_{res}$ were obtained which could not be accounted for on the basis of the assumed reaction scheme. From a straight-line least squares fit to the data in Figure V-18, we obtained a slope of 5.08. On the basis of this analysis, the measured rates in C_2H_5Br-Ar mixtures could be accounted for by a mechanism such as the one suggested at the beginning of this chapter and by another mechanism which depends more strongly on P_{Ar}. The nature of this latter reaction is not clear at the present time.

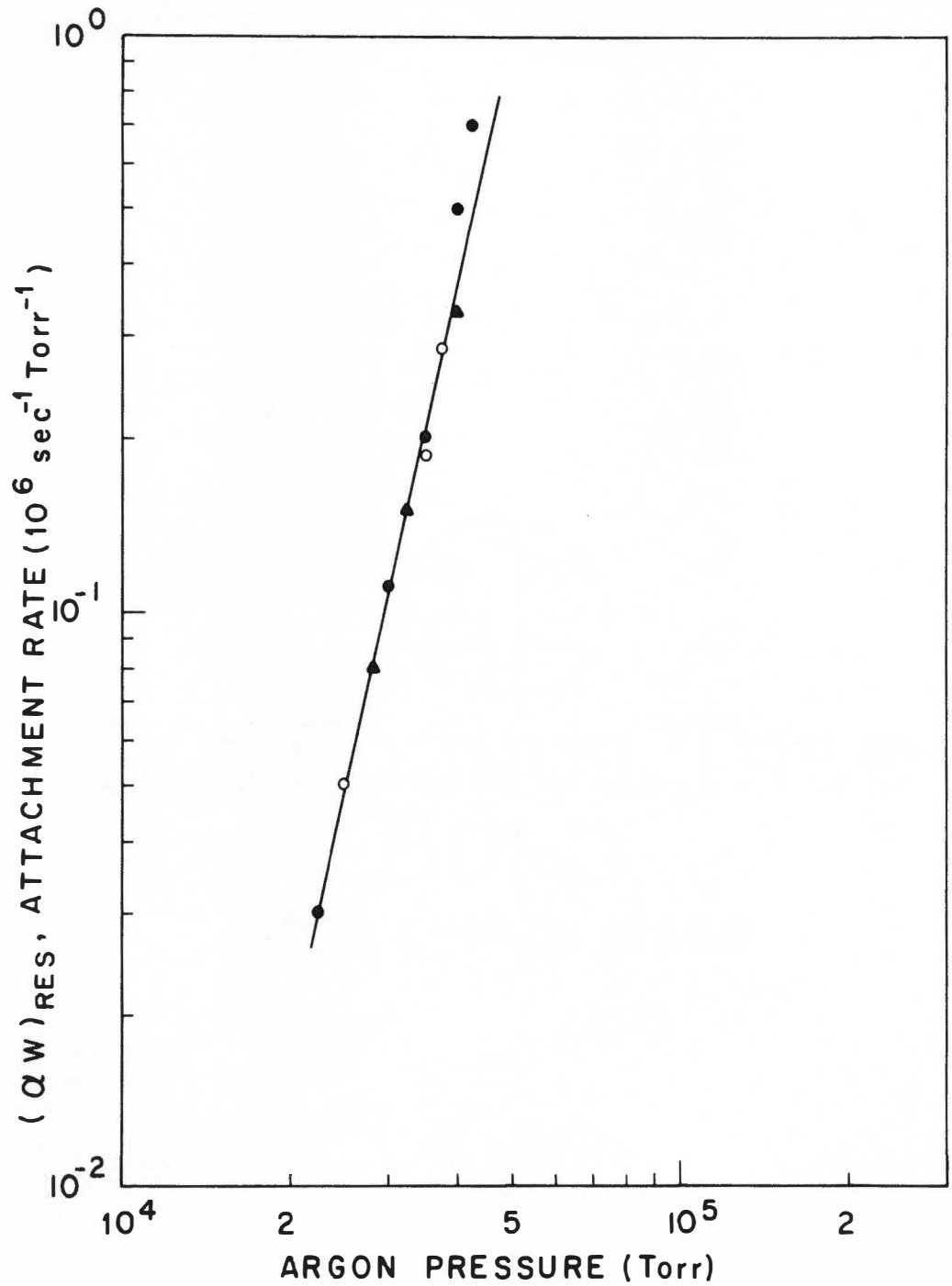

Figure V-18. The Residual Attachment Rate, $(\alpha w)_{res}$, as a Function of P_{Ar}.

6. Extrapolation of High Pressure Rates to the Liquid Phase

Any coherent picture of radiation interaction with matter must be able to relate the abundant knowledge on isolated molecules to that in the condensed phase. The ultrahigh pressure swarm experiment has been shown to be an excellent method for relating gas phase information to "liquid state" behavior. From the previous analysis, the rate k_1, interpreted as the absolute attachment rate as $P_{Ar \to \infty}$, can be found as a function of $\langle \epsilon \rangle$. Under the assumptions of the model presented earlier, we have $k_1 \approx [(\alpha w_o)]_{liquid}$. On the basis of the data presented in Figure V-18, it is obvious that the model breaks down for $P_{Ar} \geq 20,000$ Torr and that $(\alpha w)_o$ increases faster than predicted. We therefore see that k_1 is a lower limit to $(\alpha w_o)_{liquid}$. The apparent breakdown of the model was not observed in the data using N_2 as a carrier gas. However, very few E/P's could be examined in the range $P_{N_2} \geq 20,000$ Torr and the data that were taken were for low $\langle \epsilon \rangle$.

Another way of predicting liquid state attachment rates is to calculate $(\alpha w_o)_{liquid} = k_{1\ max} + (\alpha w)_{res, P_1}$ where $(\alpha w)_{res, P_1}$ ($= 1.5 \times 10^7$ sec^{-1} $Torr^{-1}$) is the residual attachment rate in Figure V-18 extrapolated to the density of liquid argon and $k_{1\ max}$ is the maximum value of k_1 in Figure V-16, page 102. The residual attachment rate is found to be roughly independent of energy over the limited range that was covered experimentally ($0.7 \leq \langle \epsilon \rangle \leq 1.0$ eV). This analysis gives $(\alpha w_o)_{liquid} \approx$

2×10^{7} sec^{-1} $Torr^{-1}$ = 0.37×10^{12} M^{-1} sec^{-1}. Attachment rates have not been measured for C_2H_5Br in liquid argon, but the value above compares favorably with 0.34×10^{12} M^{-1} sec^{-1} determined by Allen and Holroyd (1973) for C_2H_5Br in neopentane. These investigators have found a range of values of the attachment rate which depends on the solvent used; these are 1.5×10^{12} M^{-1} sec^{-1}, 1.6×10^{12} M^{-1} sec^{-1}, 6.3×10^{13} M^{-1} sec^{-1}, and 0.042×10^{12} M^{-1} sec^{-1} for C_2H_5Br in n-hexane, n-pentane, 1,2,4 trimethylpentane, and tetramethylsilane, respectively. The values of $(\alpha w)_{liquid}$ obtained in this experiment agree well with the liquid values of Allen and Holroyd considering the crudeness of the model. The model presented earlier is definitely deficient in the prediction of liquid state values because it is not possible to take solvation effects into account. Solvation would certainly shift the $k_1(\langle\epsilon\rangle)$ curve toward thermal energies as is expected to be characteristic of electrons in liquids.

CHAPTER VI

SUMMARY

In this study, electron capture mechanisms and reaction schemes have been developed for electron attachment to various molecules embedded in dense gaseous media (for N_2, $P_{N_2} \leq 27,500$ Torr; for Ar, $P_{Ar} \leq 42,000$ Torr; for C_2H_4, $P_{C_2H_4} \leq 17,000$ Torr; for C_2H_6, $P_{C_2H_6} \leq 17,500$ Torr). As the density of each medium increases, each affects the attachment rate in a different manner, indicating the profound effect and importance of the environment on the electron attachment process.

The results of a study of the capture of slow (< 1 eV) electrons by O_2 embedded in dense N_2, C_2H_4 and C_2H_6 environments was presented and discussed. Large changes were observed in both the magnitude and energy dependence of the attachment rate with increasing density of these three media. Reaction schemes were also presented to account for the pressure dependence of the attachment rate. From this analysis, an autoionization lifetime of 2×10^{-12} sec was estimated for O_2^{-*}. An extrapolation of the high pressure rates to liquid densities gave electron attachment rates of 0.74×10^{10} sec^{-1} $Torr^{-1}$ and 3.3×10^{11} sec^{-1} M^{-1} for O_2 in liquid N_2 and liquid C_2H_4, respectively. Although electron attachment to O_2 has not been measured in liquid N_2 and C_2H_4, the above values are in good agreement with those measured for O_2 in various solvents.

Benzene was found to capture slow (< 0.3 eV) electrons in high densities of N_2 and Ar with a rate which increased with increasing density. The dependence of the rate on carrier-gas density was studied and a model was presented which accounted for the experimental results. The lifetime of $C_6H_6^{-*}$ has been estimated on the basis of this model and found to vary from 1.0×10^{-12} sec at 0.04 eV to $\sim 0.2 \times 10^{-12}$ sec at 0.18 eV. The high pressure attachment rate data were extrapolated to liquid N_2 densities and a liquid rate of $\sim 1 \times 10^{9}$ sec^{-1} M^{-1} was obtained which is in good agreement with that estimated by other investigators. The finding that C_6H_6 captures electrons in the gas phase forced the conclusion that C_6H_6 has a positive electron affinity in contrast to the accepted view that $(EA)_B < 0$ eV.

Bromoethane (C_2H_5Br) has also been found to capture electrons in high densities of N_2 and Ar with a rate which increases with increasing density. $C_2H_5Br^{-*}$ can decay through dissociation, autoionization, and stabilization channels and a model is presented which predicts the relative magnitude of each of these rates as a function of $\langle \epsilon \rangle$. In general, dissociation is the most probable mode of decay for $\langle \epsilon \rangle \geq 1$ eV. The high pressure rates have also been extrapolated to liquid Ar densities and a liquid rate of 0.37×10^{12} sec^{-1} M^{-1} was found. Although attachment to C_2H_5Br has not been measured in liquid N_2 and Ar, this rate is in reasonable agreement with those obtained for C_2H_5Br in various solvents such as neopentane.

The work presented in this thesis shows that it is possible to predict electron attachment rates in liquid media from experiments performed in the high pressure gas phase. The high pressure swarm experiment is unique in that it bridges the gap between low pressure studies, where much is known about kinetic mechanisms, and studies in the condensed phase where relatively little is known about electron attachment mechanisms.

BIBLIOGRAPHY

BIBLIOGRAPHY

Allen, A. O., and R. A. Holroyd, submitted to J. Chem. Phys. (1973).

Allen, N. L., and B. A. Prew, J. Phys. B3, 1113 (1970).

Allis, W. P., "Motion of Ions and Electrons," in Handbuch der Physik, Vol. XXI (Springer-Verlag, Berlin, 1956), p. 383.

Bakale, G., and G. F. Schmidt (Private Communication, 1973).

Bardsley, J. N., A. Herzenberg, and F. Mandl, Atomic Collision Processes, edited by M. R. C. McDowell (North Holland Publishing Co., Amsterdam, 1964), p. 415.

Bardsley, J. A., A. Herzenberg, and F. Mandl. Proc. Phys. Soc. (London), 89, 321 (1966).

Bardsley, J. N., and F. Mandl, "Resonant Scattering of Electrons by Molecules," in Reports on Progress in Physics, Vol. XXXI, part 2, London, 1968.

Barbiere, D., Phys. Rev. 84, 653 (1951).

Bortner, T. E., and G. S. Hurst, Health Phys. 1, 39 (1958).

Bouby, L., and H. Abgrall, Proceedings 5th International Conference on the Physics of Atomic and Electronic Collisions (Publishing House "Nauka," Leningrad, USSR, 1967), p. 584.

Bouby, L., F. Fiquet-Fayard, and Y. Le Coat, Intern. J. Mass Spectr. and Ion Phys. 3, 439 (1970).

Chanin, L. M., A. V. Phelps, and M. A. Biondi, Phys. 128, 219 (1962).

Chapman, S., and T. G. Cowling, The Mathematical Theory of Non-Uniform Gases, Second Edition (Cambridge University Press, London, 1952).

Christodoulides, A. A., and L. G. Christophorou, J. Chem. Phys. 54, 4691 (1971).

Christophorou, L. G., Atomic and Molecular Radiation Physics (John Wiley and Sons, Inc., London, 1971a).

Christophorou, L. G., "Recent Studies on Electron Attachment," in Proceedings of the Third Tihany Conference on Radiation Chemistry (Tihany, Hungary, 1971b).

Christophorou, L. G., J. Phys. Chem. 76, 3730 (1972).

Christophorou, L. G., and R. P. Blaunstein, Rad. Res. 37, 229 (1969).

Christophorou, L. G., and R. P. Blaunstein, Chem. Phys. Letters 12, 173 (1971).

Christophorou, L. G., R. P. Blaunstein, and D. Pittman, Chem. Phys. Letters 18, 509 (1973).

Christophorou, L. G., E. L. Chaney, and A. A. Christodoulides, Chem. Phys. Letters 3, 363 (1969).

Christophorou, L. G., R. N. Compton, G. S. Hurst, and P. W. Reinhardt, J. Chem. Phys. 43, 4273 (1965).

Christophorou, L. G., and R. E. Goans, J. Chem. Phys. (in press).

Christodoulides, L. G., D. L. McCorkle, and V. E. Anderson, J. Phys. B4, 1163 (1971).

Collins, P. M., L. G. Christophorou, and J. G. Carter, Oak Ridge National Laboratory Report ORNL-TM 2614 (1970).

Compton, R. N., L. G. Christophorou, and R. H. Huebner, Phys. Letters 23, 656 (1966).

Cottrell, T. L., and I. C. Walker, Trans. Faraday Soc. 61, 1585 (1965).

Duncan, C. W., and I. C. Walker, Faraday Trans. II 68, 1800 (1972).

Eldridge, H. B., Oak Ridge National Laboratory Report ORNL-3090 (1962).

Engelhardt, A. G., A. V. Phelps, and C. G. Risk, Phys. Rev. 135, A1566 (1964).

Fairstein, E., IRE Trans. on Nuclear Sci. NS-8, 136 (1961).

Fox, R. E., W. M. Hickam, D. J. Grave, and T. Kjeldaas, Jr., Rev. Sci. Instr. 26, 1101 (1955).

Gant, K. S., L. G. Christophorou, and D. Pittman (Private Communication, 1973).

Gardner, C. L., J. Chem. Phys. 45, 572 (1966).

Gilding, L. J., and J. G. Kloosterboer, Chem. Phys. Letters 21, 127 (1973).

Goans, R. E., and L. G. Christophorou, J. Chem. Phys. (in press).

Heijtink, G. J., and P. J. Zandstra, Mol. Phys. 3, 371 (1960).

Huber, B., Diplomarbeit, Institute fur Angewandte Physik, University of Hamburg (1969).

Huber, B., Z. fur Naturforschung 24a, 578 (1969).

Kowalski, E., Nuclear Electronics (Springer-Verlag, Berlin, 1970).

Landolt, H. H., and R. Bornstein, "Tables on Chemical Data," Zahlenwerte und Funktionen, Vol. 1, part 3 (Springer-Verlag, Berlin, 1951), p. 511.

Linder, F., and H. Schmidt, Abstracts of the 24th Annual Gaseous Electronics Conference, paper W1 (Gainsville, Florida, 1971).

Loeb, L. B., Basic Processes of Gaseous Electronics, Second Edition (University of California Press, Berkeley, 1960).

Massey, H. S. W., and E. H. S. Burhop, Electronic and Ionic Impact Phenomena (Clarendon Press, Oxford, 1952).

Maxwell, J. B., Data Book on Hydrocarbons (Van Nostrand, New York, 1950).

McCorkle, D. L., L. G. Christophorou, and V. E. Anderson, J. Phys. B. 5, 1211 (1972).

McDaniel, E. W., Collision Phenomena in Ionized Gases (John Wiley and Sons, Inc., New York, 1964).

Nelson, D. R., and G. E. Whitesides (Private Communication, 1968).

O'Malley, T. F., Phys. Rev. 150, 14 (1966).

Present, R. D., Kinetic Theory of Gases (McGraw-Hill Co., New York, 1958).

Ramsauer, C., Ann. Physik 64, 513 (1921).

Richards, J. T., and J. K. Thomas, Chem. Phys. Letters 10, 317 (1971).

Ritchie, R. H., and G. E. Whitesides, Oak Ridge National Laboratory Report ORNL-3081 (1961).

Stockdale, J. A., L. G. Christophorou, and G. S. Hurst, J. Chem. Phys. 47, 3267 (1967).

Szent-Gyorgyi, A., I. Isenberg, and S. Baird, Proc. Nat. Acad. Sci. 46, 1444 (1960).

Szent-Gyorgyi, A., Science 161, 988 (1968).

Townsend, J. S., Phil. Trans. Roy. Soc. London A193, 129 (1900).

Tuttle, T. R., Jr., and S. I. Weissman, J. Am. Chem. Soc. 80, 5342 (1958).

Vogt, E., and G. Wannier, Phys. Rev. 95, 1190 (1954).

Wagner, E. B., F. J. Davis, and G. S. Hurst, J. Chem. Phys. 47, 3138 (1967).

Walker, I. C., (Private Communication, 1973).

Walters, R. J., J. H. Tracht, E. B. Weinberger, and J. K. Rodgers, Chemical Engineering Progress 50, 511 (1954).

Wu, T. Y., Kinetic Equations of Gases and Plasmas (Addison-Wesley Publishing Co., Reading, Mass., 1966).

VITA

Ronald Earl Goans was born in Clinton, Tennessee on August 12, 1946. He attended elementary schools in that city and was graduated from Clinton High School in 1964. He entered the University of Tennessee in June, 1964 and in June, 1968, he received a Bachelor of Science degree in Engineering Physics. In the fall of 1968 he accepted a graduate assistantship at the University of Tennessee and began study toward a Master's degree. He received this degree in December, 1969. In September, 1969 he accepted an Atomic Energy Commission Special Fellowship in Health Physics and began work toward a Doctor of Philosophy degree with a major in Physics. In September, 1972, he accepted an Oak Ridge Associated Universities Laboratory Participantship. The Doctor of Philosophy degree was awarded in June, 1974. He is a member of Tau Beta Pi and Sigma Pi Sigma.

He is married to the former Judy Winegar of Knoxville, Tennessee.